Dark matter with

+ DM sector

at the LHC

Tae Min Hong

on behalf of the
ATLAS Collaboration

WIN2019, Bari, Italy
June 7, 2019

https://agenda.infn.it/event/13938/contributions/88576

University of
Pittsburgh

Outline

http://cern.ch/Atlas/GROUPS/PHYSICS/CombinedSummaryPlots/EXOTICS

- Theory — Approaches, Complementarity
- Exp't — LHC, ATLAS
- Results

DM associated production

- Mono-jet
- Mono-Higgs ($b\bar{b}$)

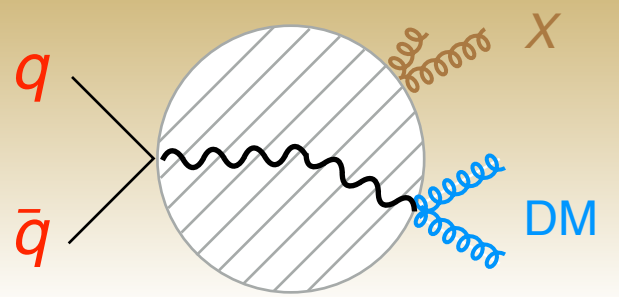

DM mediators

- Decay to di-fermions ($q\bar{q}$, $b\bar{b}$, $\ell\ell$)
- Higgs as mediator

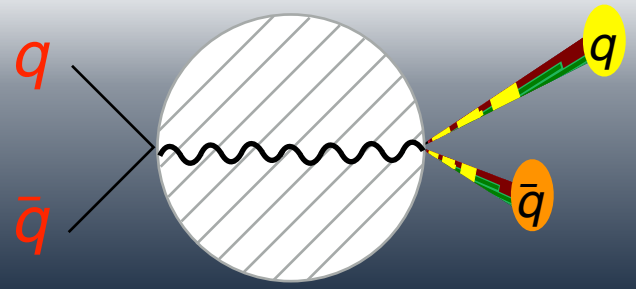

- Tools — Trigger, Boosted jets
- Future — Projections

TM Hong
Pittsburgh

I will highlight only a handful of recent results

How simple?

"Everything should be made as simple as possible, but not simpler."

~ Einstein

Effective Theories

(Run 1)

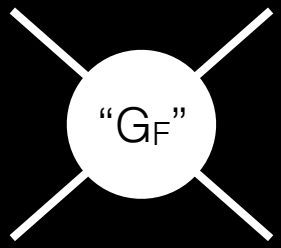

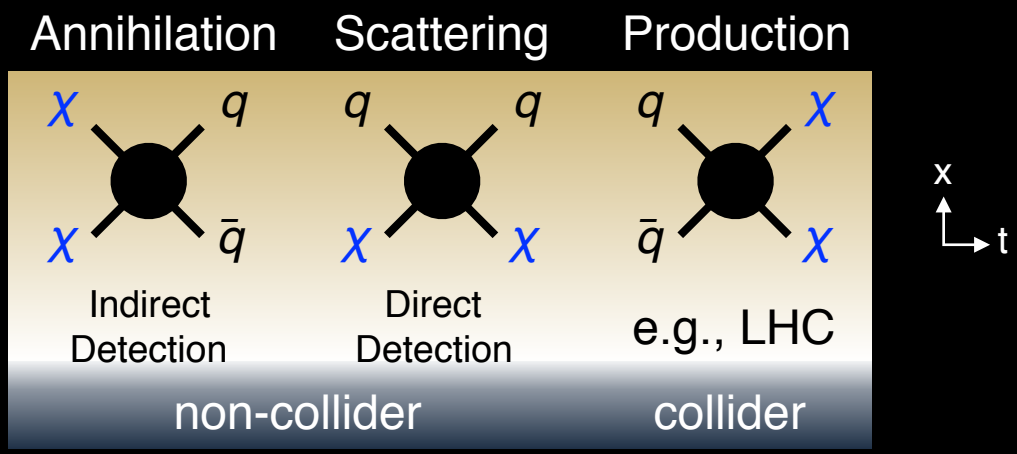

Various approaches are complementary

How simple?

"Everything should be made as simple as possible, but not simpler."

~ Einstein

Effective Theories

(Run 1)

more complex, complete

more simple, agnostic

Simplified models

(Run 2)

[1603.04156]

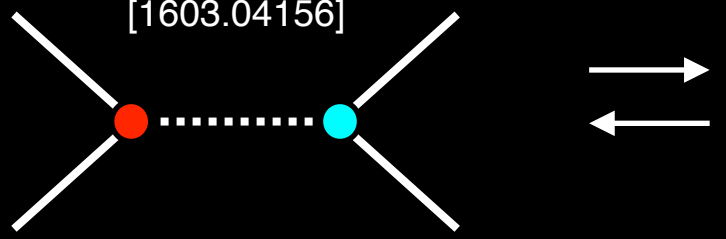

- Large q^2
- Low m_χ

Annihilation	Scattering	Production	LHC	
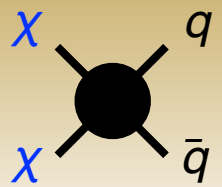	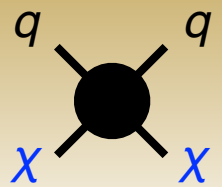	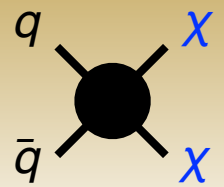	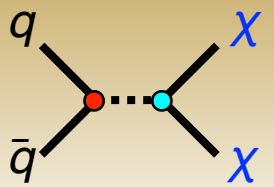	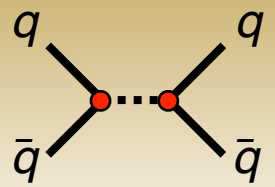
Indirect Detection	Direct Detection	e.g., LHC	e.g., Z', ϕ	e.g., di-jet
non-collider		collider	DM + mediator	mediator

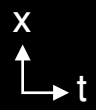

Various approaches are complementary

Neutral third party

Features of mediator

^ prompt, colorless, etc.

Property	Spin 0	Spin 1
Charge Q	0	
Mass m	?	
Mediator is similar to	H [1609.09079]	γ, Z, Z'
Lorentz structure	scalar 1 pseudosc. γ_5	vector γ^μ axial v. $\gamma^\mu \gamma_5$
Coupling "g"	$\propto$ mass	$\propto$ charge
Consequences	$m_b \gg m_d$	$Q_b = Q_d$
Example chan.	mono-b	di-jet

Complementary

Neutral third party

Features of mediator

^ prompt, colorless, etc.

Property	Spin 0	Spin 1
Charge Q	0	
Mass m	?	
Mediator is similar to	H [1609.09079]	γ, Z, Z'
Lorentz structure	scalar 1 pseudosc. γ_5	vector γ^μ axial v. $\gamma^\mu\gamma_5$
Coupling "g"	$\propto$ mass	$\propto$ charge
Consequences	$m_b \gg m_d$	$Q_b = Q_d$
Example chan.	mono-b	di-jet

Model dependence

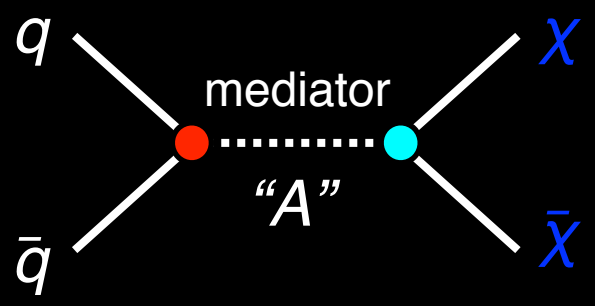

Lagrangian terms

$g_q\,\bar{q}qA$ matter-mediator

$g_\chi\,\bar{\chi}\chi A$ DM-mediator

4-5 in the matrix element

v

Counting parameters

g_q	m_q	m_A	g_χ	m_χ	m_A
❶	known	❷	❸	❹	-

Complementary

2d exclusion plots
assumes 2 parameters

LHC intro

Define pileup, E_T^{miss}

Along beampipe

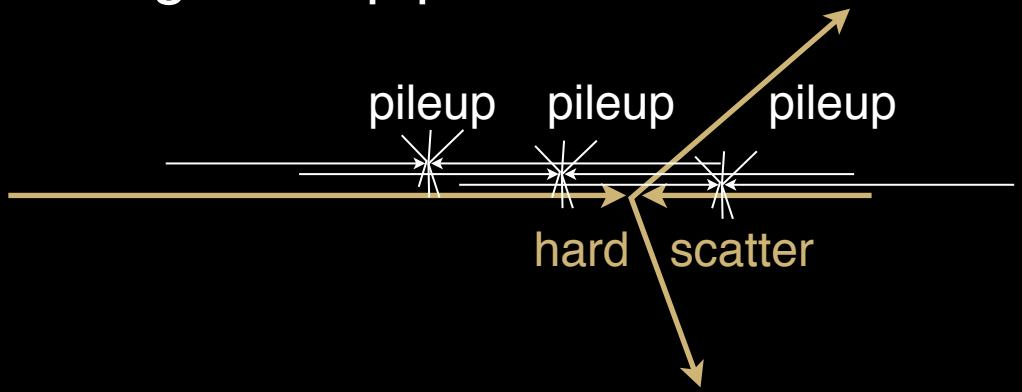

Transverse to beampipe

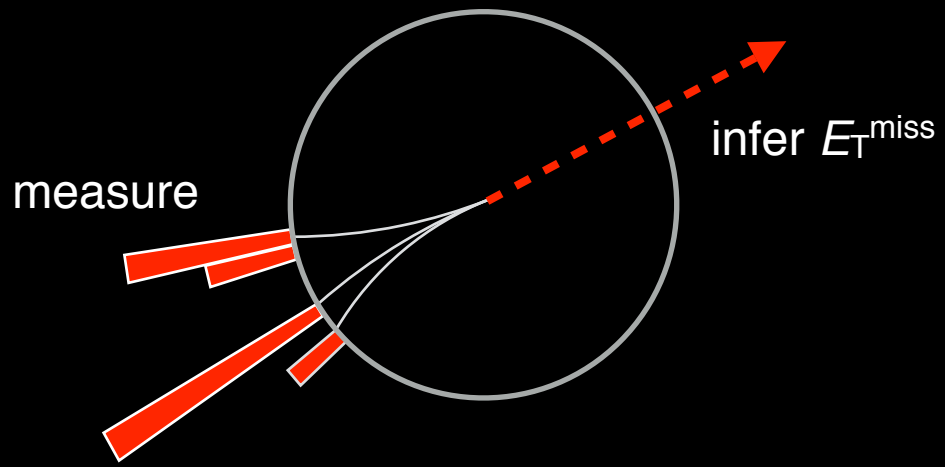

Higher pileup → more challenging to $\begin{matrix}\text{measure}\\\text{trigger on}\end{matrix}$ jets, E_T^{miss}

LHC intro

Define pileup, E_T^{miss}

Along beampipe

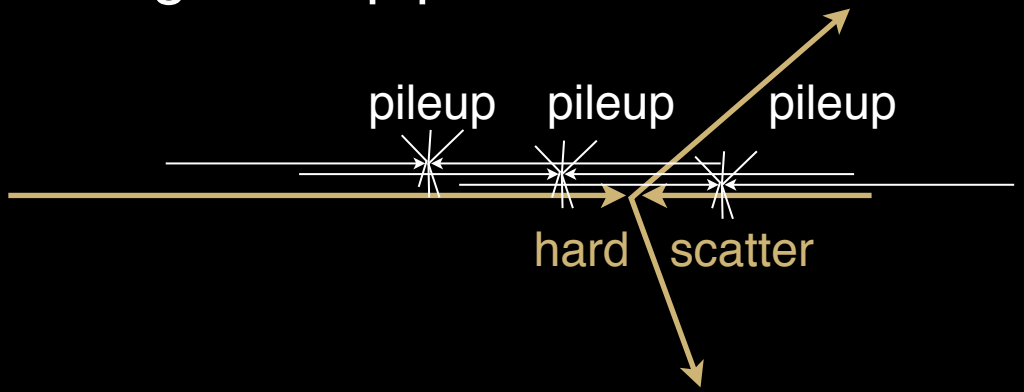

Transverse to beampipe

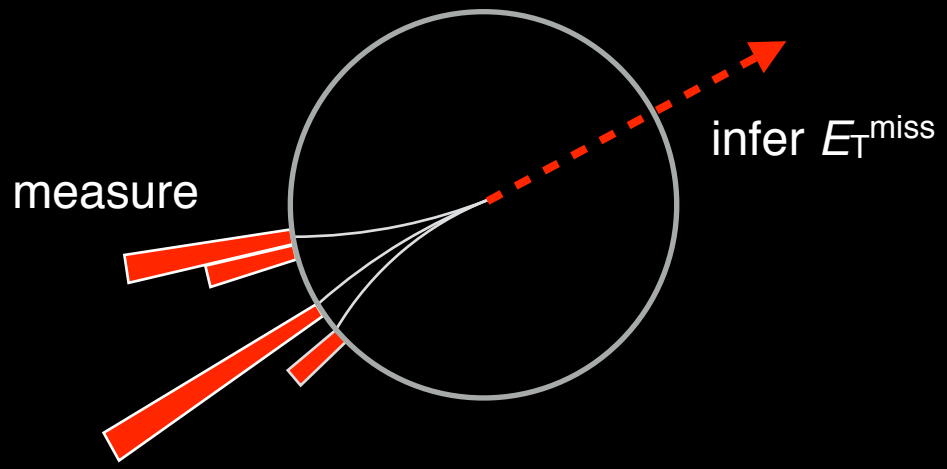

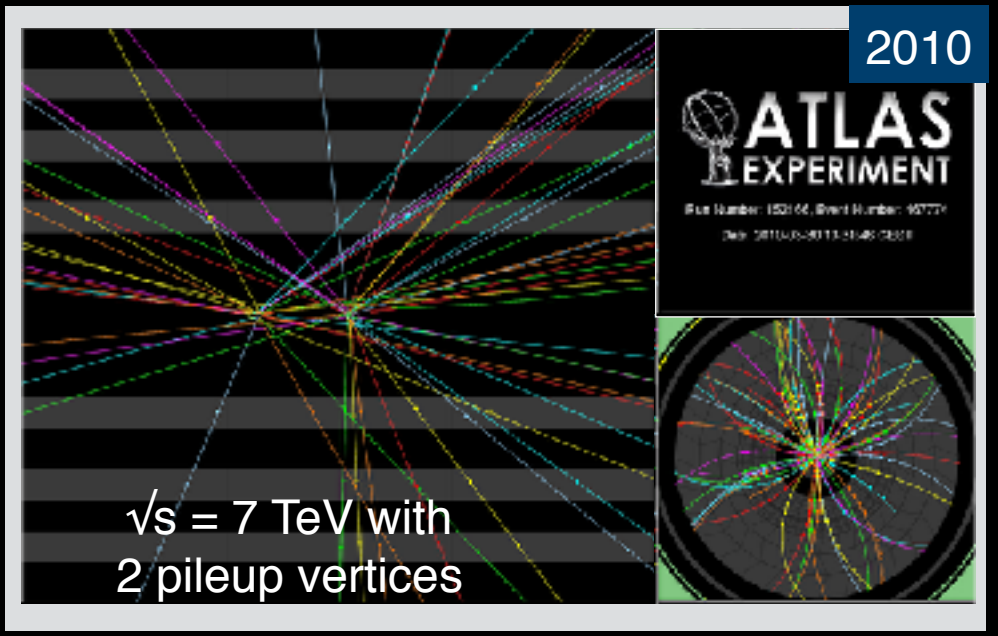

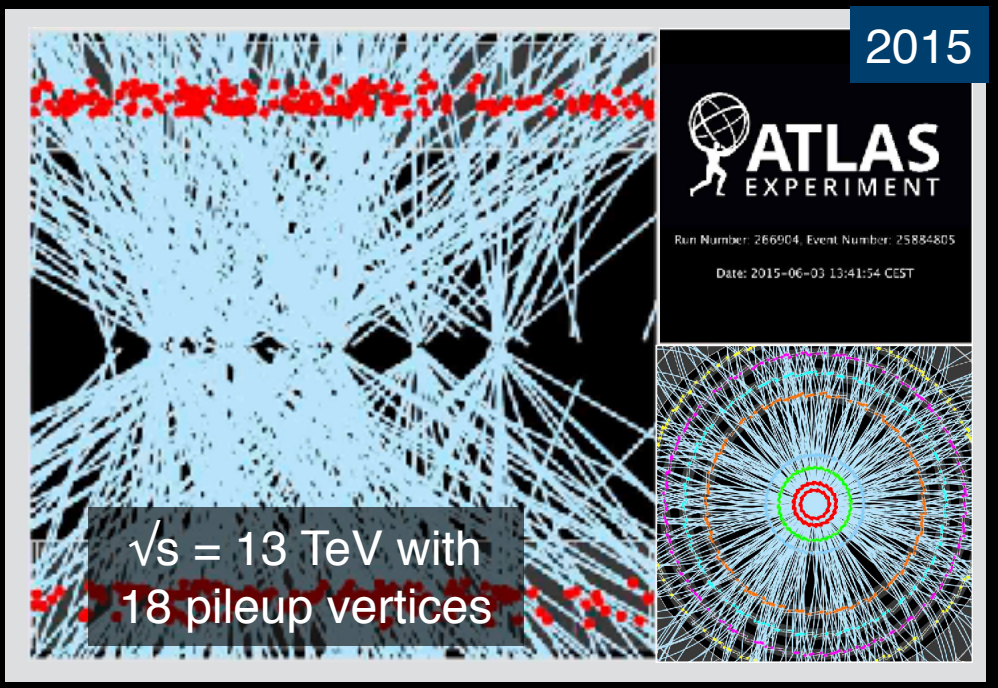

Higher pileup → more challenging to measure / trigger on jets, E_T^{miss}

ATLAS data collection

Higher simultaneous *pp* collisions per bunch crossing, pileup ⟨μ⟩

Integrated luminosity

http://cern.ch/twiki/bin/view/AtlasPublic/LuminosityPublicResultsRun2

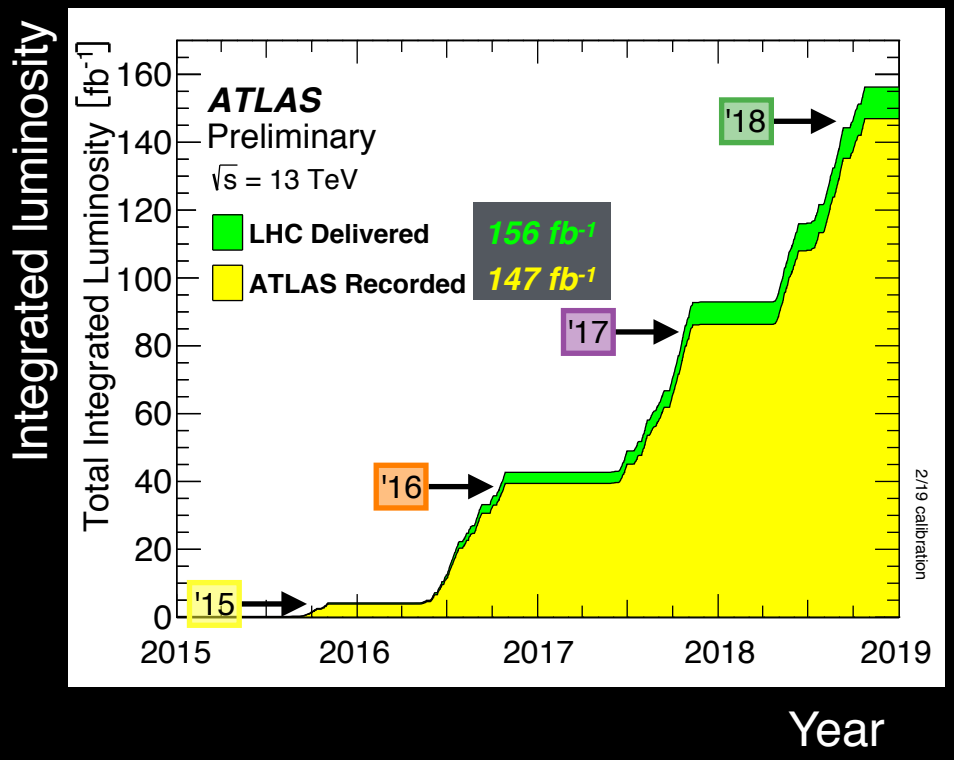

Pileup distribution

http://cern.ch/twiki/bin/view/AtlasPublic/LuminosityPublicResultsRun2

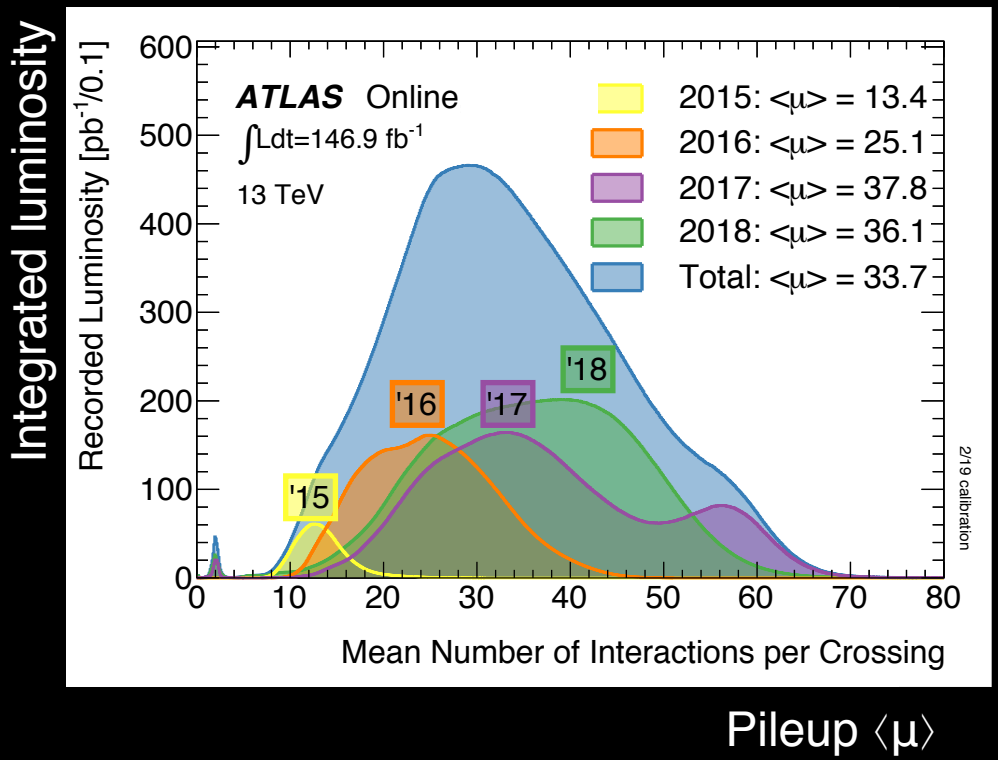

Steeper slope every year

Increase from 10s → near 40

Results in this talk use 36 fb^{-1}, 80 fb^{-1}, 145 fb^{-1}

2015 - 16 - 17 - 18

ATLAS trigger system (L1, HLT)

Trigger rates and efficiencies

L1 trigger rate vs. instantaneous luminosity (2018)

http://cern.ch/twiki/bin/view/AtlasPublic/TriggerOperationPublicResults

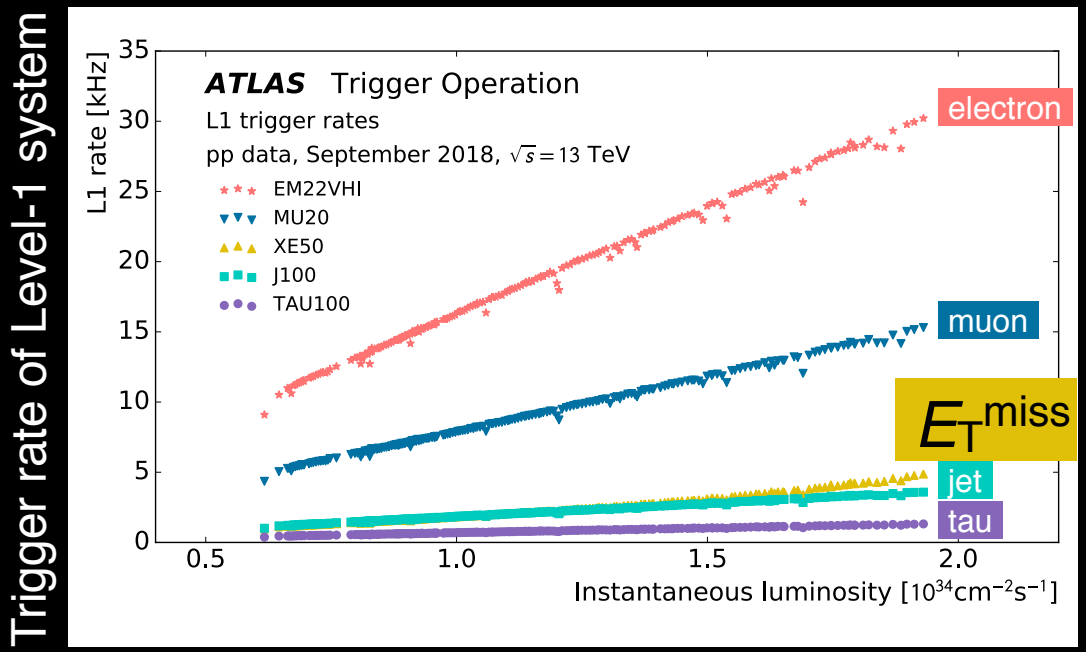

Instantaneous luminosity, proportional to pileup ⟨μ⟩

Mostly linear, few exponential

HLT E_T^{miss} trigger efficiency for each year

http://cern.ch/twiki/bin/view/AtlasPublic/MissingEtTriggerPublicResults

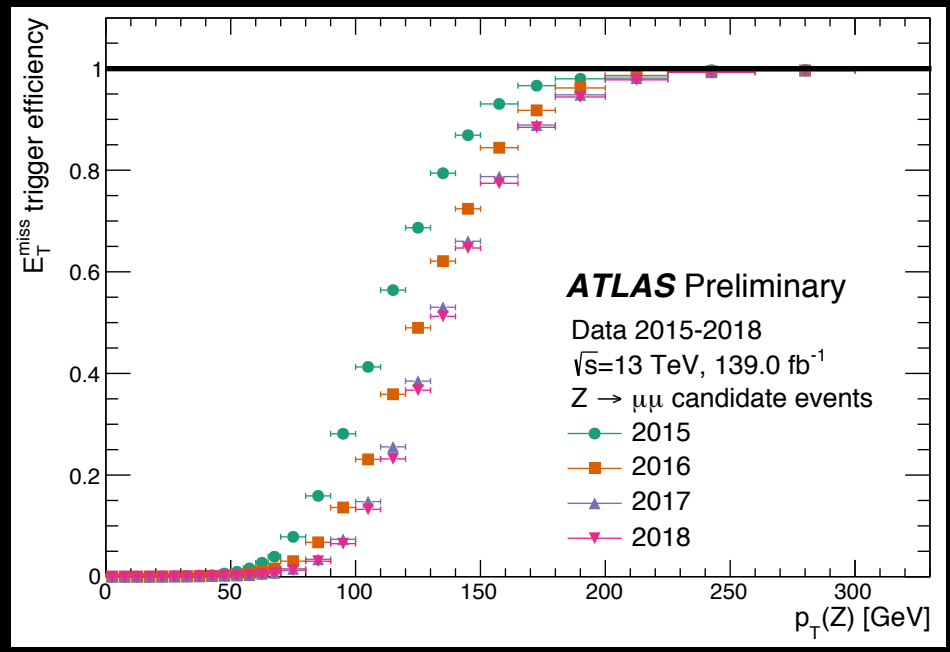

p_T of $Z_{\mu\mu}$

shifting

Increase in pileup ⟨μ⟩ → higher E_T^{miss} threshold

TM Hong
Pittsburgh

ATLAS trigger system (L1, HLT)

Trigger rates and efficiencies

L1 trigger rate vs. instantaneous luminosity (2018)

http://cern.ch/twiki/bin/view/AtlasPublic/TriggerOperationPublicResults

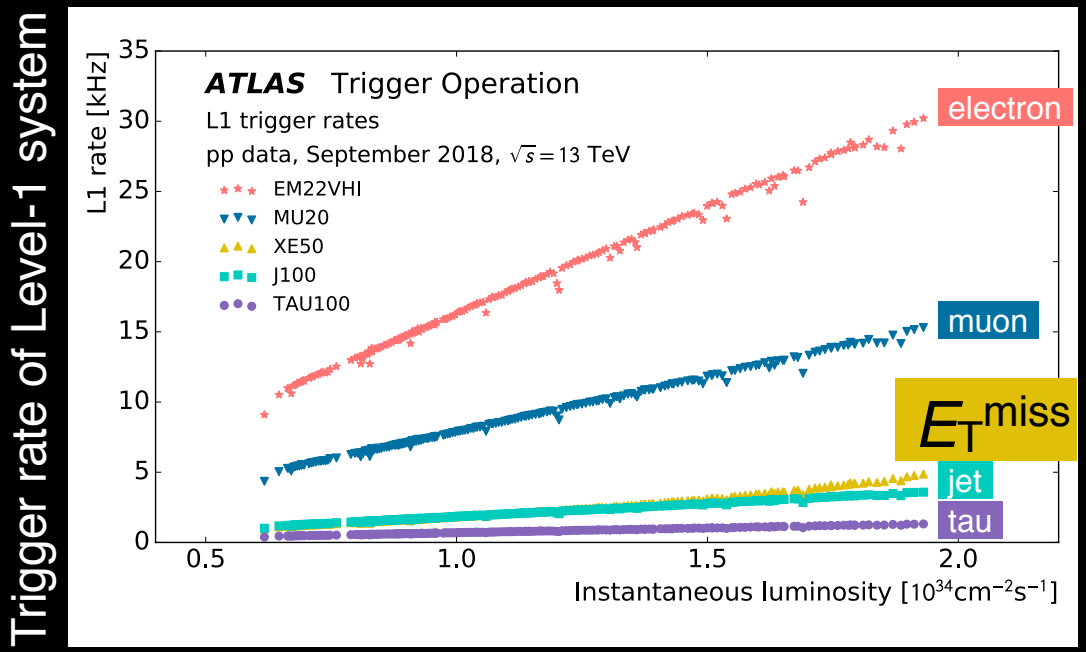

Instantaneous luminosity, proportional to pileup ⟨μ⟩

Mostly linear, few exponential

HLT E_T^{miss} trigger efficiency for each year

http://cern.ch/twiki/bin/view/AtlasPublic/MissingEtTriggerPublicResults

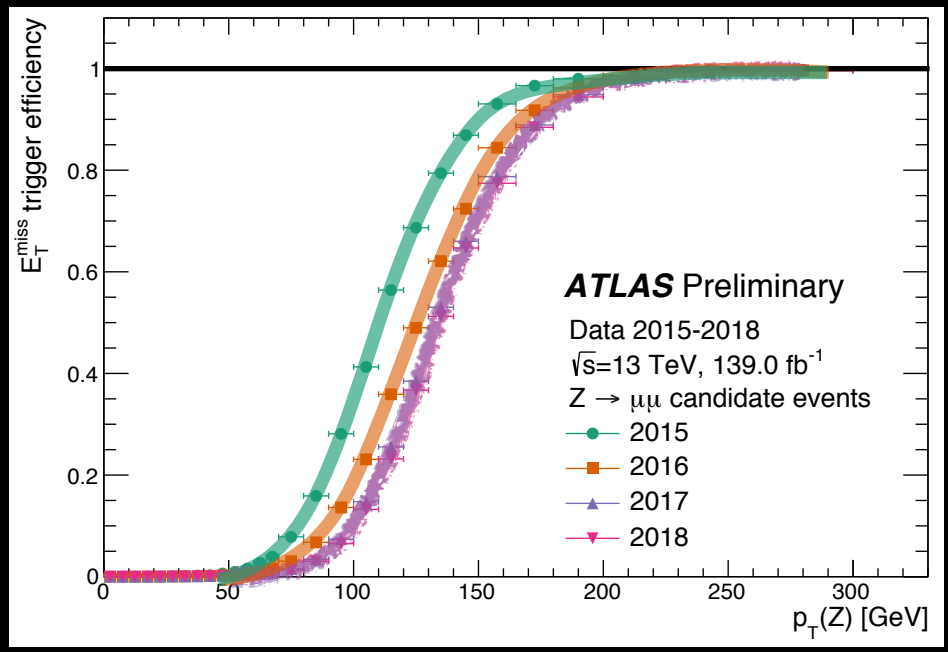

p_T of $Z_{\mu\mu}$

shifting

Increase in pileup ⟨μ⟩ → higher E_T^{miss} threshold

Mono-jet

Event display

Example signal models

axial-vec. mediator WIMP

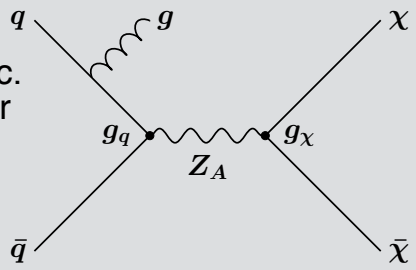

colored mediator WIMP

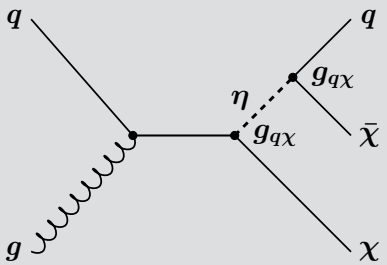

SUSY

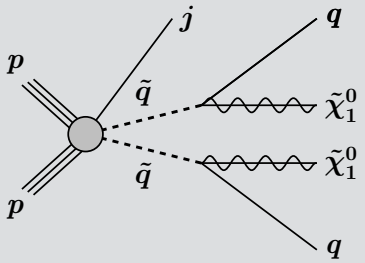

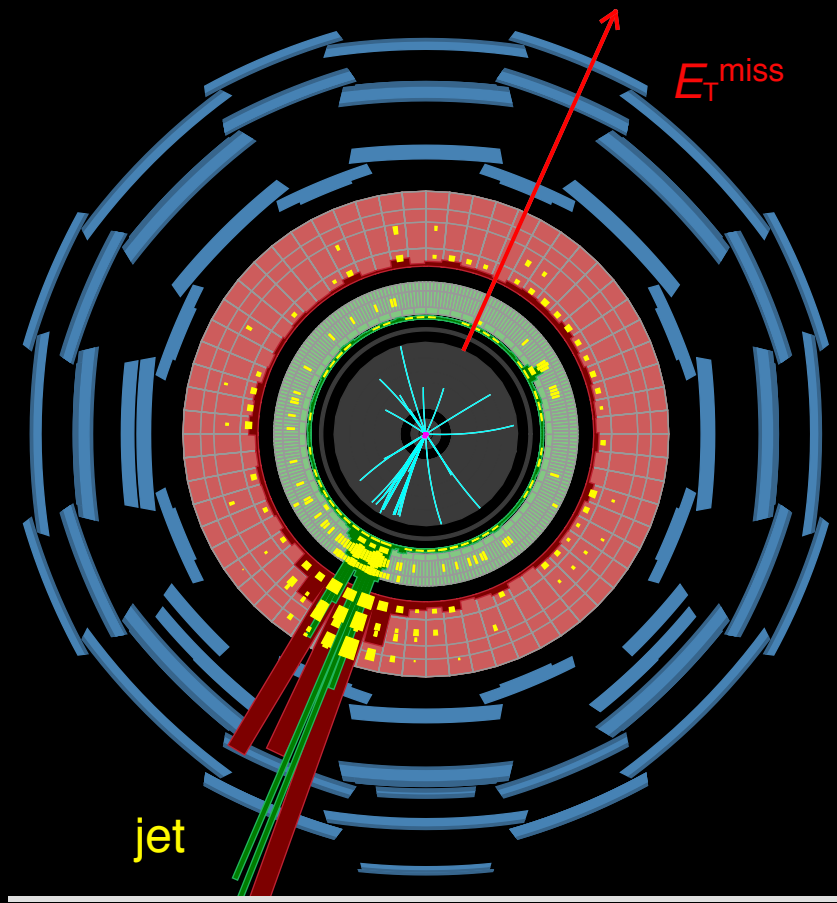

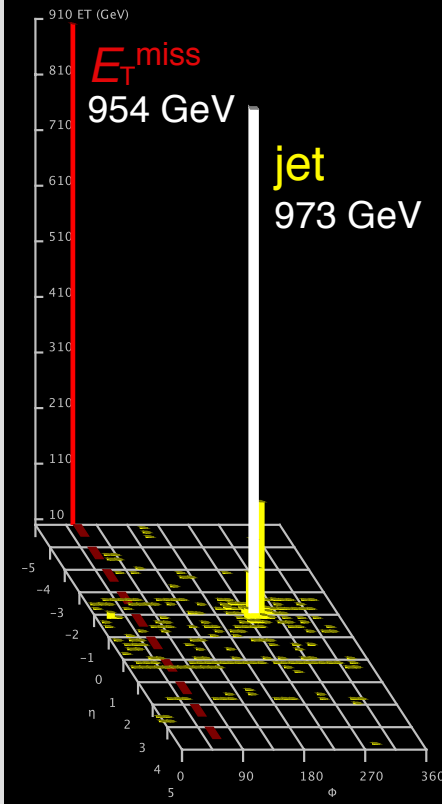

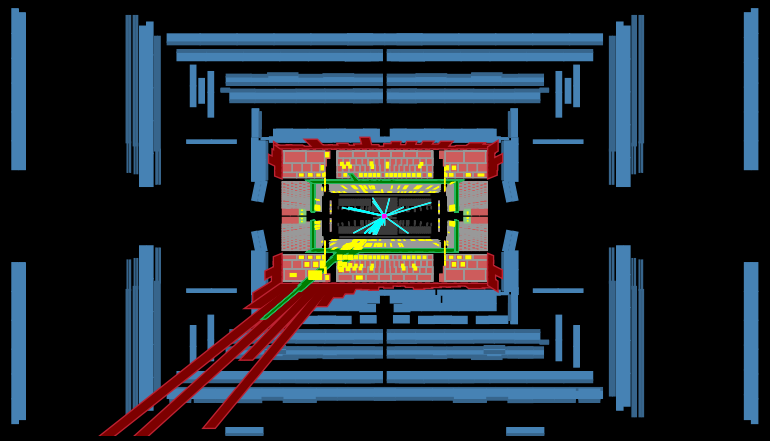

PRD 94 (2016) 032005

ATLAS EXPERIMENT

Run Number: 279284, Event Number: 606734214

Date: 2015-09-14 12:05:34 CEST

Many signal models, same signature

TM Hong

Pittsburgh

Mono-jet

Event display

Example signal models

axial-vec. mediator WIMP

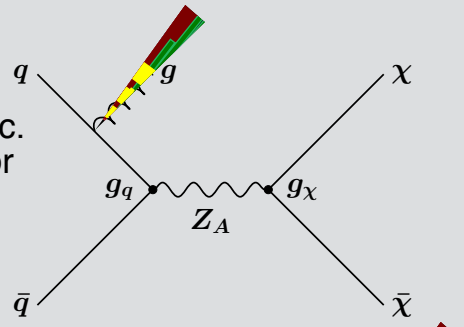

colored mediator WIMP

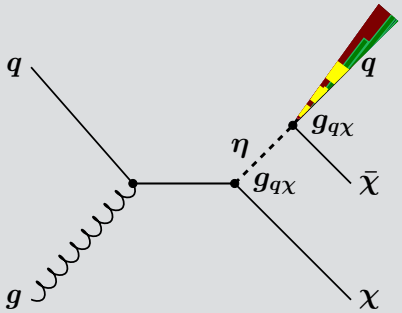

SUSY

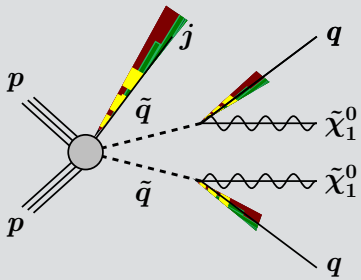

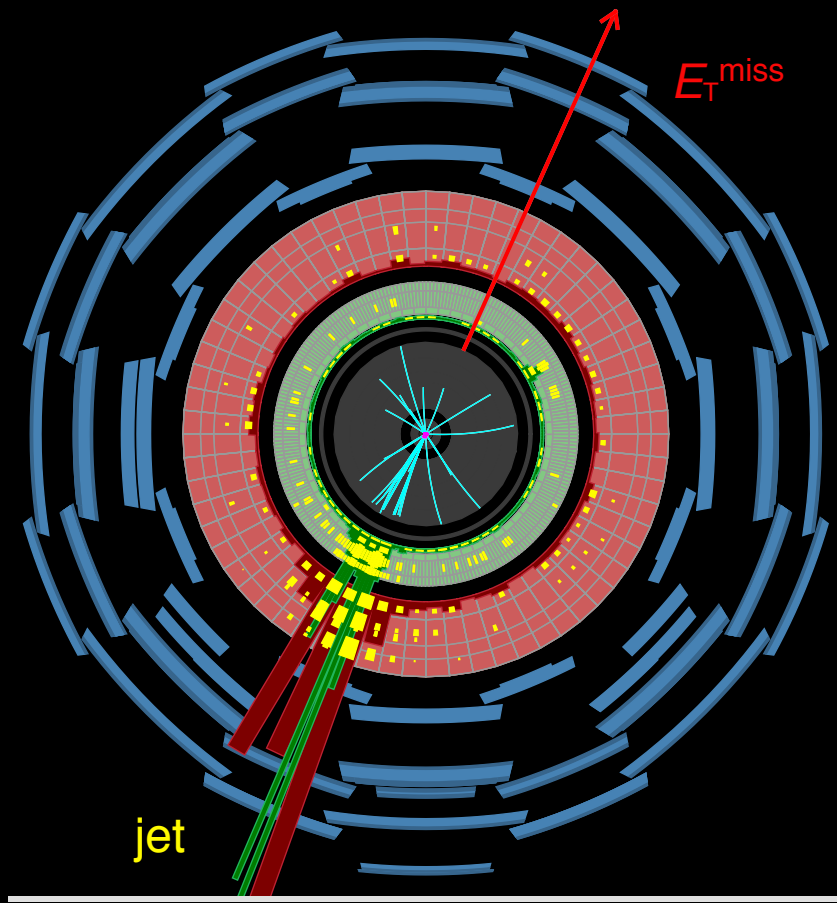

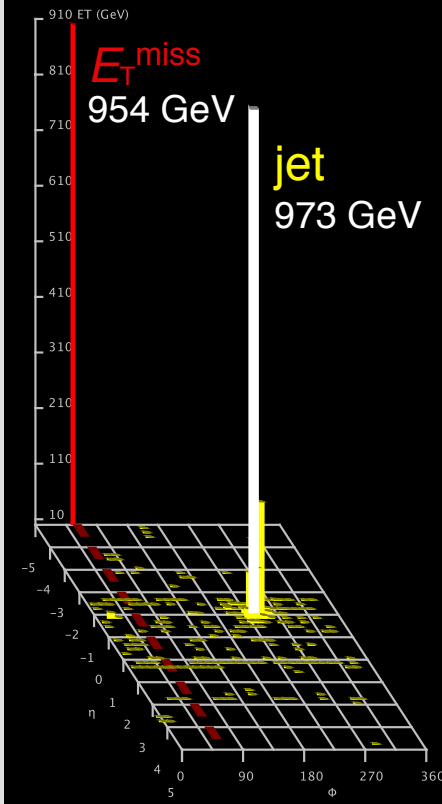

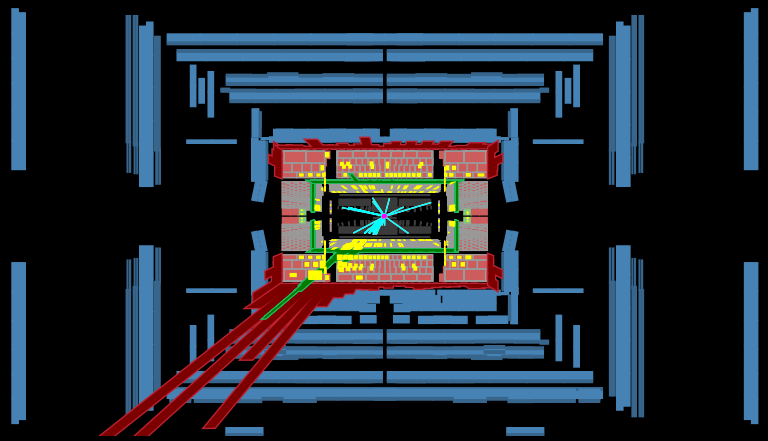

PRD 94 (2016) 032005

ATLAS EXPERIMENT

Run Number: 279284, Event Number: 606734214

Date: 2015-09-14 12:05:34 CEST

Many signal models, same signature

TM Hong

Pittsburgh

Mono-jet

JHEP 01 (2018) 126, 36 fb^{-1}

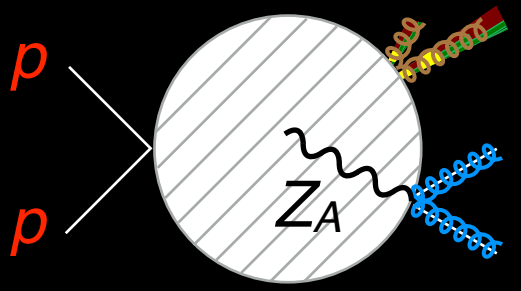

Looking at tail of E_T^{miss} distribution

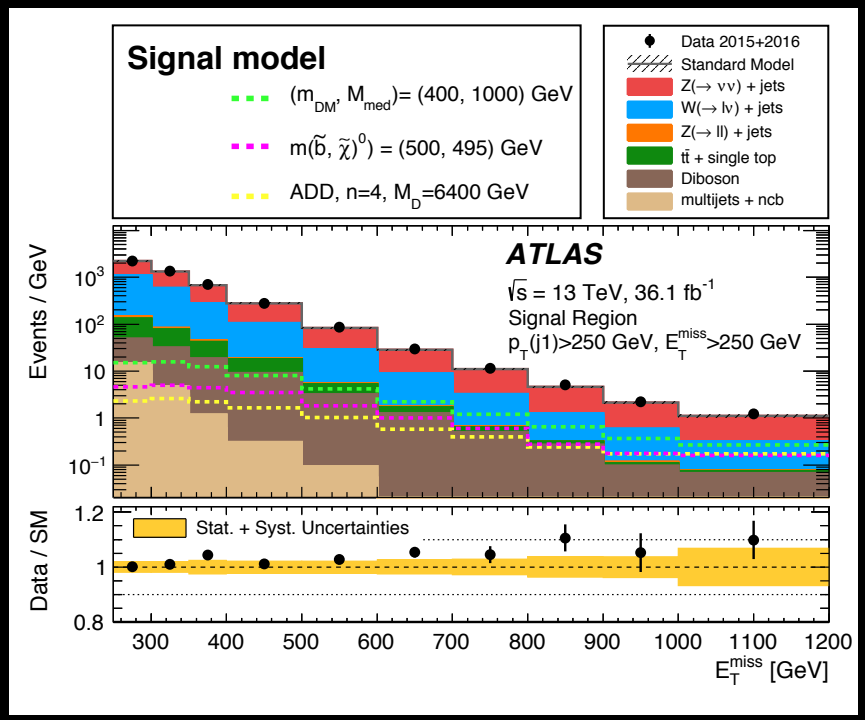

Ratio Distribution

E_T^{miss}

- Theory: p_T modeling of W, Z in collaboration with theorists 2-10% [EPJC 77 (2017) 829]
- Exp't: $W_{\ell\nu}$, $Z_{\ell\ell}$ control samples to normalize MC

DM mediator interpretation

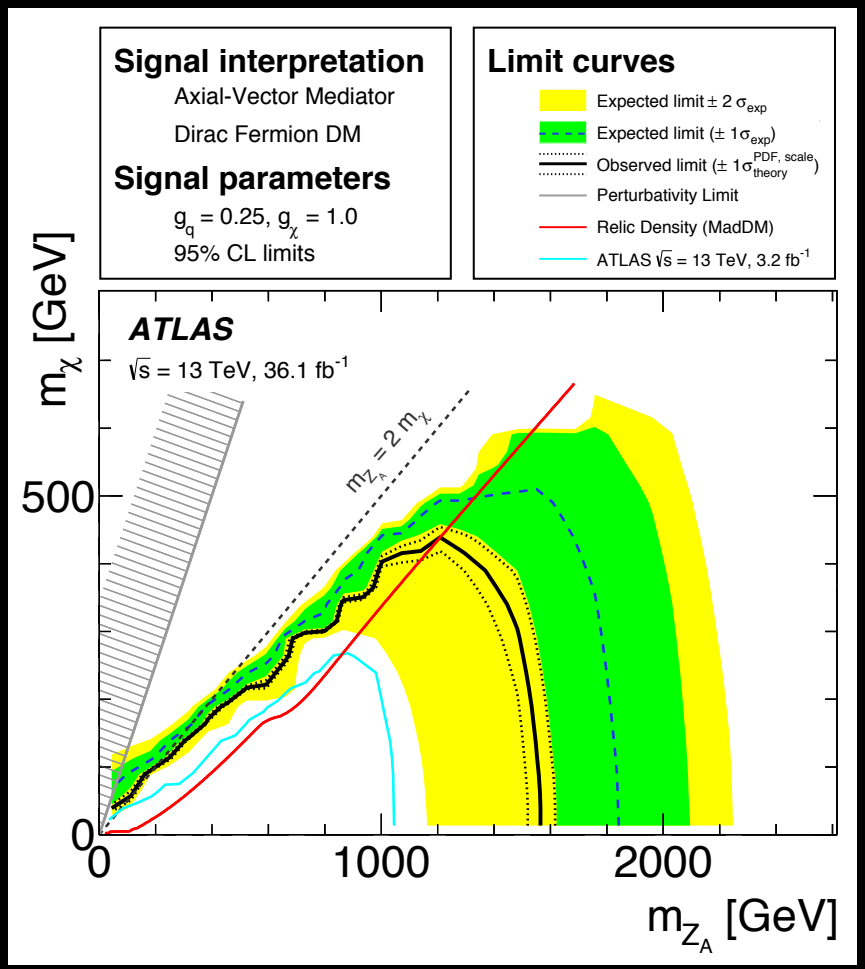

m_{DM}

$m_{mediator}$

Exclude 0 - 0.5 TeV DM for 0 - 1.5 TeV mediator

TM Hong
Pittsburgh

Mono-jet

JHEP 01 (2018) 126, 36 fb^{-1}

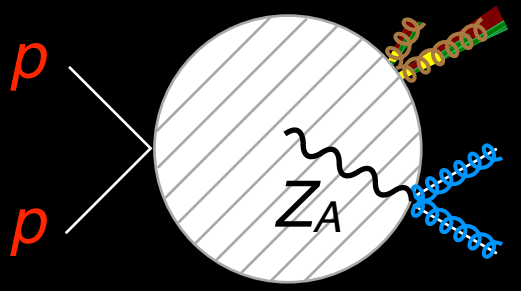

Looking at tail of E_T^{miss} distribution

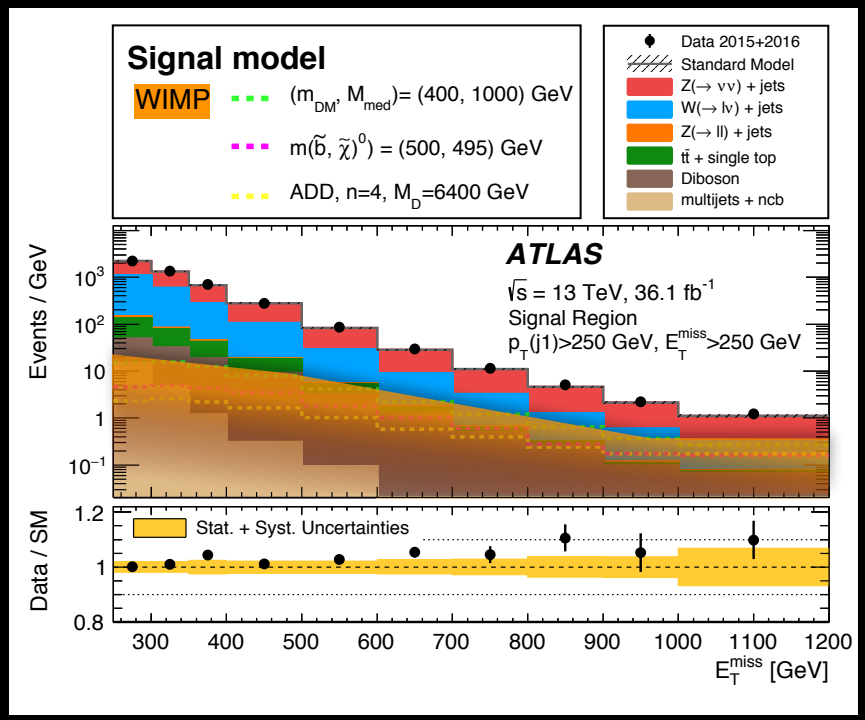

Ratio Distribution

E_T^{miss}

- Theory: p_T modeling of W, Z in collaboration with theorists 2-10% [EPJC 77 (2017) 829]
- Exp't: $W_{\ell\nu}$, $Z_{\ell\ell}$ control samples to normalize MC

DM mediator interpretation

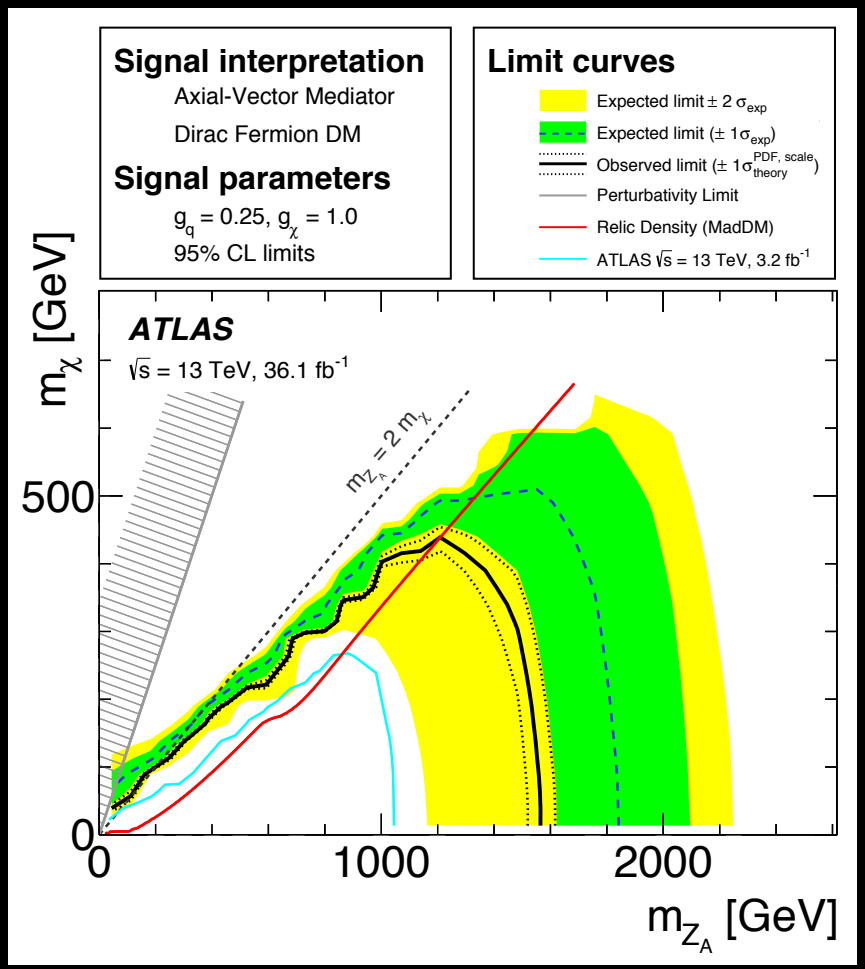

m_{DM}

$m_{mediator}$

Exclude 0 - 0.5 TeV DM for 0 - 1.5 TeV mediator

TM Hong
Pittsburgh

Mono-jet

JHEP 01 (2018) 126, 36 fb^{-1}

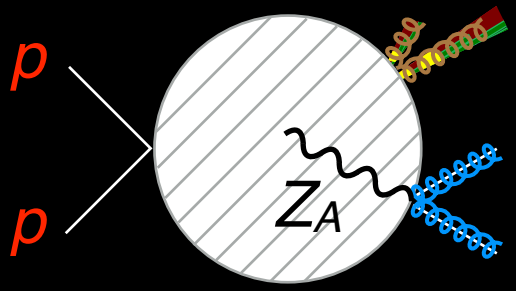

Looking at tail of E_T^{miss} distribution

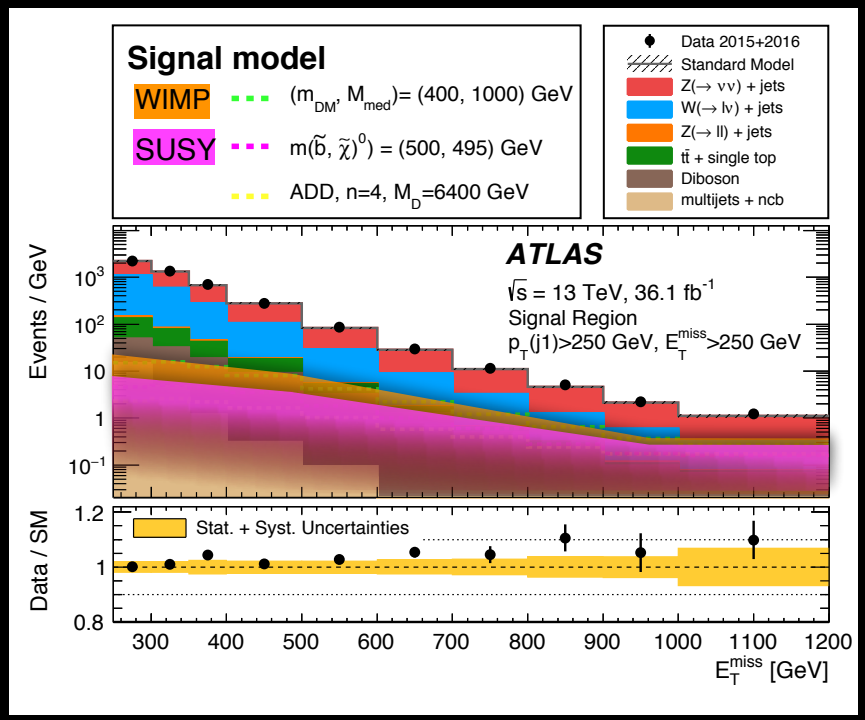

E_T^{miss}

- Theory: p_T modeling of W, Z in collaboration with theorists 2-10% [EPJC 77 (2017) 829]
- Exp't: $W_{\ell\nu}$, $Z_{\ell\ell}$ control samples to normalize MC

DM mediator interpretation

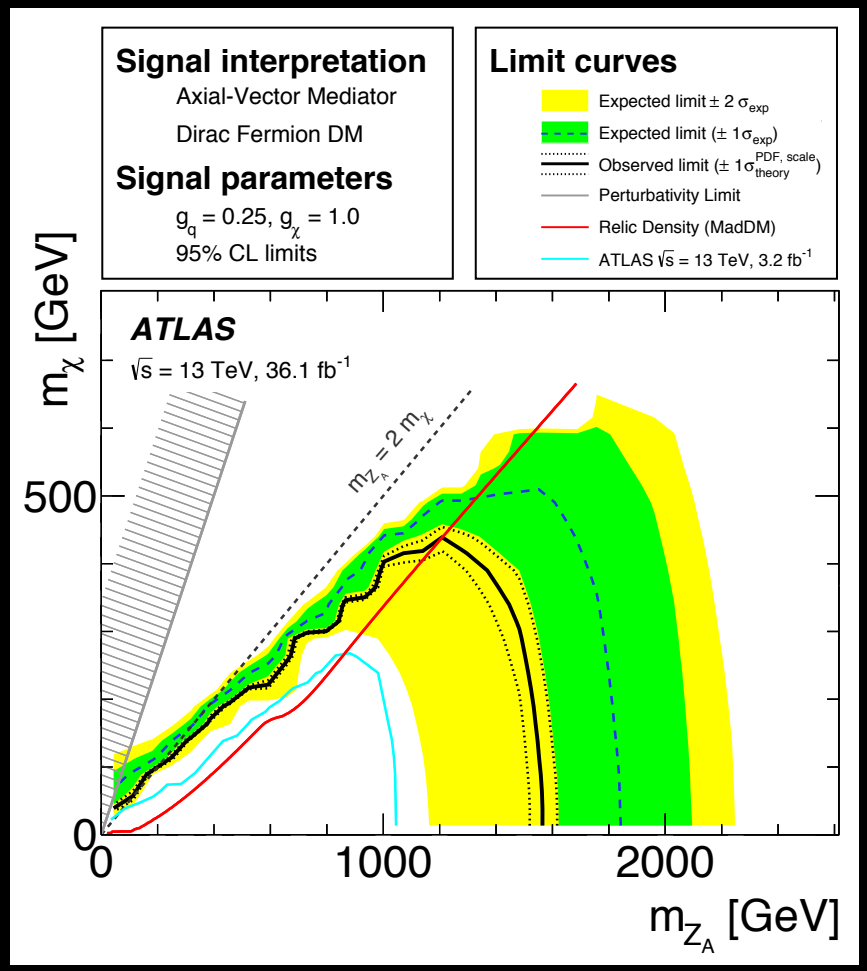

Exclude 0 - 0.5 TeV DM for 0 - 1.5 TeV mediator

TM Hong
Pittsburgh

Mono-jet

JHEP 01 (2018) 126, 36 fb^{-1}

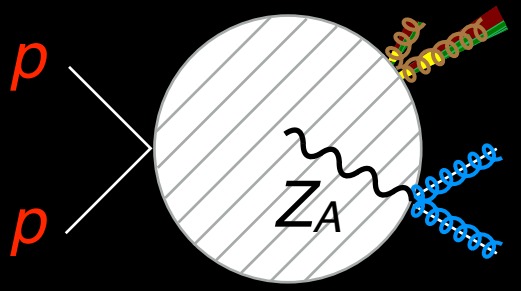

Looking at tail of E_T^{miss} distribution

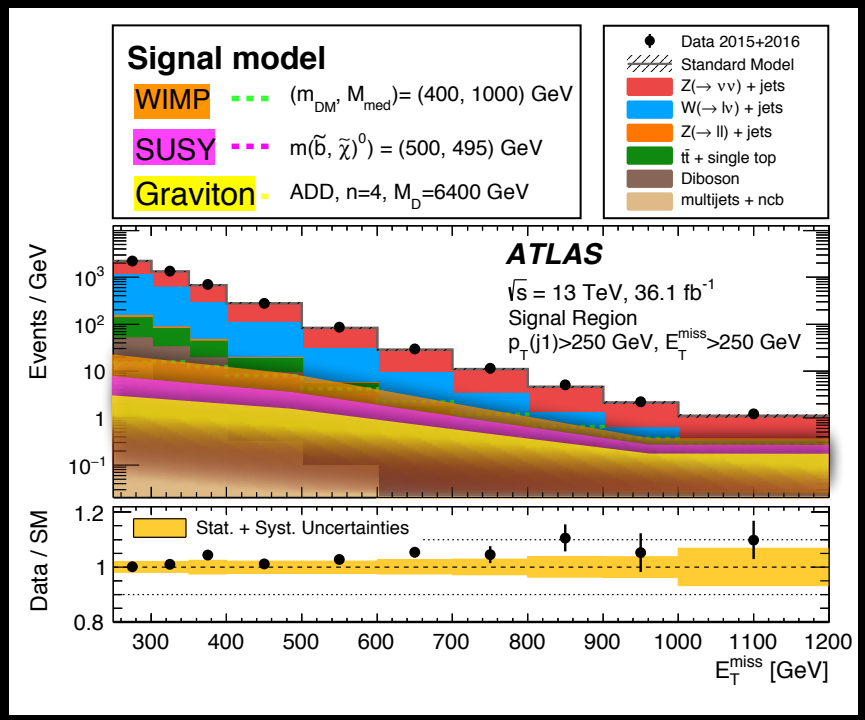

Ratio Distribution

E_T^{miss}

- Theory: p_T modeling of W, Z in collaboration with theorists 2-10% [EPJC 77 (2017) 829]
- Exp't: $W_{\ell\nu}$, $Z_{\ell\ell}$ control samples to normalize MC

DM mediator interpretation

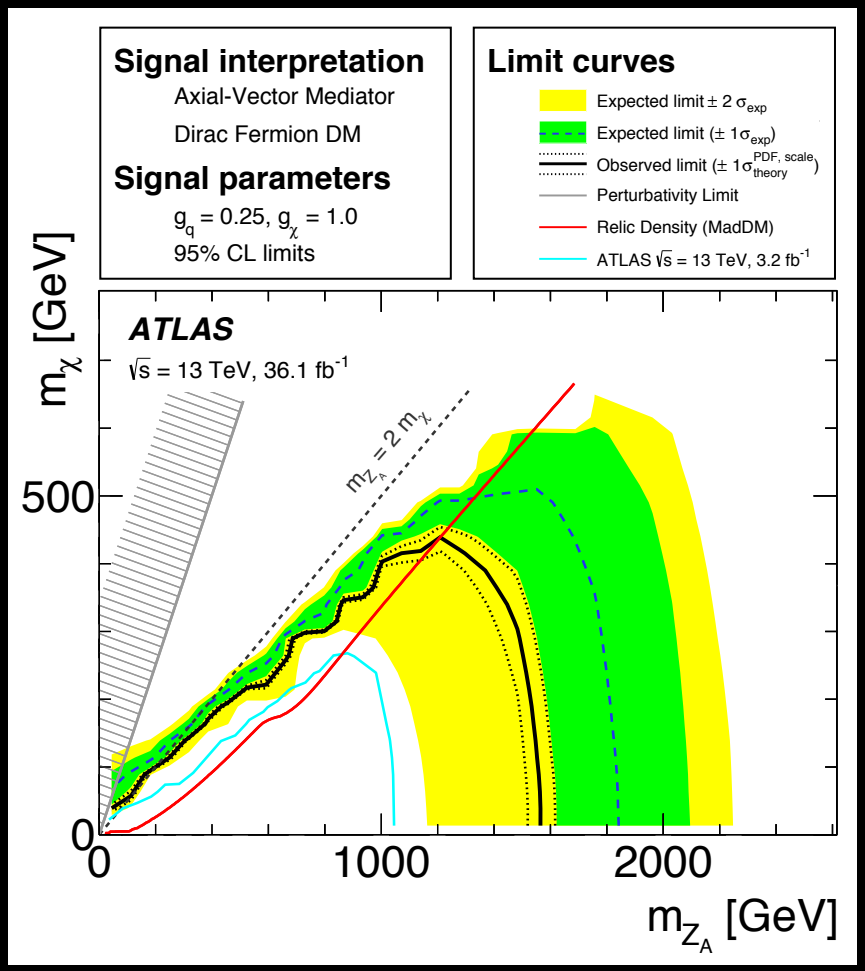

m_{DM}

$m_{mediator}$

Exclude 0 - 0.5 TeV DM for 0 - 1.5 TeV mediator

TM Hong
Pittsburgh

Mono-jet

JHEP 01 (2018) 126, 36 fb^{-1}

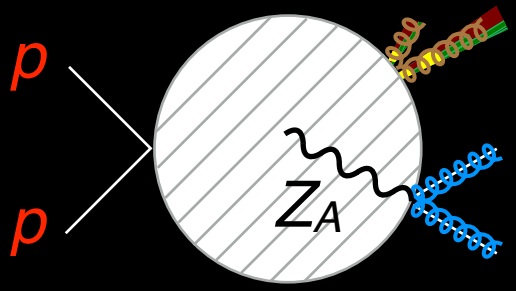

Looking at tail of E_T^{miss} distribution

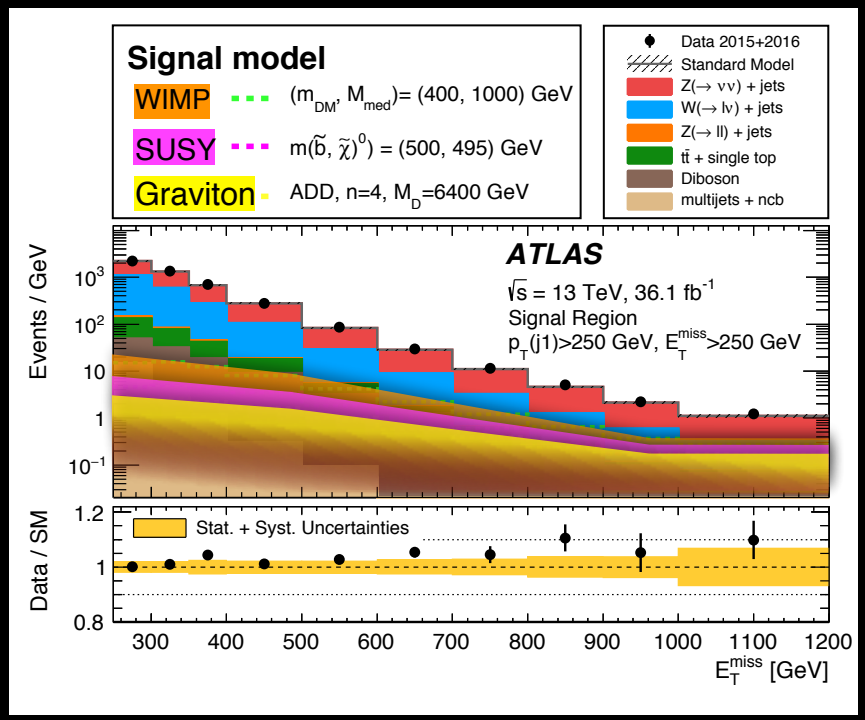

- Theory: p_T modeling of W, Z in collaboration with theorists 2-10% [EPJC 77 (2017) 829]
- Exp't: $W_{\ell\nu}$, $Z_{\ell\ell}$ control samples to normalize MC

DM mediator interpretation

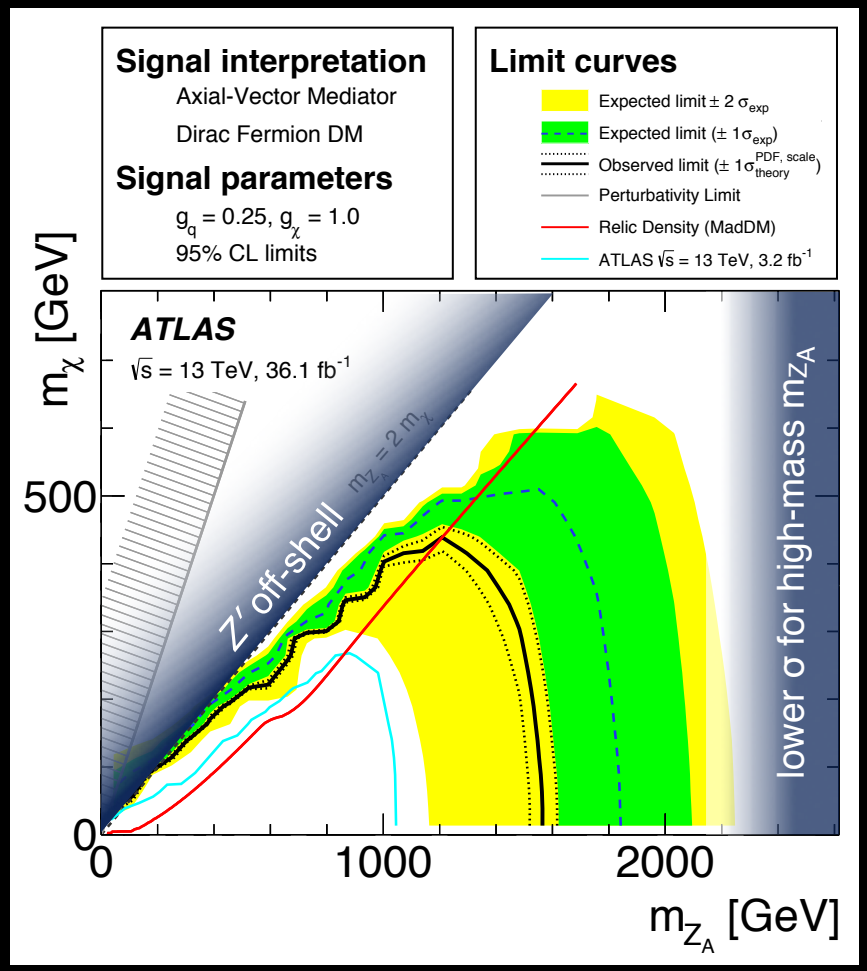

Exclude 0 - 0.5 TeV DM for 0 - 1.5 TeV mediator

Mono-jet

JHEP 01 (2018) 126, 36 fb^{-1}

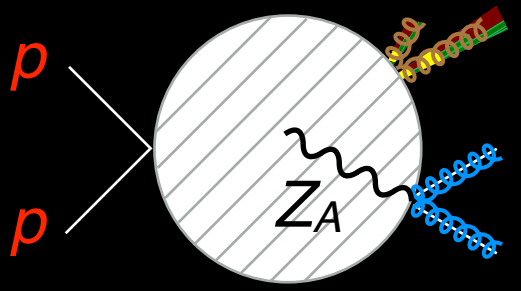

Looking at tail of E_T^{miss} distribution

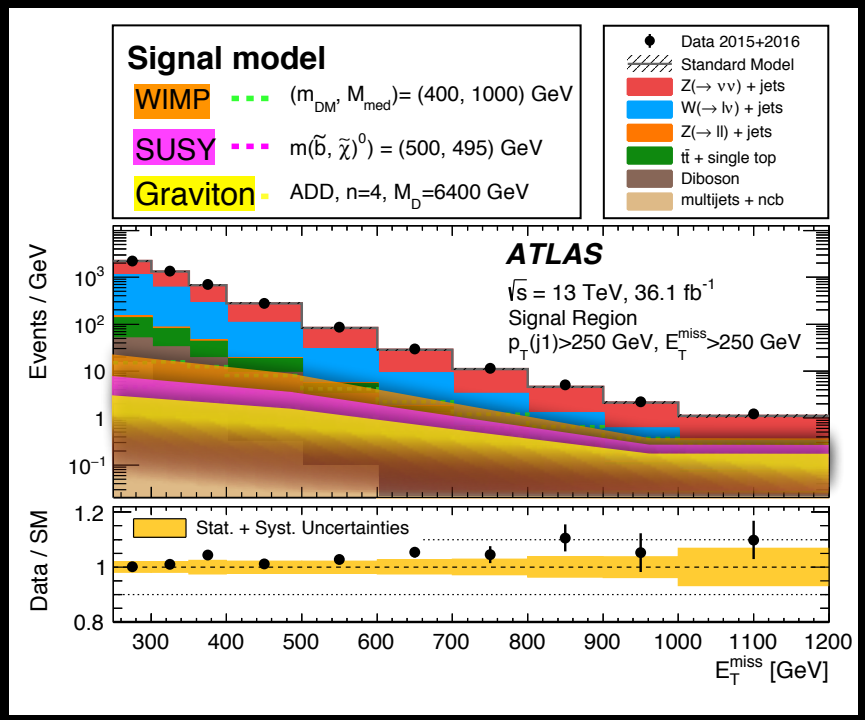

- Theory: p_T modeling of W, Z in collaboration with theorists 2-10% [EPJC 77 (2017) 829]
- Exp't: $W_{\ell\nu}$, $Z_{\ell\ell}$ control samples to normalize MC

DM mediator interpretation

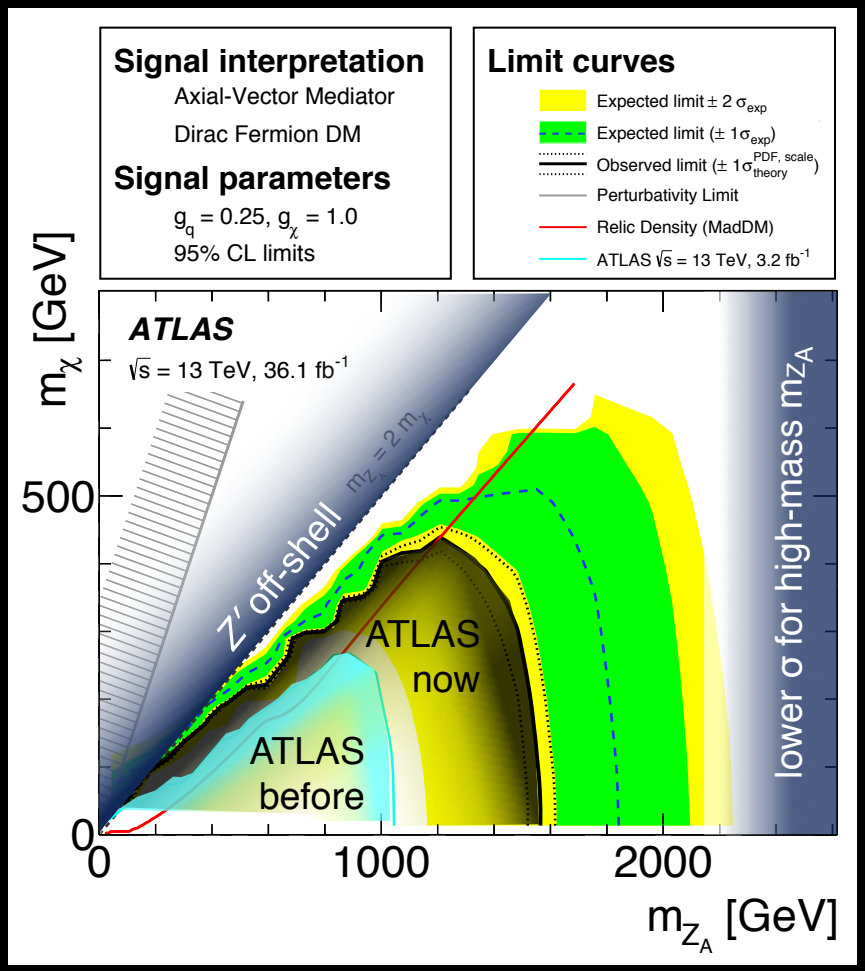

Exclude 0 - 0.5 TeV DM for 0 - 1.5 TeV mediator

Mono-Higgs, $H_{b\bar{b}}$

ATLAS-CONF-2018-039, 80fb^{-1}

- Tool: Boosted, variable-radius, track jets
- Exp't: Peak in $m_{\text{fat-jet}}$ & excess in E_T^{miss} (bins)
- Theory: *H* from ISR is Yukawa suppressed, so signal is BSM

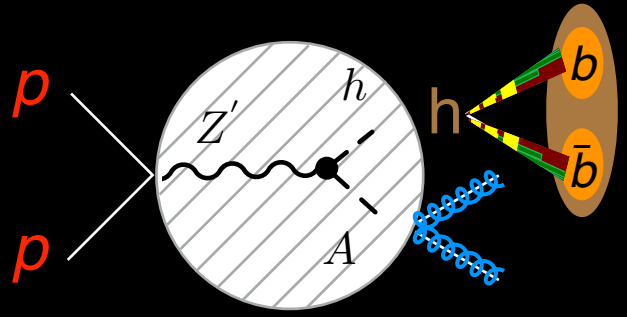

Large-R jet
- ΔR = 1.0
- p_T > 200 GeV

Track jet
- ΔR is p_T-dep.
- p_T^{trk} > 0.5 GeV

Scan of invariant mass

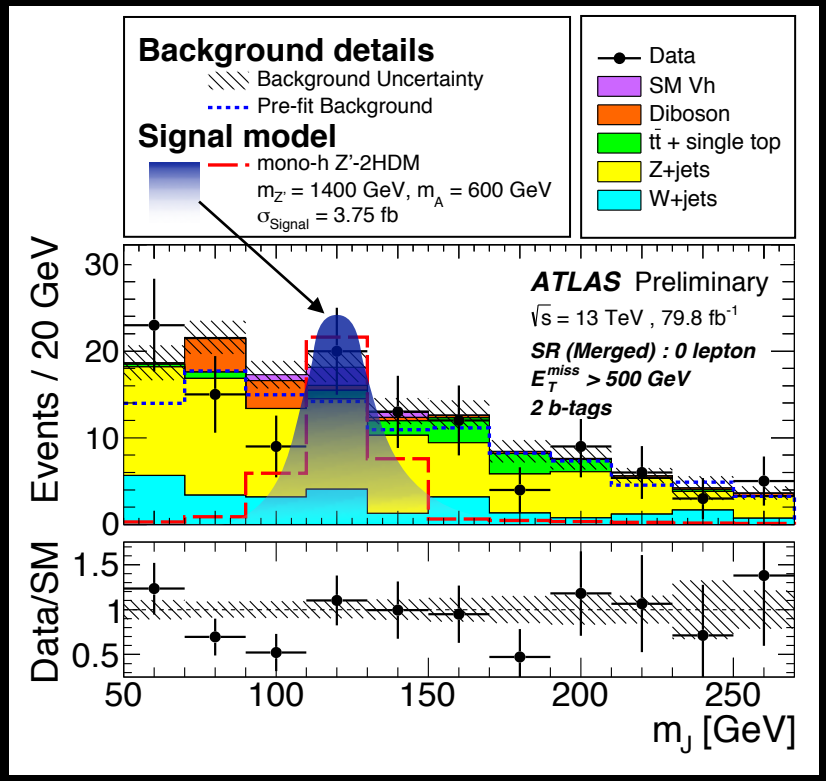

$m_{\text{fat-jet}}$

DM mediator interpretation

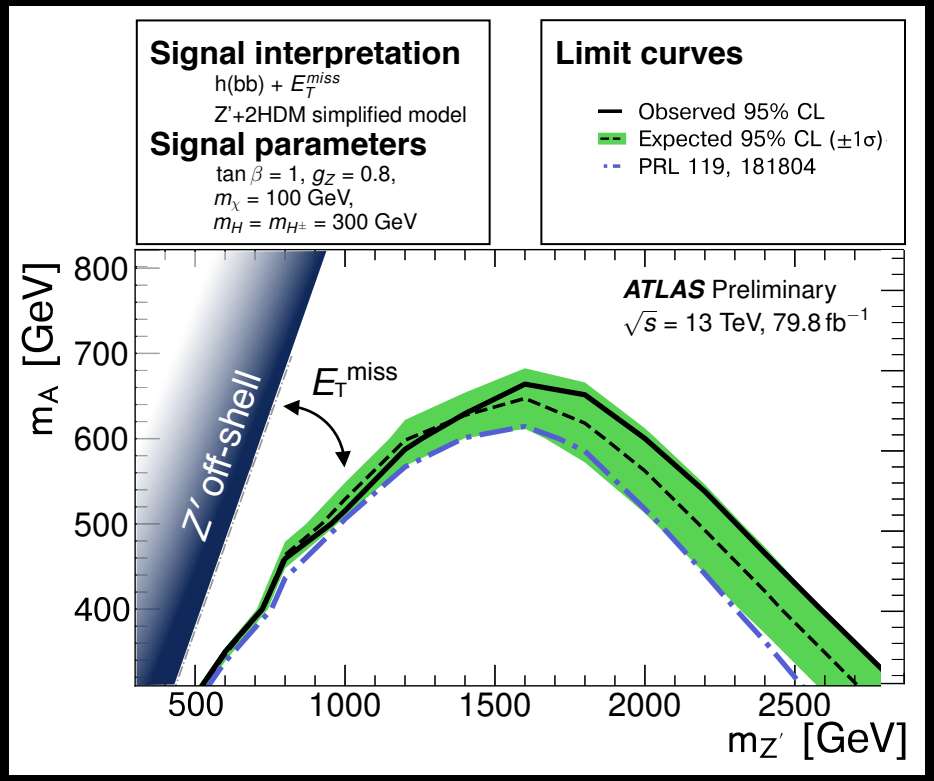

$m_{\text{mediator-}A}$

$m_{\text{mediator-}Z'}$

TM Hong
Pittsburgh

Tool: Track-jet technology for fat-jets

High-mass di-jet

ATLAS-CONF-2019-007, 139 fb^{-1}

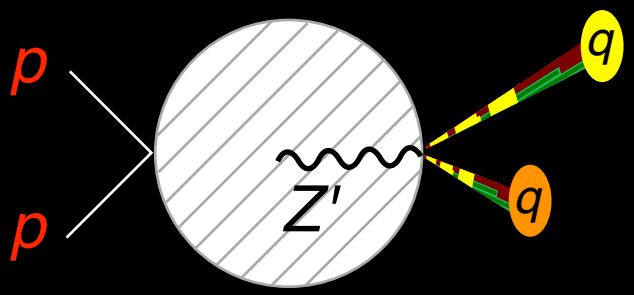

Trigger jet
- p_T > 420 GeV

Subleading jet
- p_T > 150 GeV

Scan of invariant mass

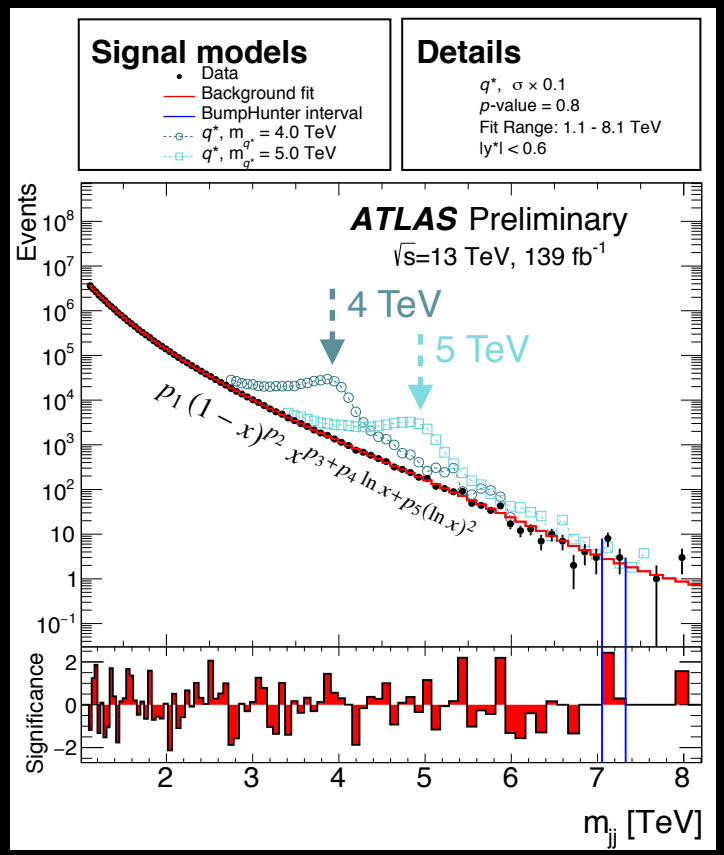

$m_{\text{di-jet}}$

Excited quark interpretation

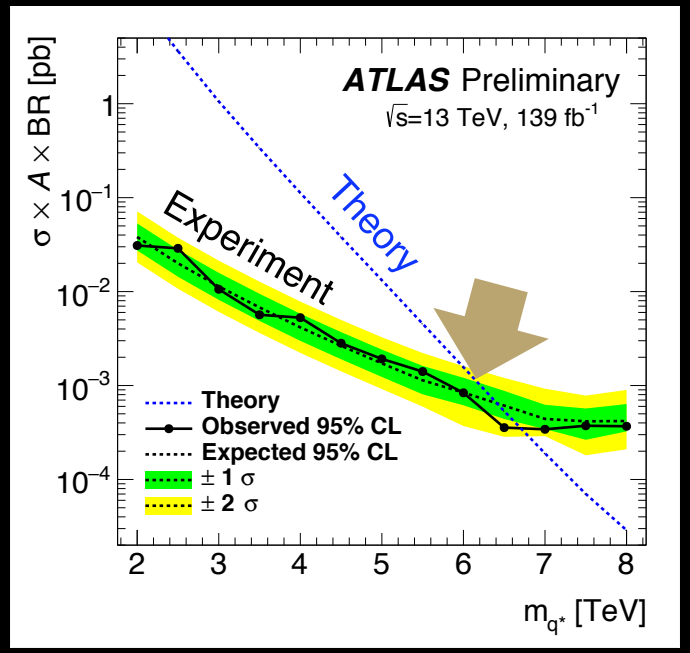

$m_{\text{excited-quark}}$

- Exp't: JES ~ 1-3%, $m_{\text{di-jet}}$ resolution ~ 3%
- Tool: Use lowest threshold single-jet trigger

TM Hong
Pittsburgh

The "high" di-jet mass range is limited by trigger

Joke

Once you have a collider,

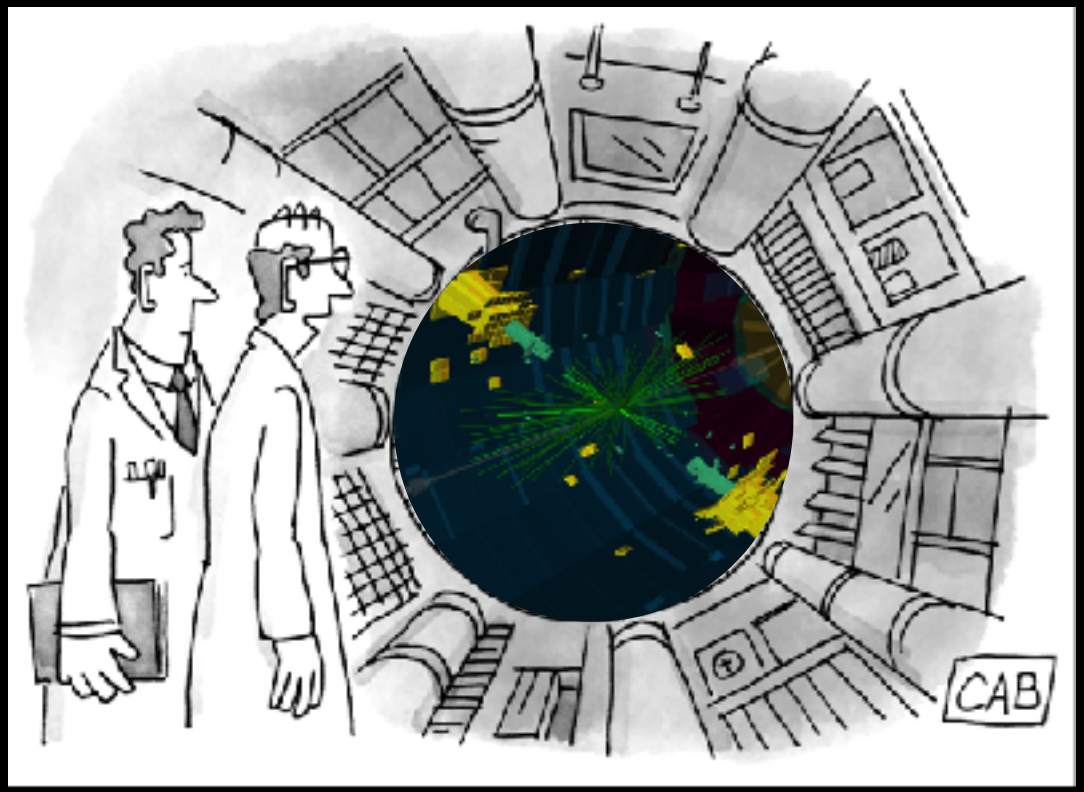

every problem starts to look like a particle.

Joke

Once you have a collider,

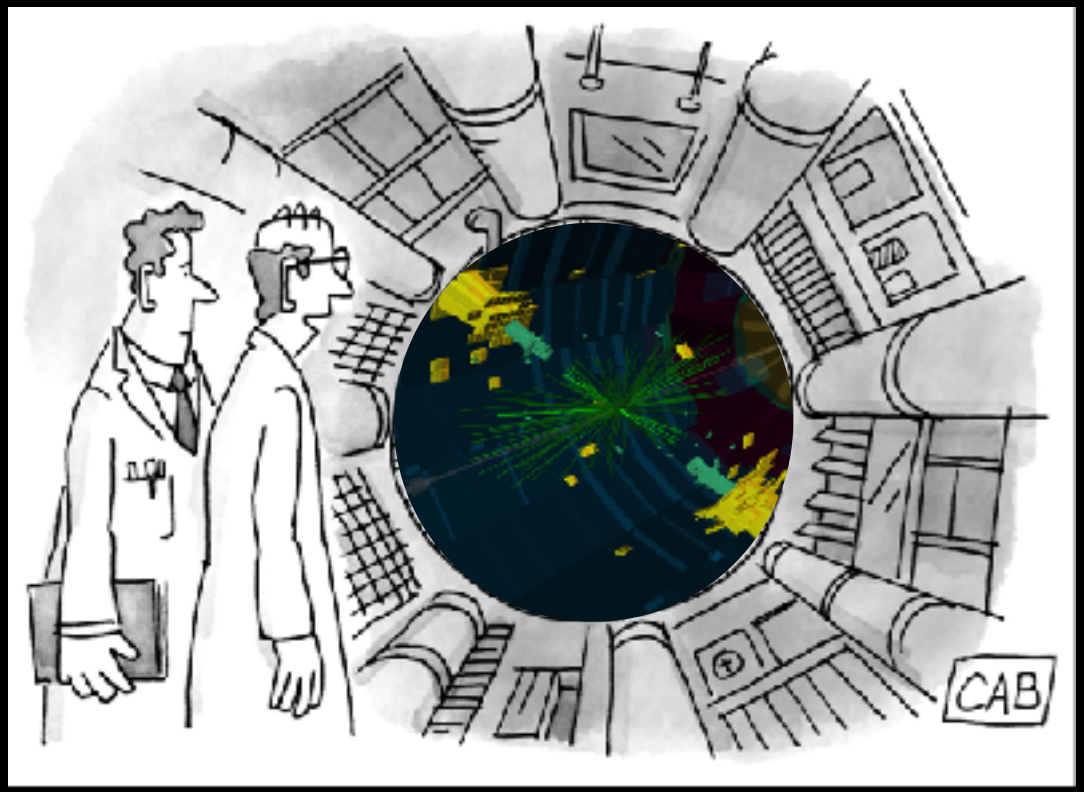

~~every problem~~ starts to look like a ~~particle~~.

your analysis dark matter mediator

Interpretation

JHEP 05 (2019) 142,
up to 36 fb^{-1}

- Di-fermion results exclude rectangular regions →
- Mono-X results exclude triangular region →

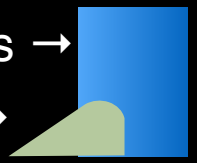

Cartoon

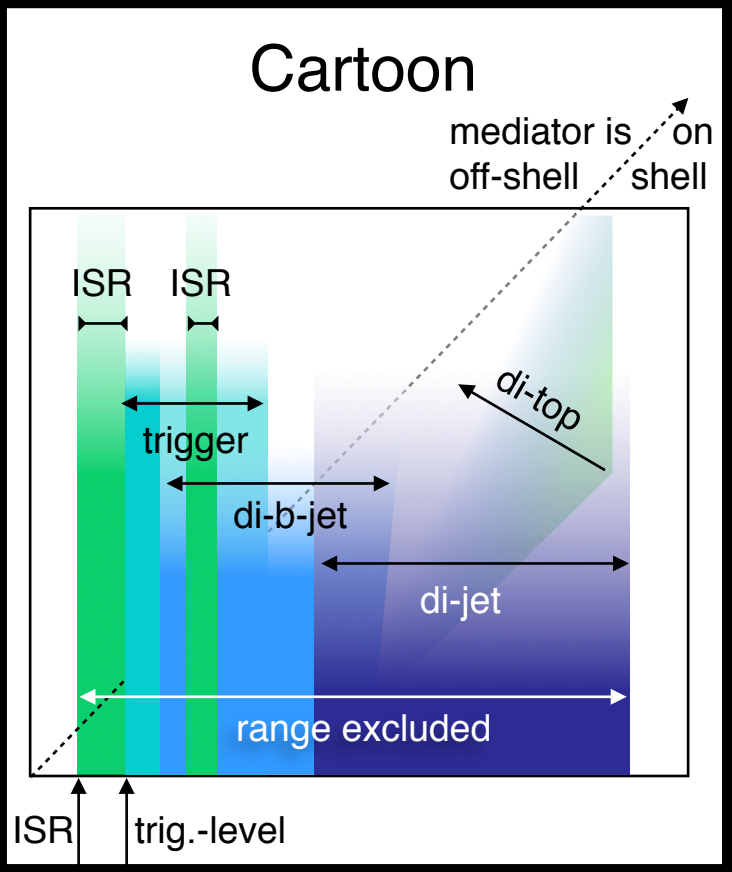

DM & DM mediator interpretation

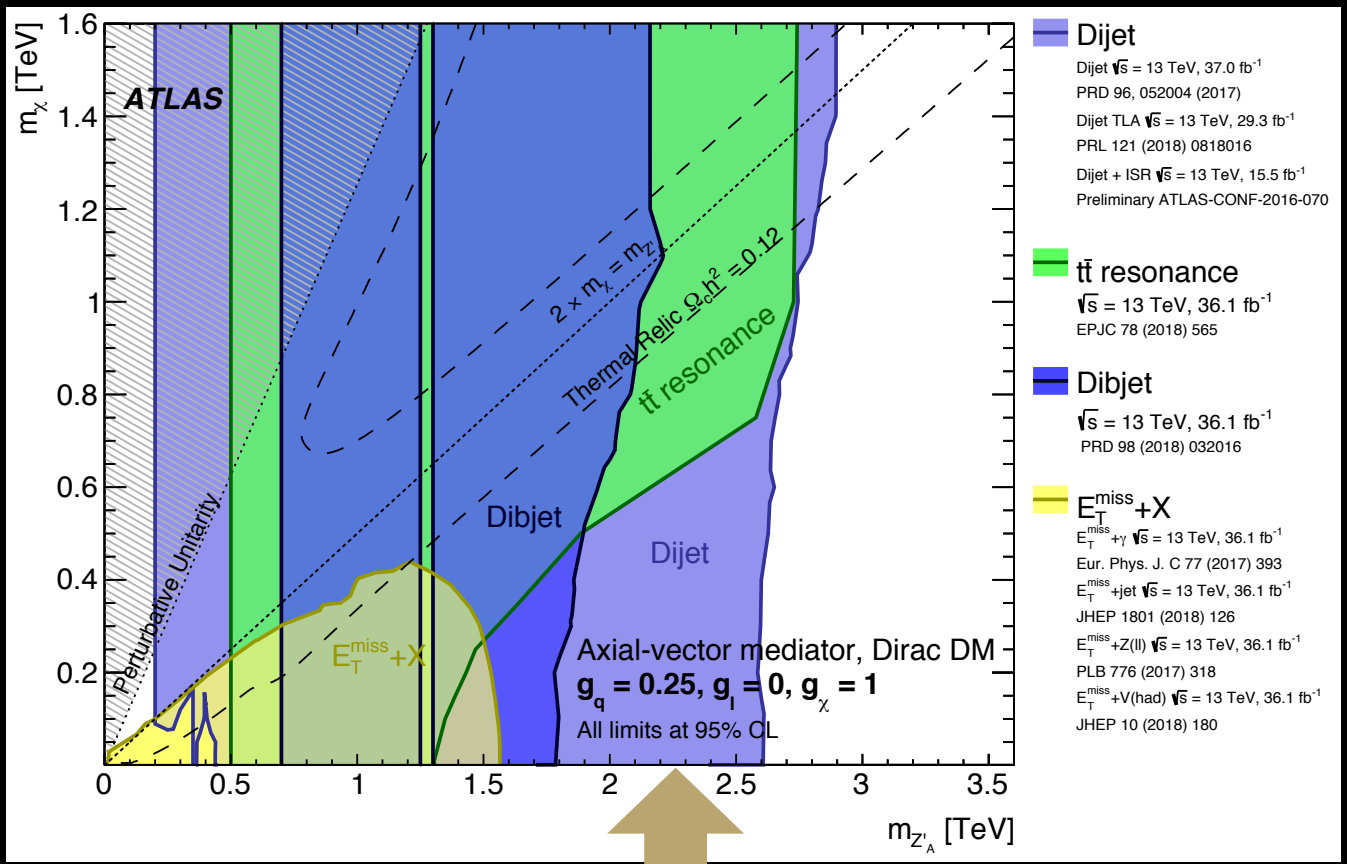

$m_{mediator}$

model assumptions

TM Hong
Pittsburgh

Rectangular exclusion because independent of m_{DM}

Low-mass di-jet

[1901.10917], ~80 fb^{-1}

Scan of invariant mass

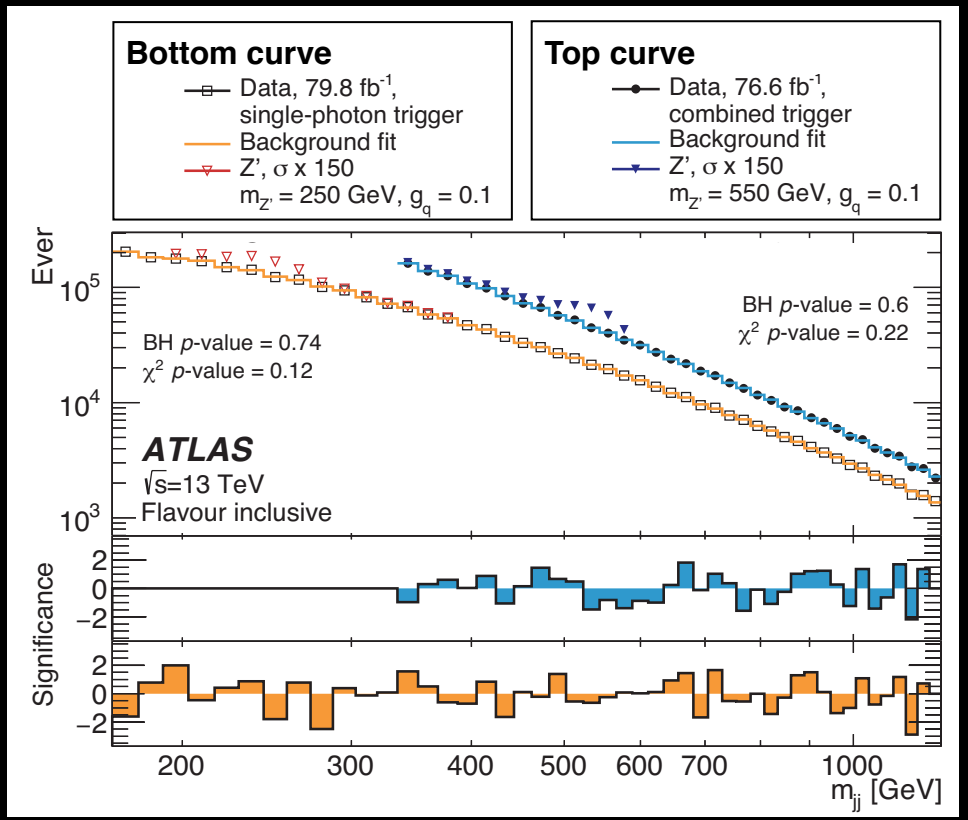

Distribution

Significance

$m_{di\text{-}jet}$

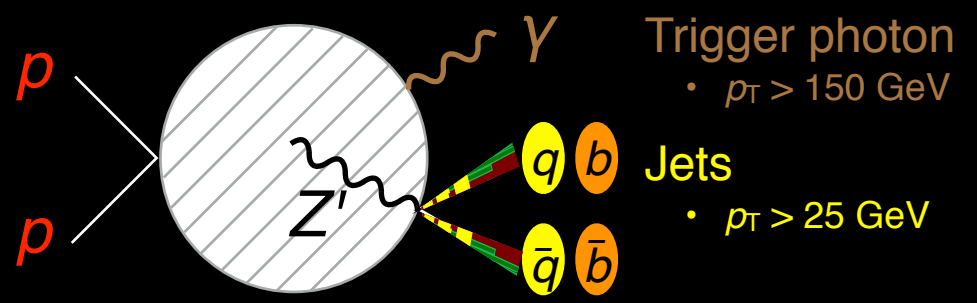

$q\bar{q}$ → mediator → $q\bar{q}$, so only 2 parameters

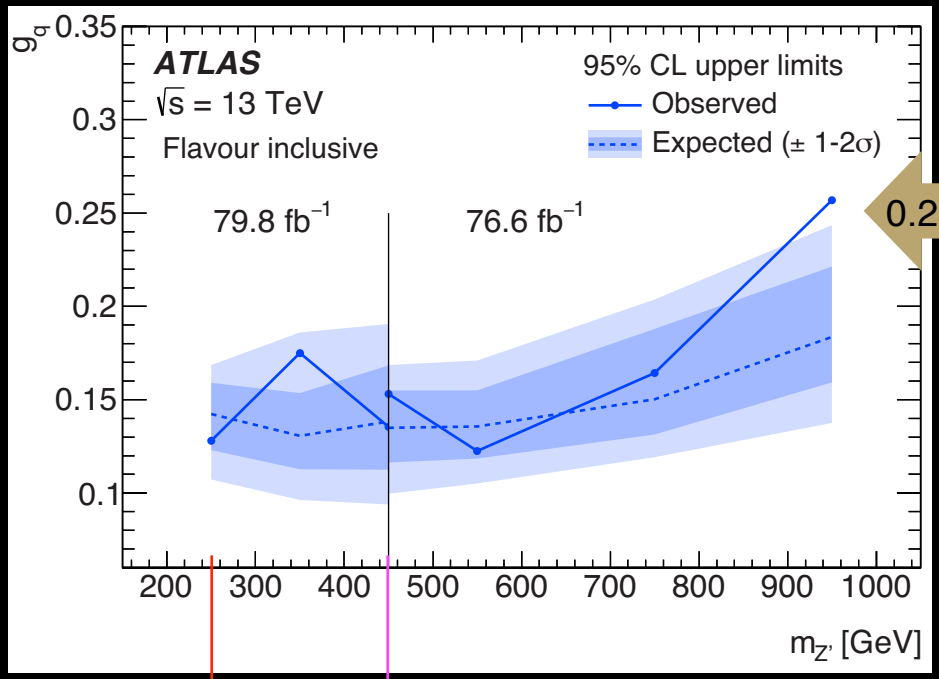

Mediator-quark coupling

$m_{mediator}$

- Tool: Add photon trigger to reach lower $m_{di\text{-}jet}$
- Exp't: Also analysis with two b-tag

photon + two jet trigger

lowest threshold single-photon trigger

Tool: Photon trigger to probe lower masses

Low-mass di-jet

[1901.10917], ~80 fb^{-1}

Scan of invariant mass

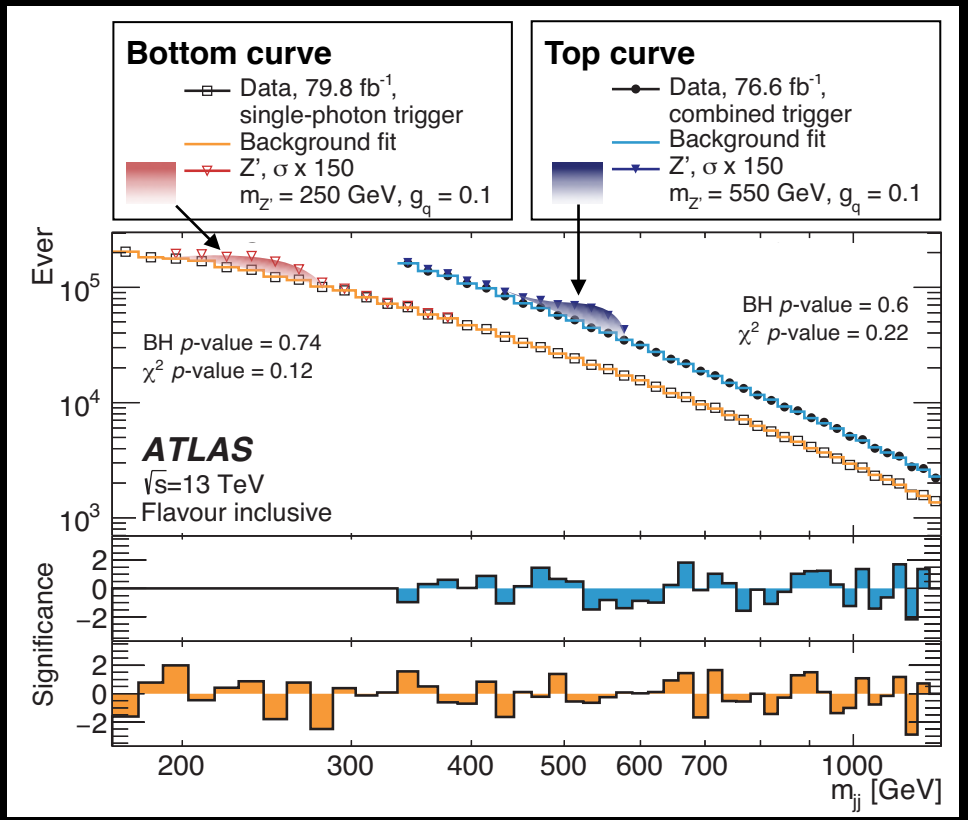

m$_{\text{di-jet}}$

- Tool: Add photon trigger to reach lower m$_{\text{di-jet}}$
- Exp't: Also analysis with two b-tag

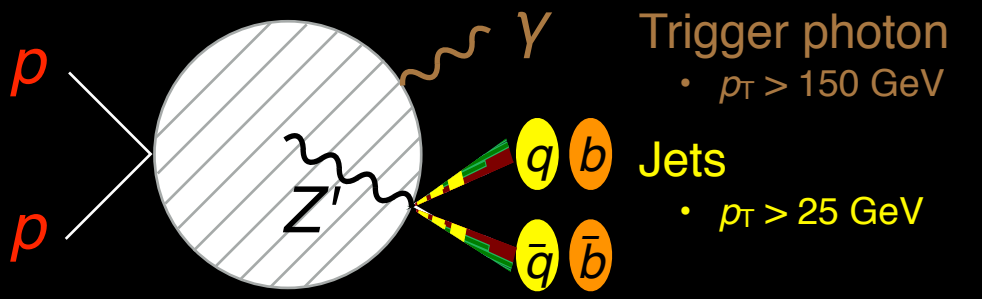

$q\bar{q}$ → mediator → $q\bar{q}$, so only 2 parameters

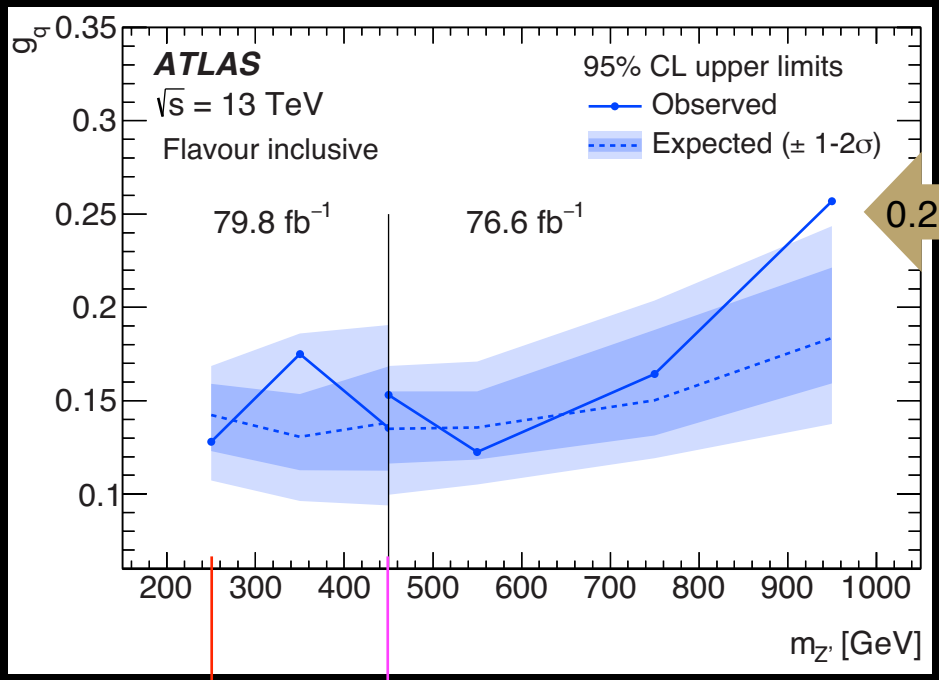

m$_{\text{mediator}}$

photon + two jet trigger

lowest threshold single-photon trigger

TM Hong
Pittsburgh

Tool: Photon trigger to probe lower masses

Boosted di-b-jet

ATLAS-CONF-2018-052, 81 fb^{-1}

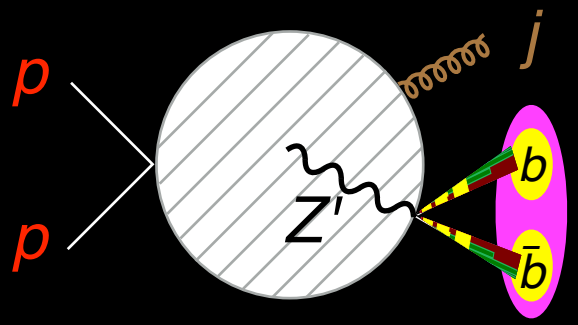

Large radius jet
- $\Delta R = 1.0$
- $p_T > 480$ GeV
- $2\, m_J / p_T > 1$

Track jet
- ΔR is p_T-dep.
- $p_T > 10$ GeV

- Tool: Boosted, variable-radius, track jets
- Exp't: 5σ peak for *W*, *Z* & hint of Higgs, top

Scan of invariant mass

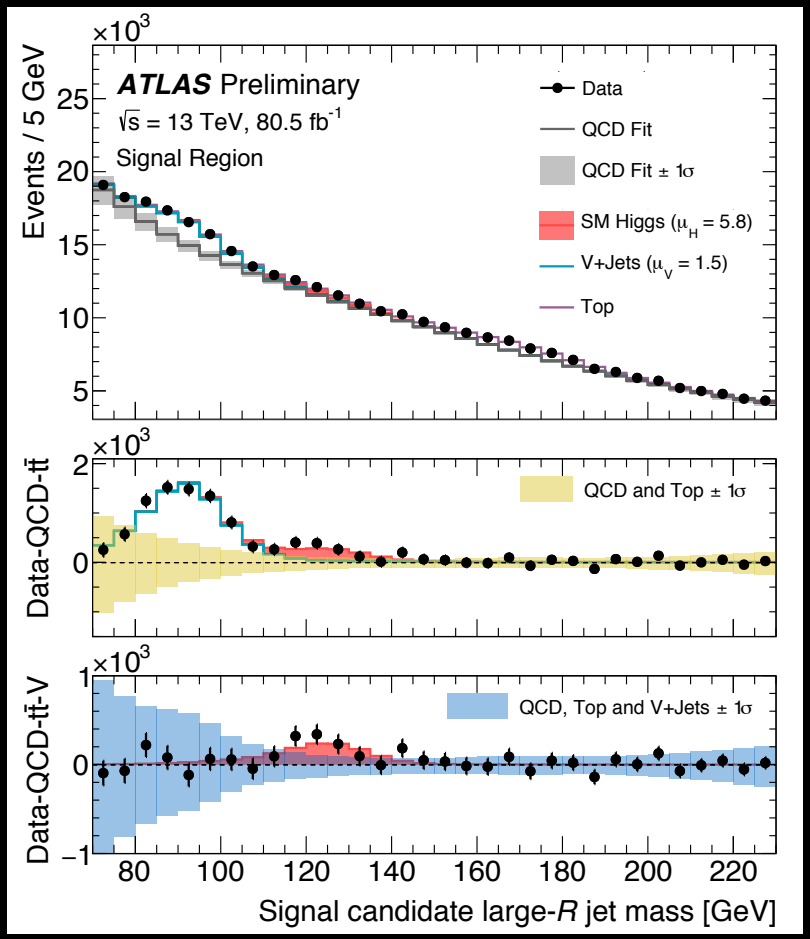

$q\bar{q} \rightarrow$ mediator $\rightarrow q\bar{q}$, so only 2 parameters

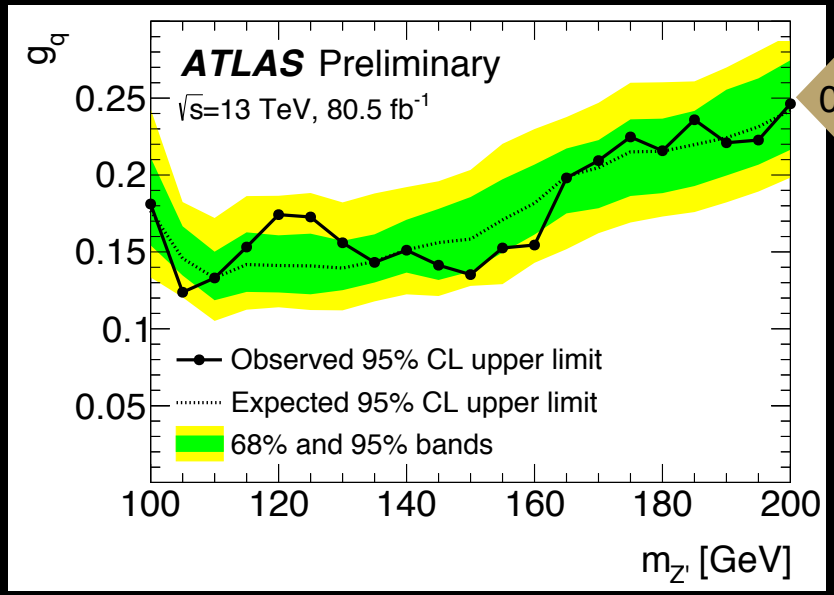

Tool: Track-jet technology for fat-jets (again!)

TM Hong
Pittsburgh

Boosted di-b-jet

ATLAS-CONF-2018-052, 81 fb^{-1}

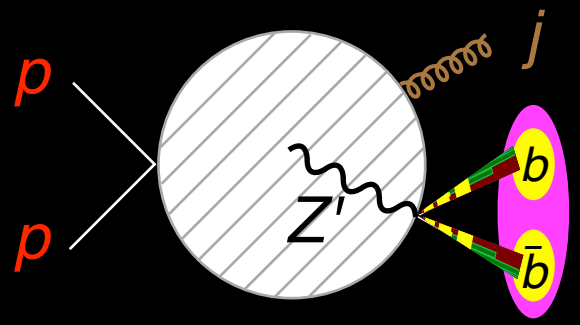

Large radius jet
- $\Delta R = 1.0$
- $p_T > 480$ GeV
- $2\ m_J / p_T > 1$

Track jet
- ΔR is p_T-dep.
- $p_T > 10$ GeV

- Tool: Boosted, variable-radius, track jets
- Exp't: 5σ peak for *W*, *Z* & hint of Higgs, top

Scan of invariant mass

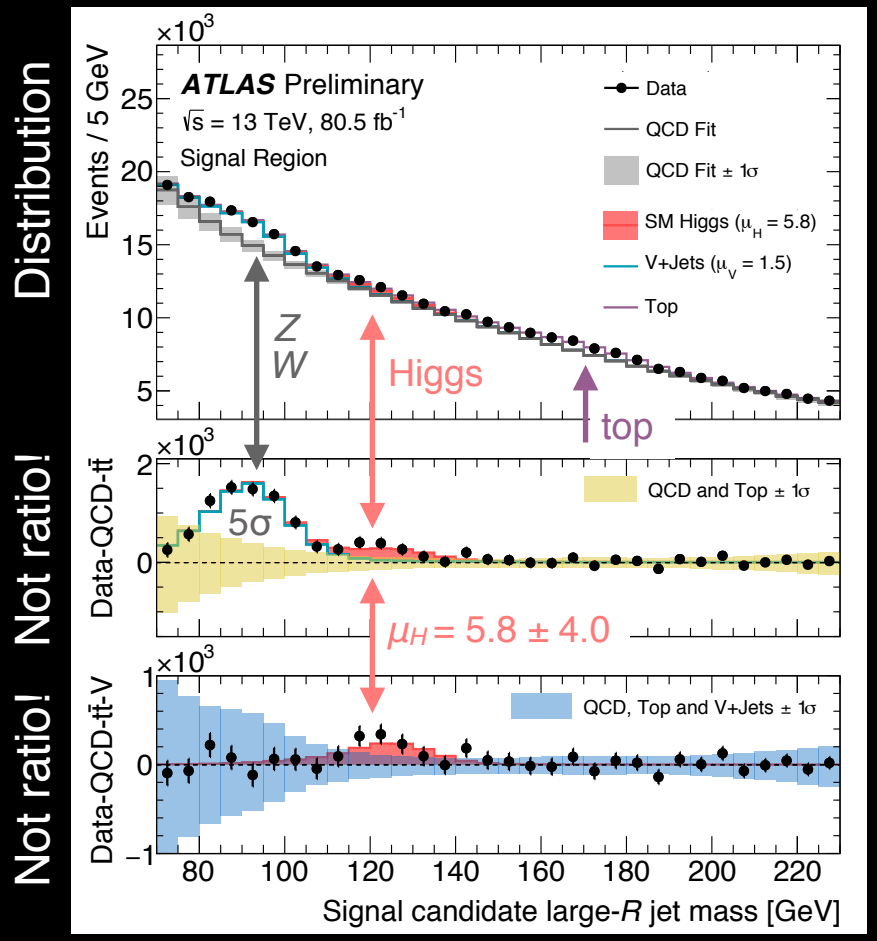

$q\bar{q} \rightarrow$ mediator $\rightarrow q\bar{q}$, so only 2 parameters

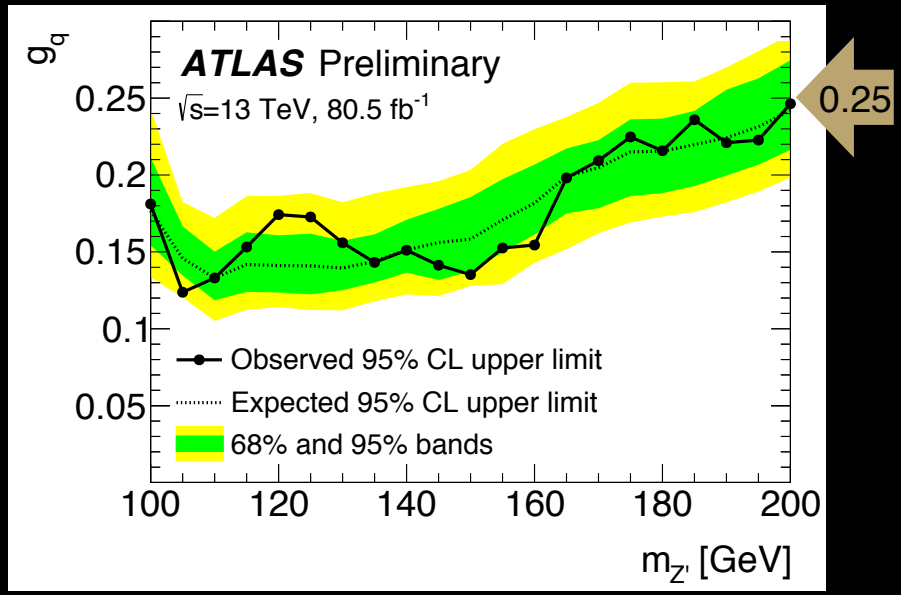

Tool: Track-jet technology for fat-jets (again!)

TM Hong
Pittsburgh

Di-fermion summary, leptophobic

JHEP 05 (2019) 142, up to 36 fb^{-1} Generic features for non-LHC, LHC

Cartoon

m_χ [GeV]

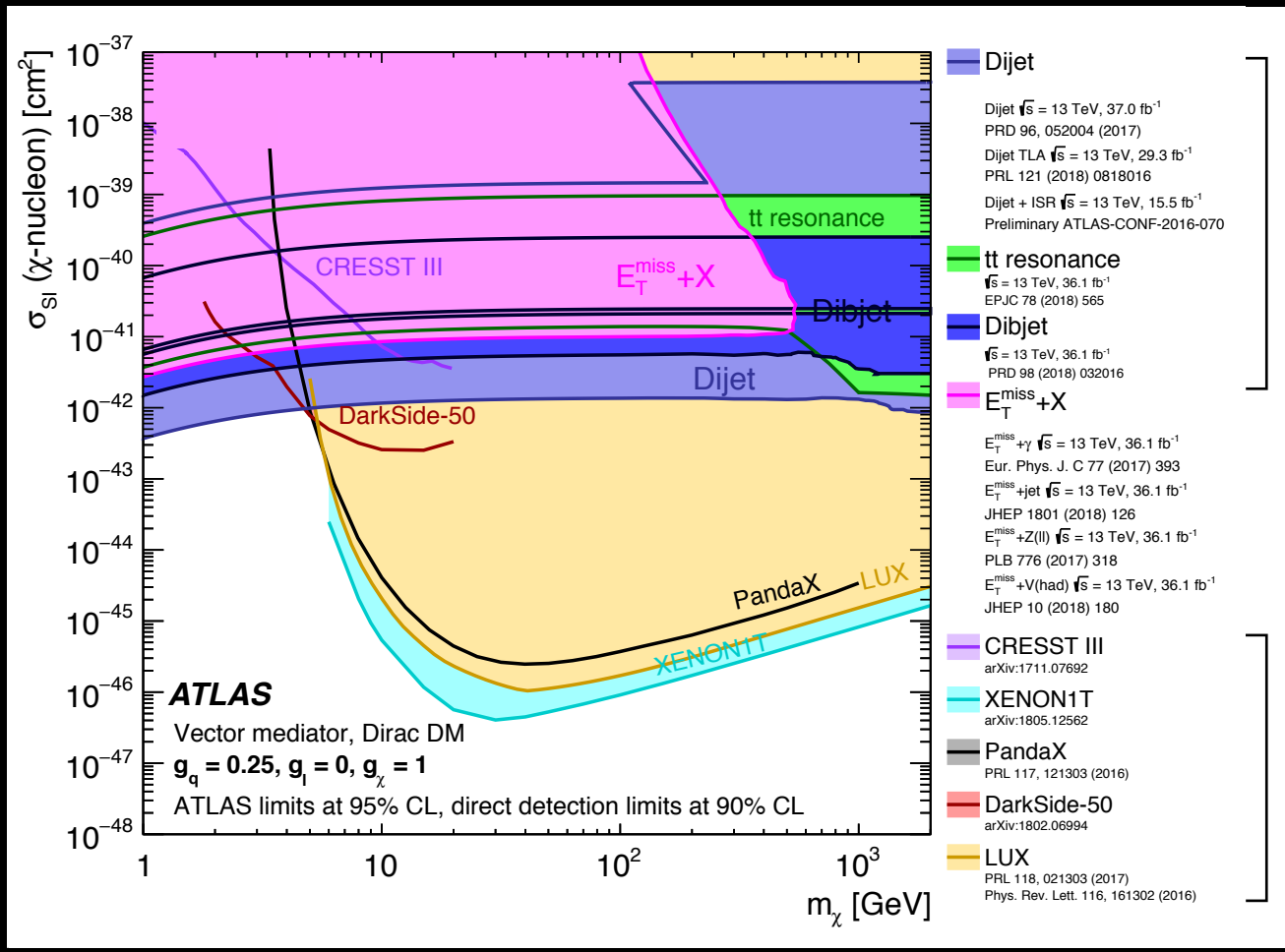

Spin Independent interpretation

Complementary among various LHC results

Di-fermion summary, leptophobic

JHEP 05 (2019) 142, up to 36 fb^{-1} Generic features for non-LHC, LHC

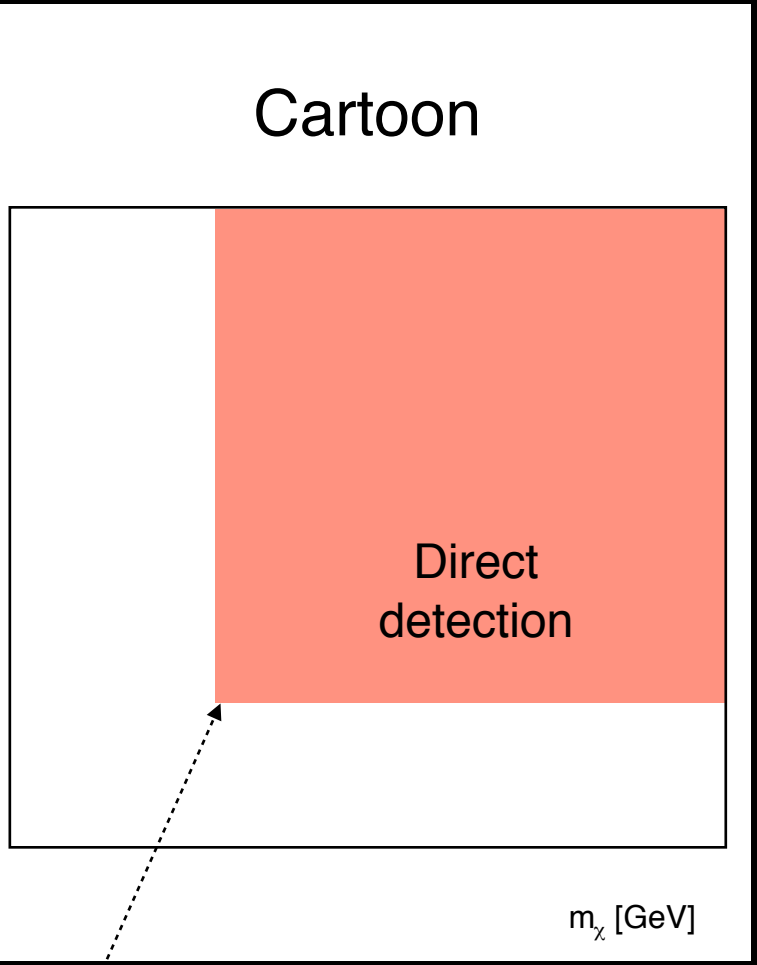

exp't limit
O(1) GeV

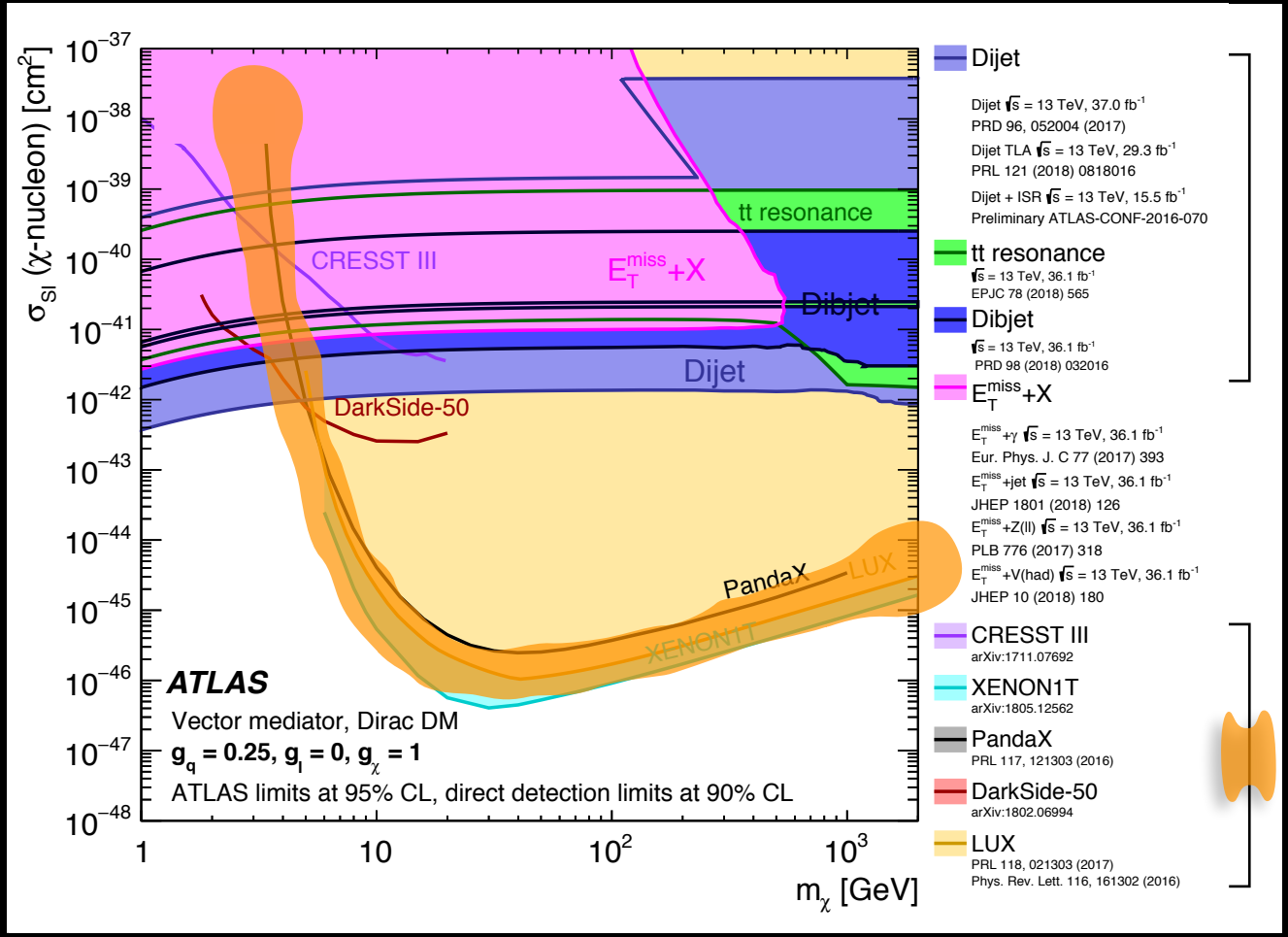

Spin Independent interpretation

TM Hong
Pittsburgh

Complementary among various LHC results

Di-fermion summary, leptophobic

JHEP 05 (2019) 142, up to 36 fb^{-1} Generic features for non-LHC, LHC

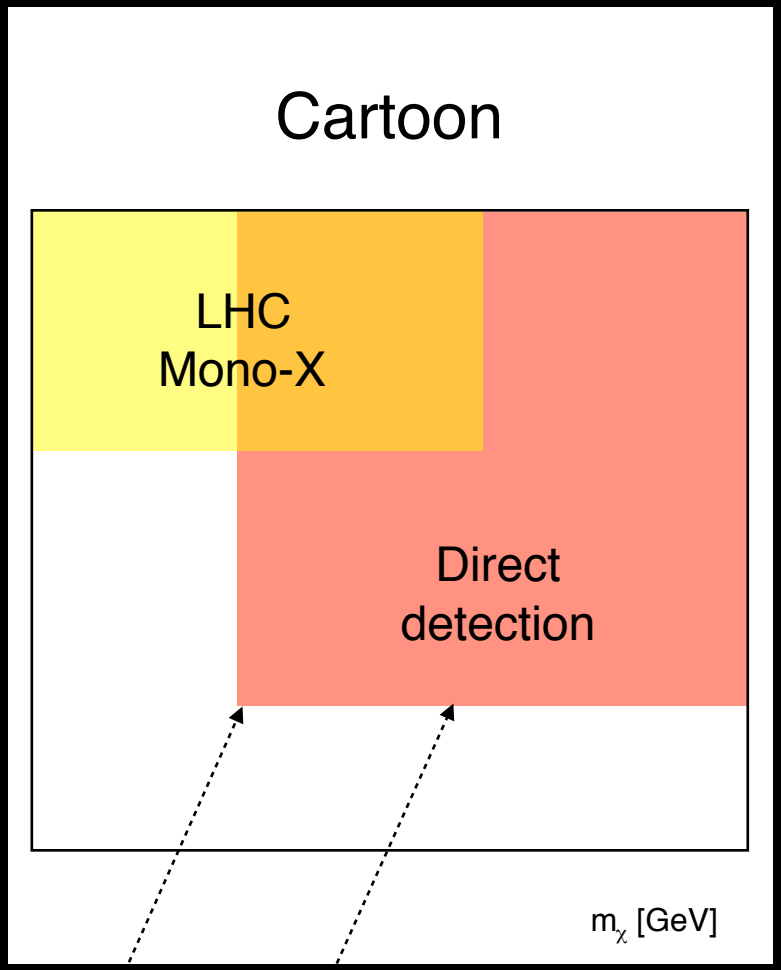

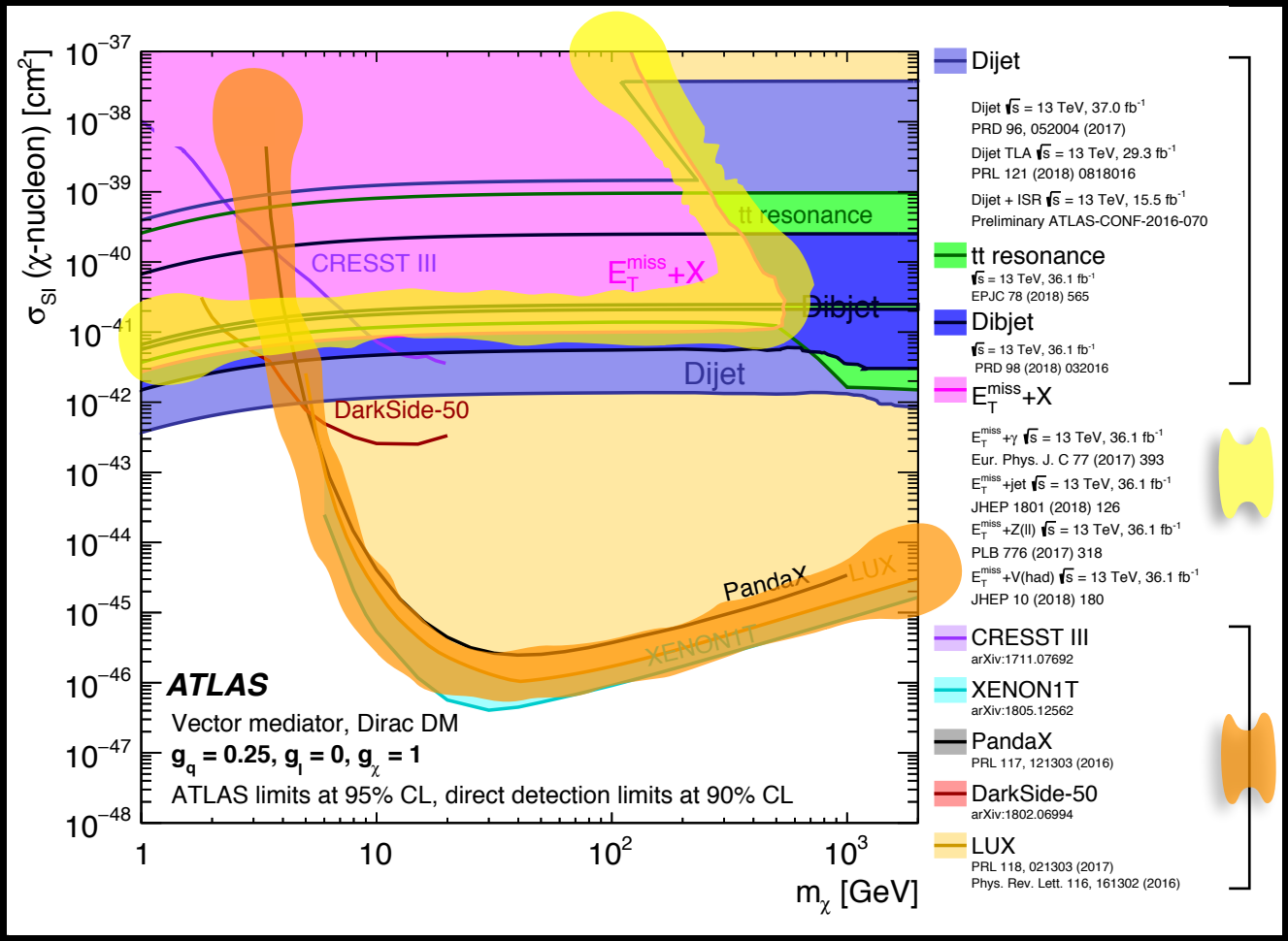

exp't limit
O(1) GeV

$m_{mediator}$
O(100) GeV

Spin Independent interpretation

TM Hong
Pittsburgh

Complementary among various LHC results

Di-fermion summary, leptophobic

JHEP 05 (2019) 142, up to 36 fb^{-1} Generic features for non-LHC, LHC

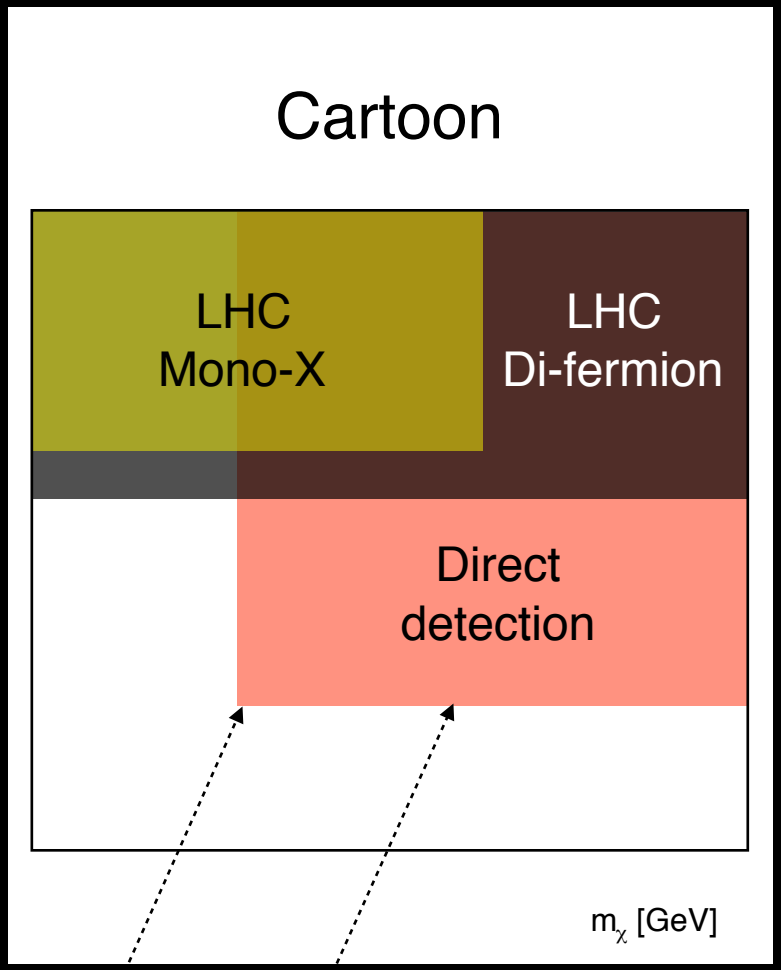

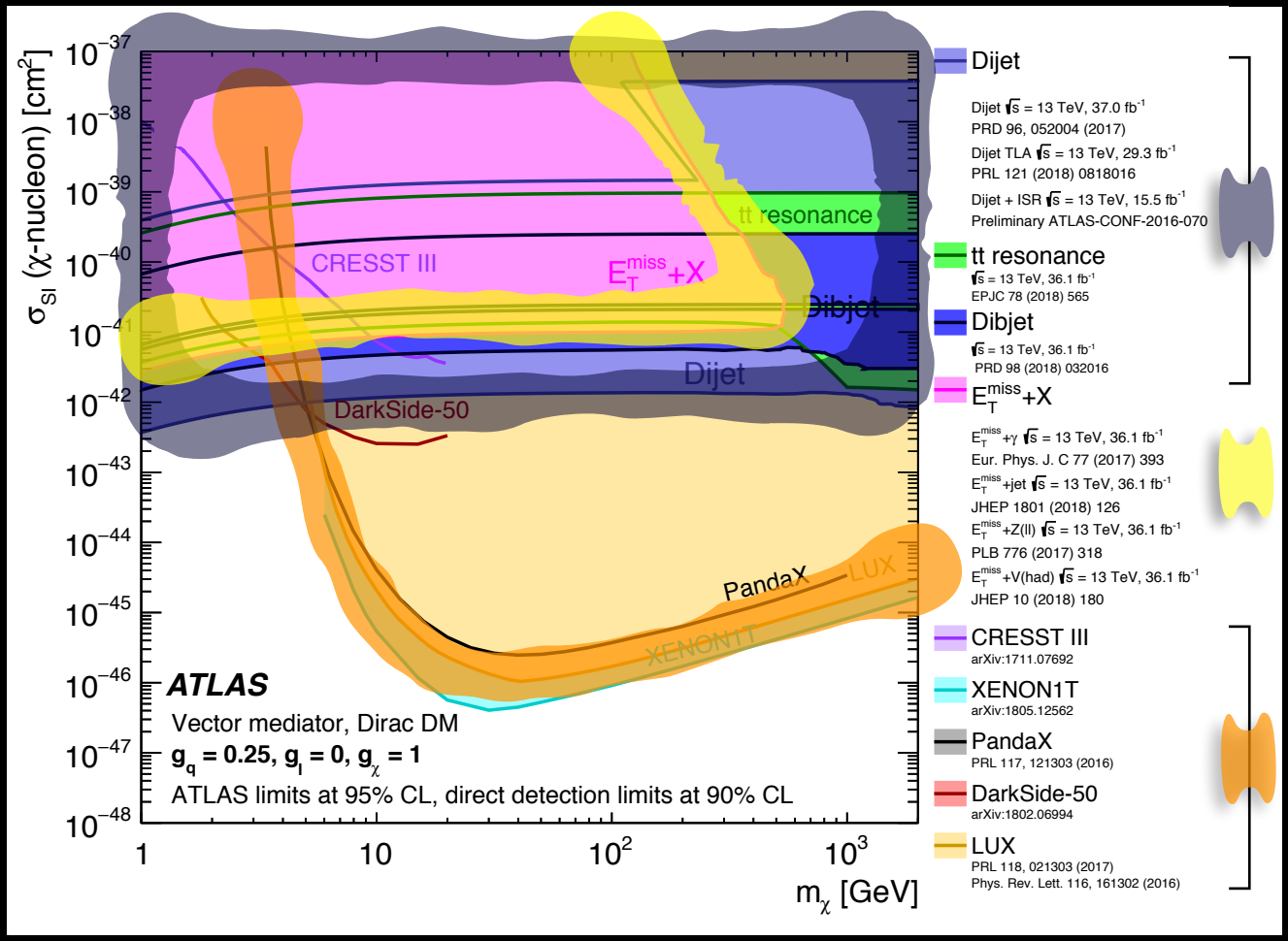

exp't limit
O(1) GeV

$m_{mediator}$
O(100) GeV

Spin Independent interpretation

TM Hong
Pittsburgh

Complementary among various LHC results

Di-lepton

[1903.06248], 139 fb^{-1}

Scan of invariant mass

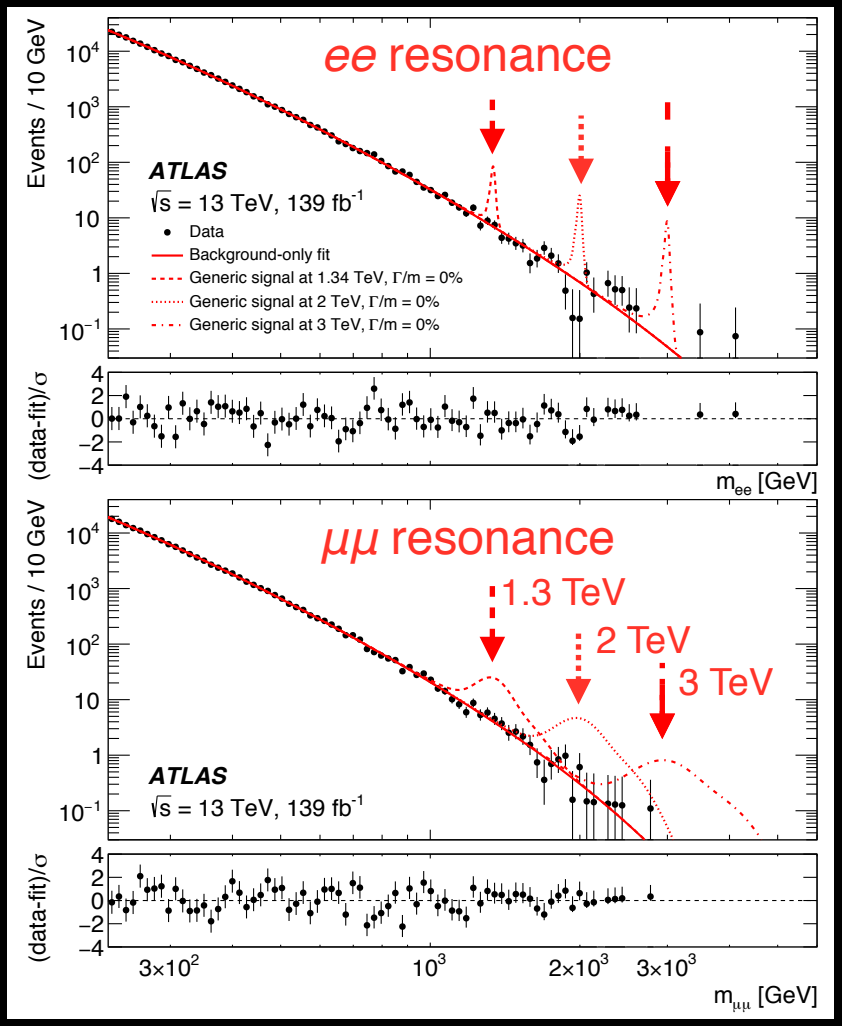

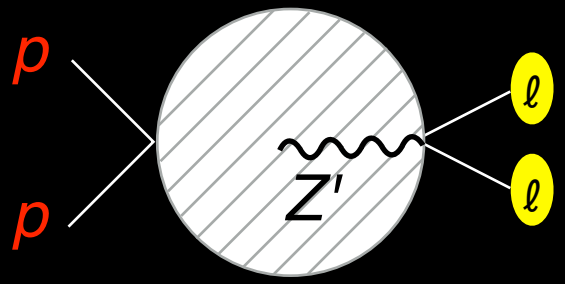

For $m_{Z'} \gg 1$ TeV, the ℓ resolution is

- electrons ~ 1%
- muons ~ tens %

Z' interpretation

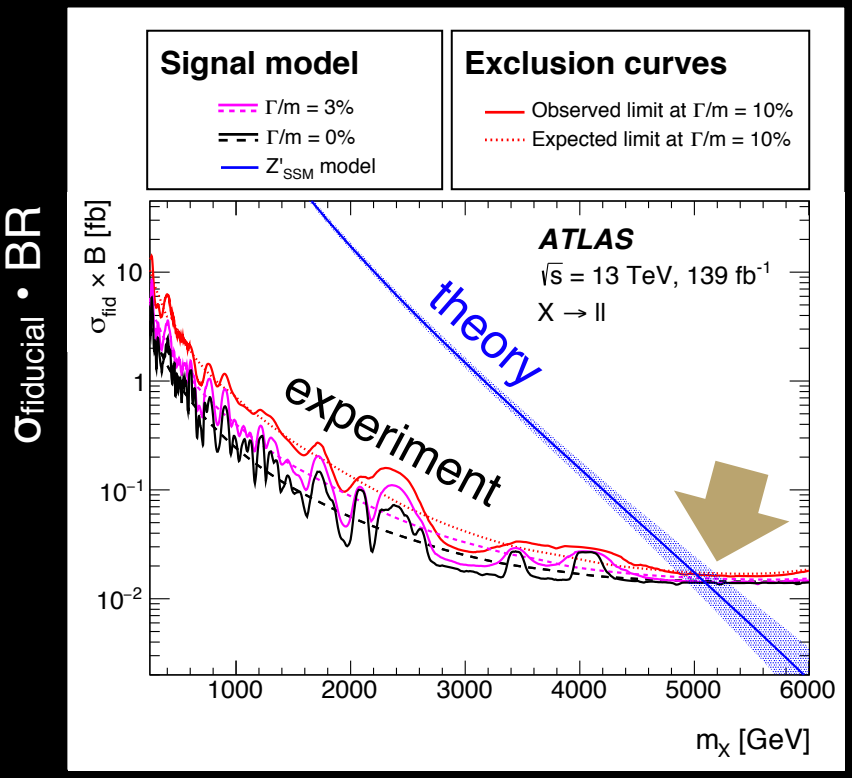

Excude Z' mass to 5 TeV

Di-fermion summary, leptophilic

JHEP 05 (2019) 142, up to 36 fb^{-1} Generic features for non-LHC, LHC

Cartoon

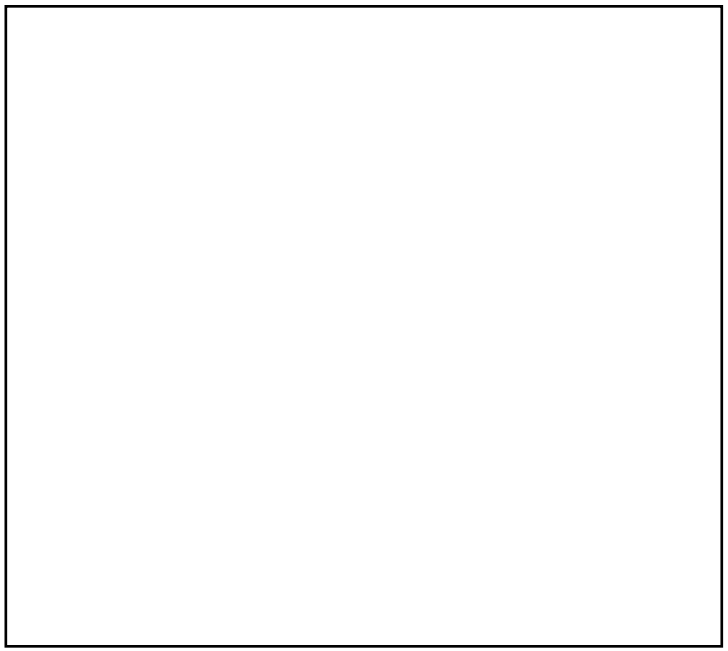

m_χ [GeV]

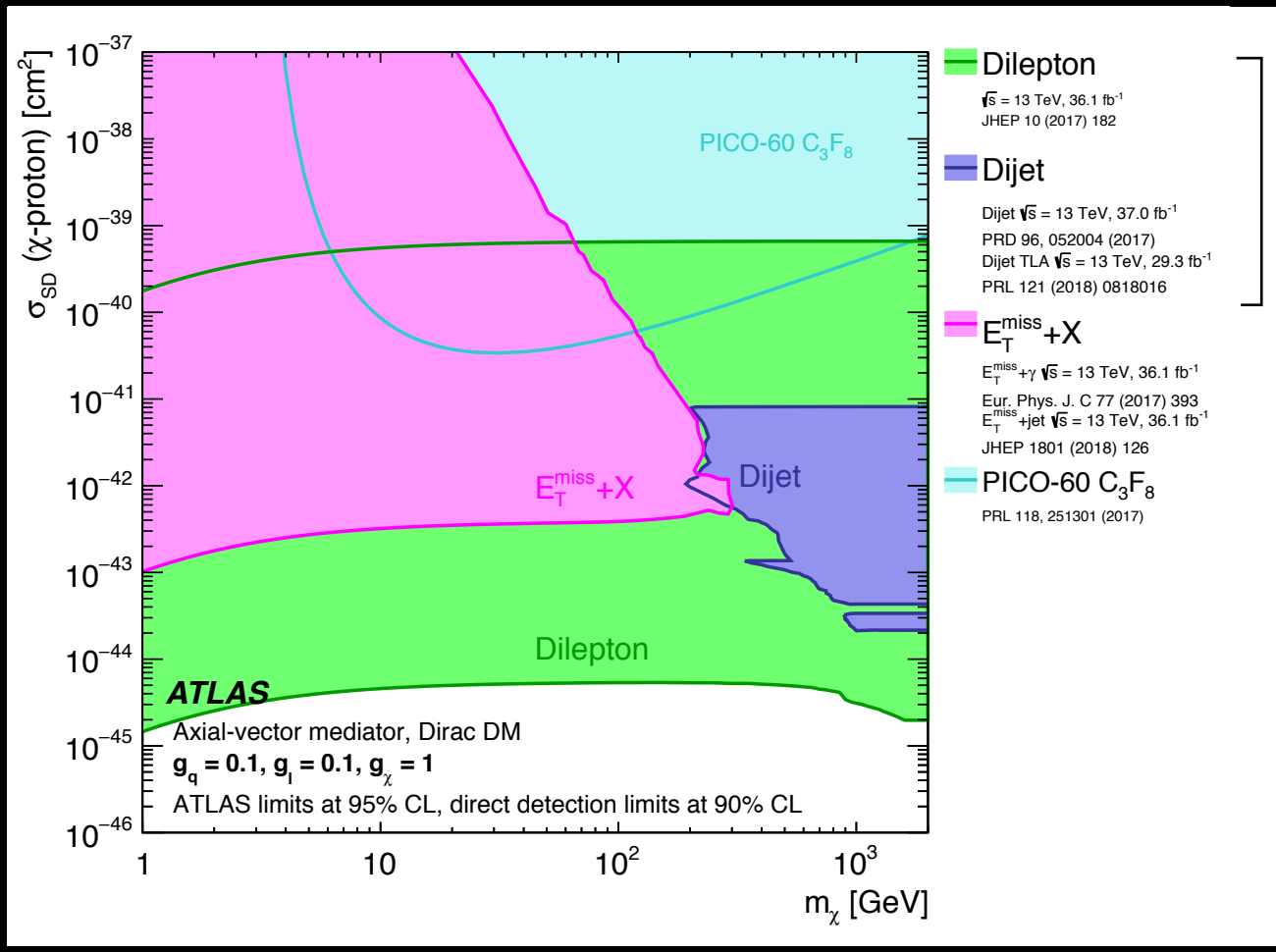

Spin Dependent interpretation

Different channels excluding different parameters

Di-fermion summary, leptophilic

JHEP 05 (2019) 142, up to 36 fb^{-1} Generic features for non-LHC, LHC

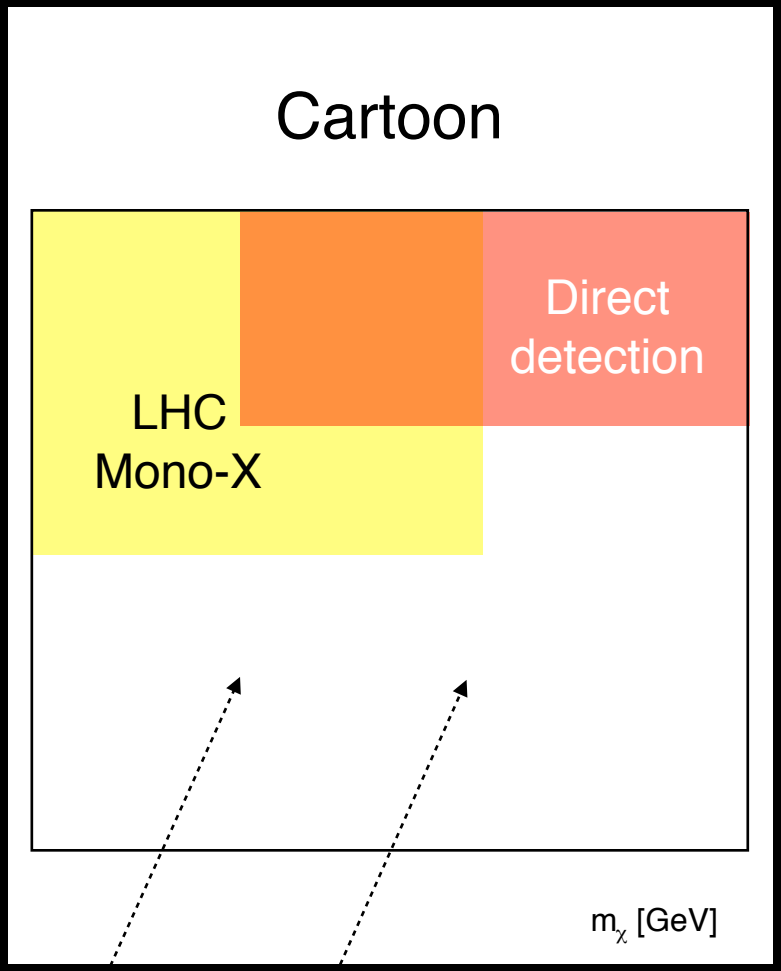

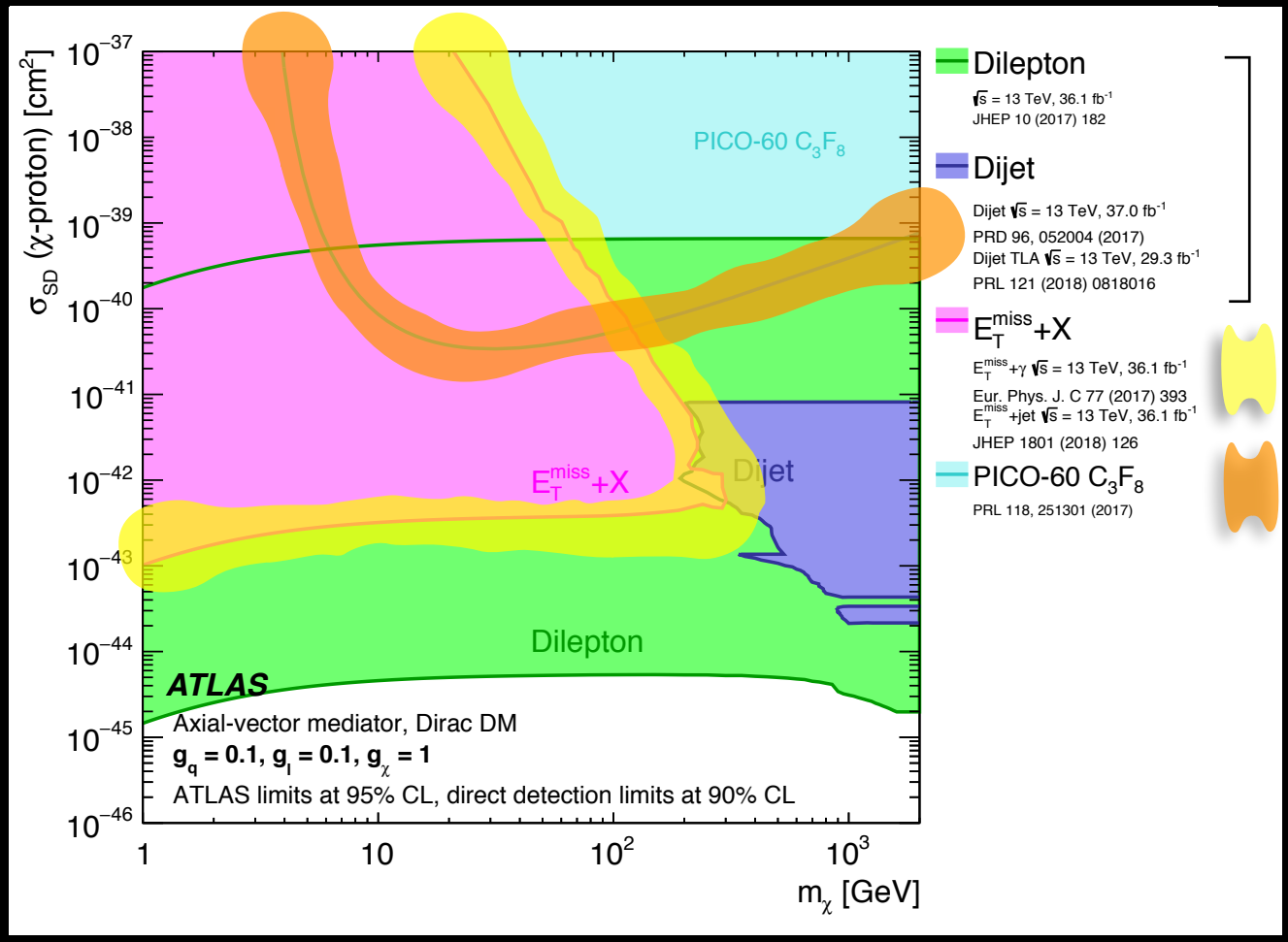

exp't limit
O(1) GeV

$m_{mediator}$
O(100) GeV

Spin Dependent interpretation

Different channels excluding different parameters

Di-fermion summary, leptophilic

JHEP 05 (2019) 142, up to 36 fb^{-1} Generic features for non-LHC, LHC

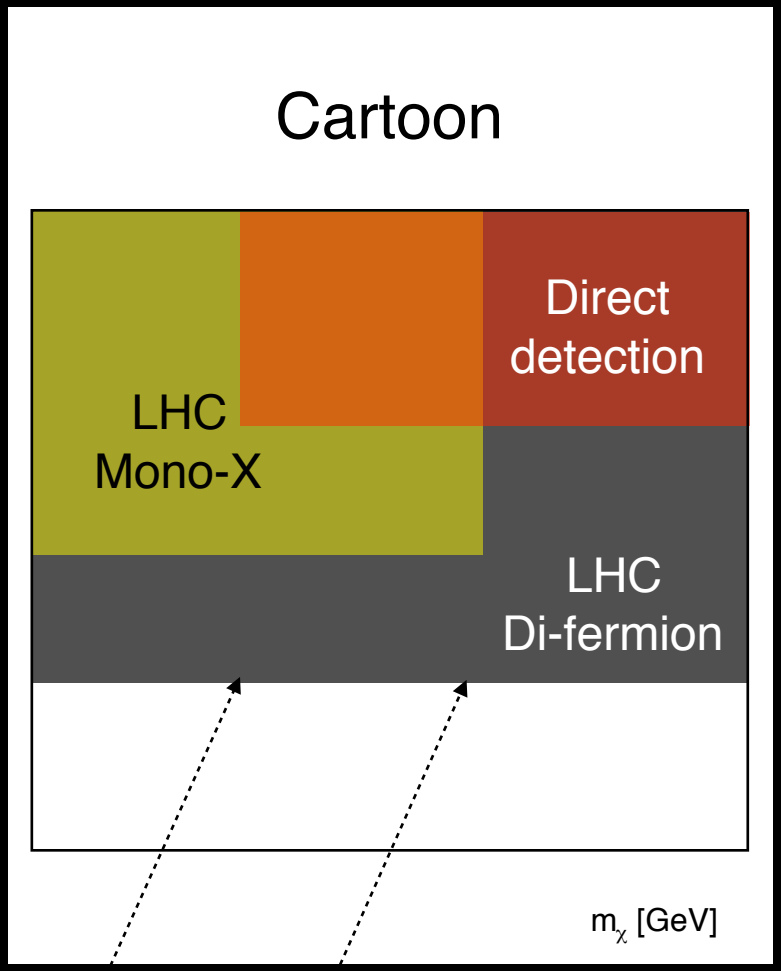

exp't limit
O(1) GeV

m$_{mediator}$
O(100) GeV

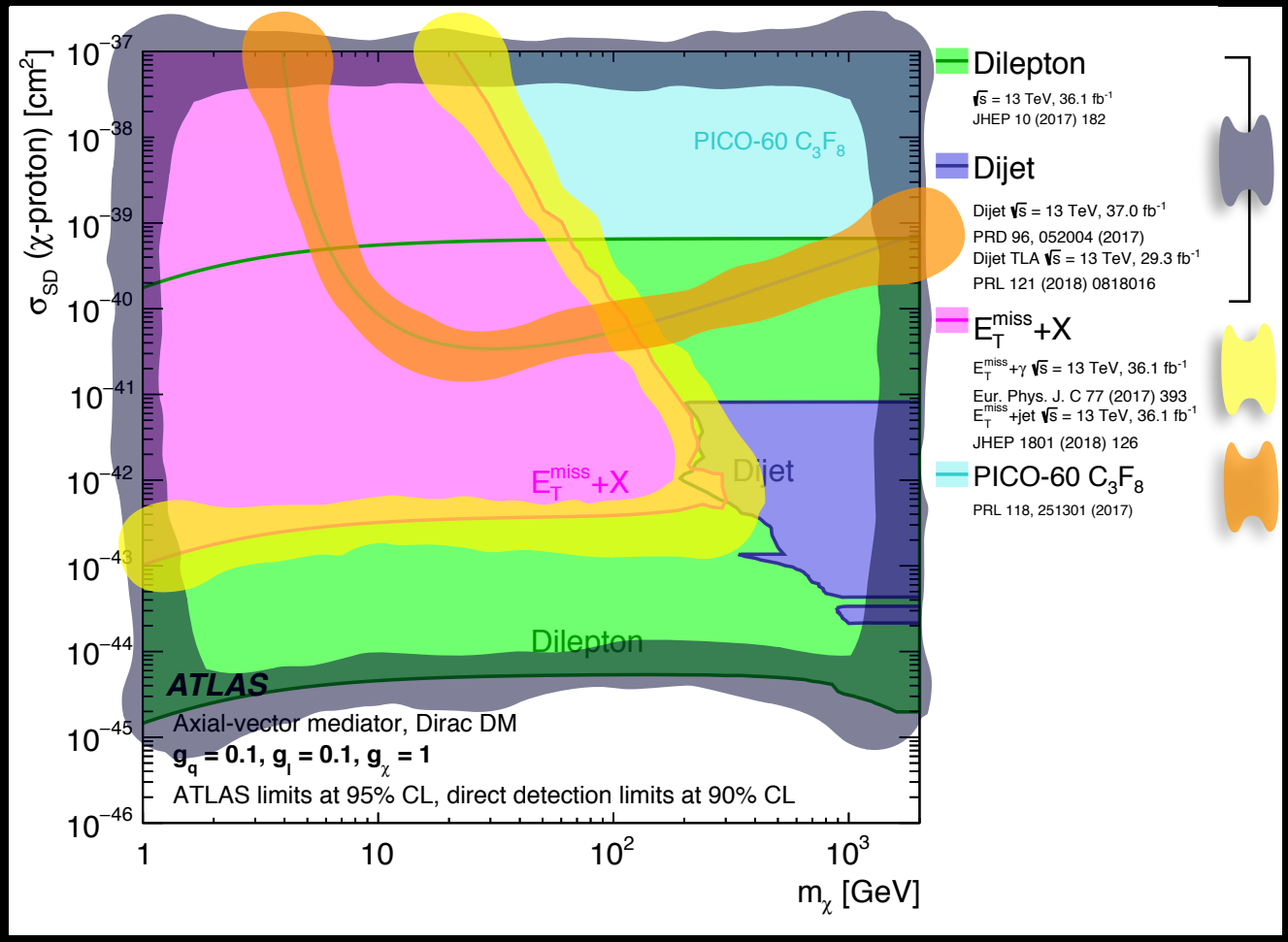

Spin Dependent interpretation

Different channels excluding different parameters

Higgs → DM: VBF

Phys. Lett. B 4 (2019) 024, 36 fb^{-1}

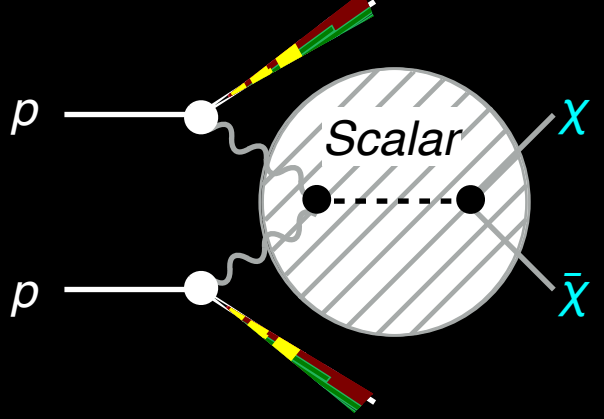

DM χ

E_T^{miss} > 180 GeV

lowest thresh. trigger

$m_{di\text{-}jet}$ > 1 TeV

Look for excess in tail of distributions

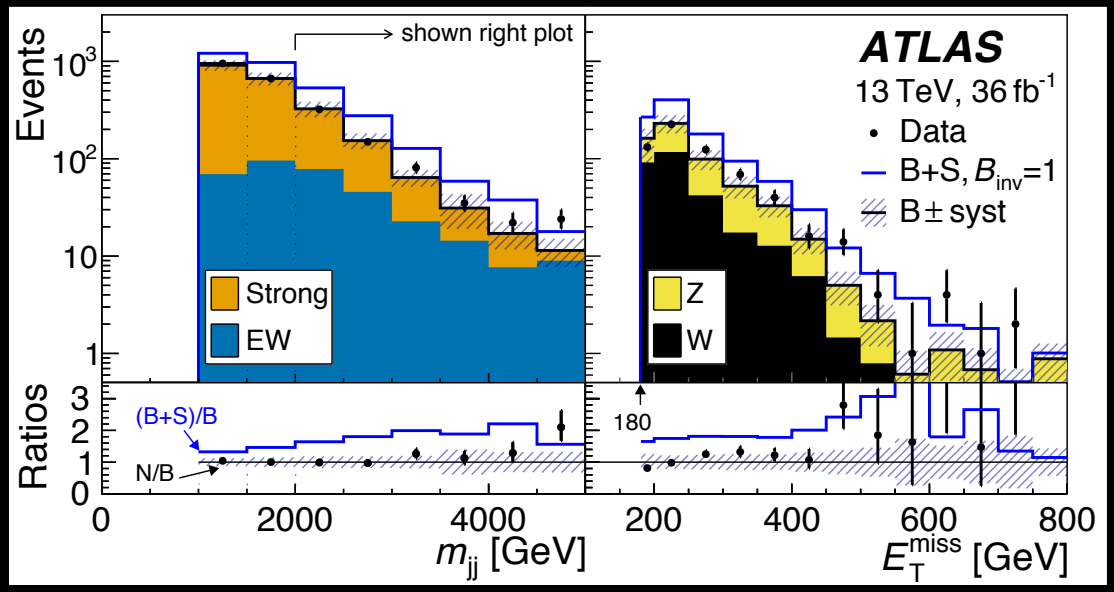

"No model" interpretation

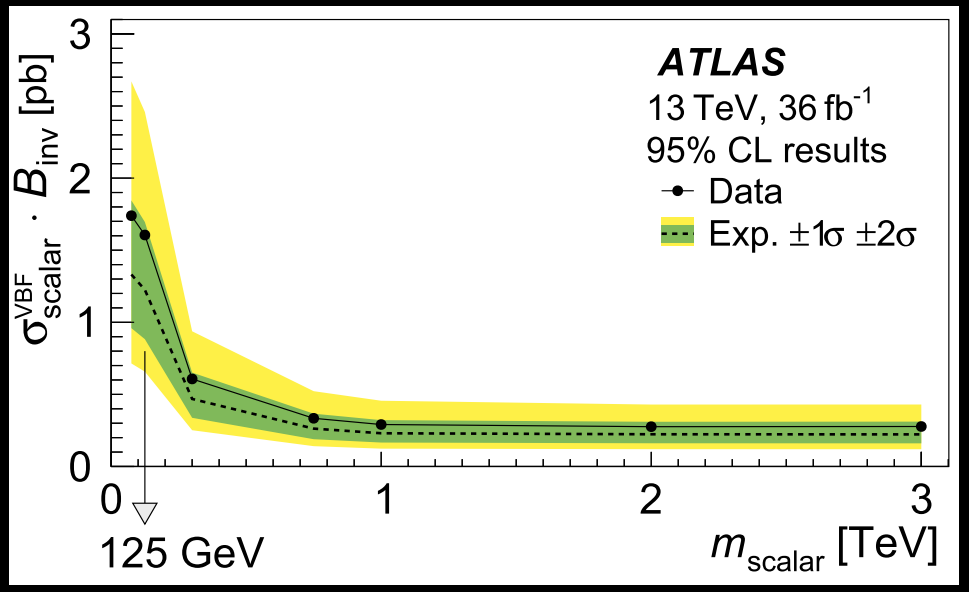

- Tool: E_T^{miss} trigger, focus on Higgs at 125 GeV
- Exp't: $W_{\ell\nu}$, $Z_{\ell\ell}$ control samples to normalize MC
- Interpret: Repeat cuts for higher m_{scalar}

- Observed limit 0.37 in Higgs BR
- Expected limit 0.28 in Higgs BR

TM Hong

Pittsburgh

Large background, so like a precision measurement

Higgs → DM: Combination

[1904.05105], 36 fb^{-1} (and Run-1)

Individual channels

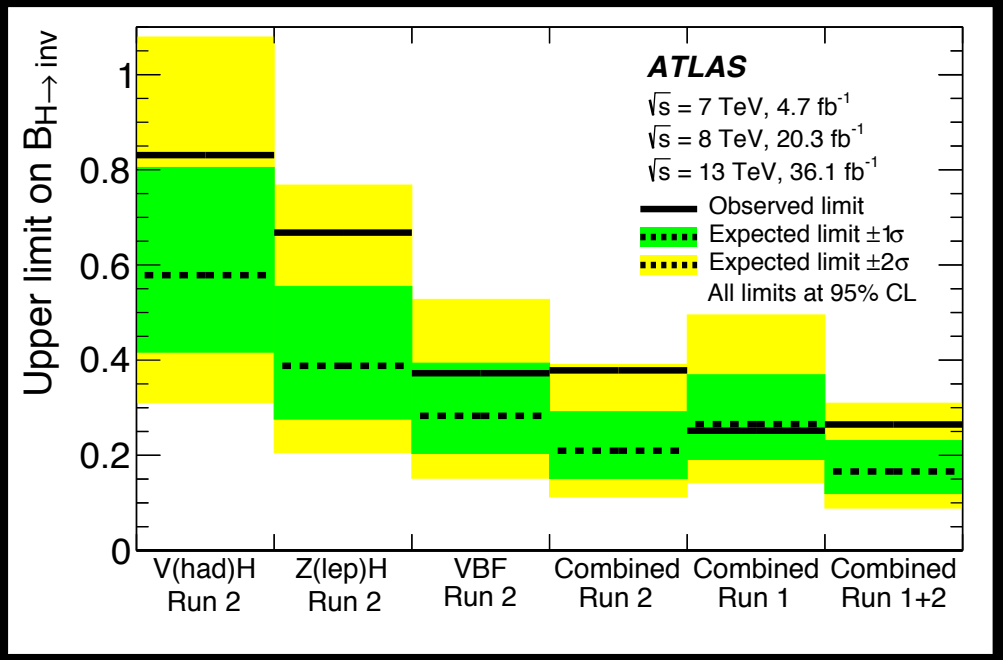

Higgs portal

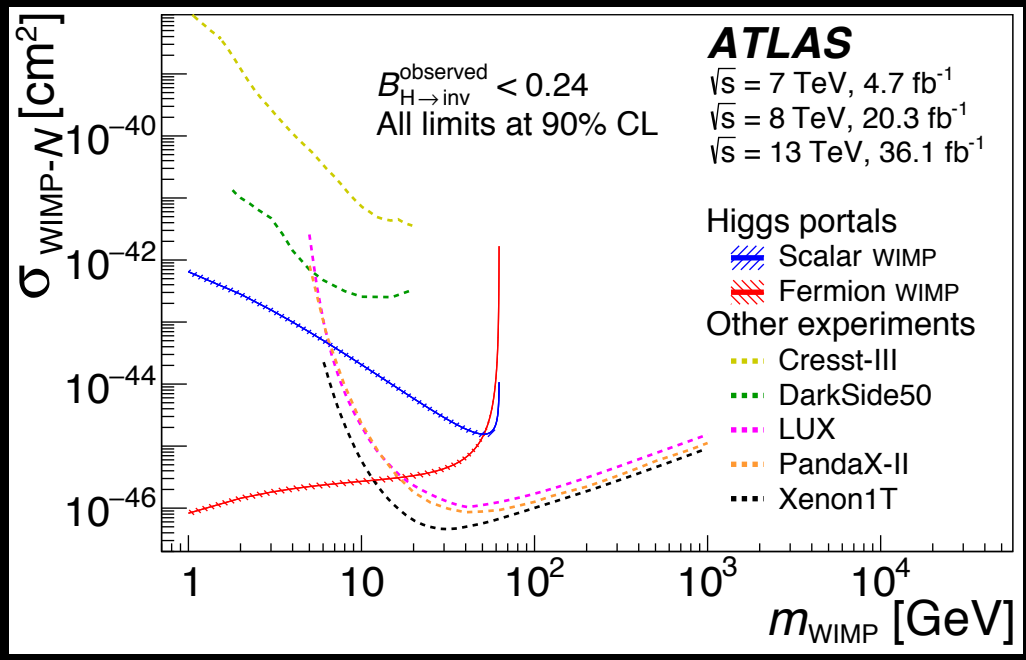

Previous slide

- Observed limit 0.26 in Higgs BR at 95% CL
- Expected limit 0.17 in Higgs BR "

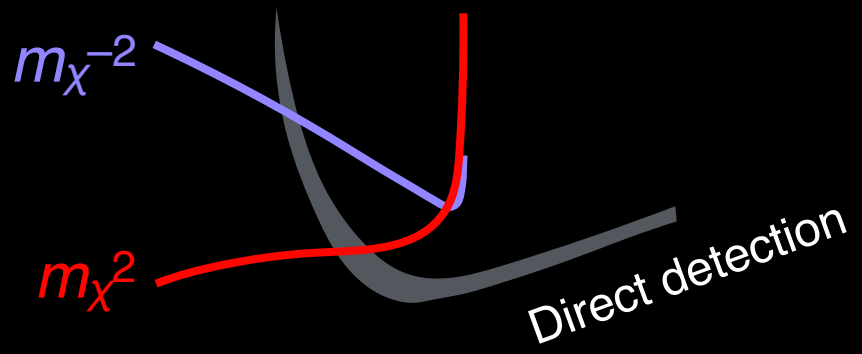

Complementarity between LHC & direct detection

Future

Projections, Upgrades, Community effort

HL-LHC Mono-jet
ATL-PHYS-PUB-2018-043

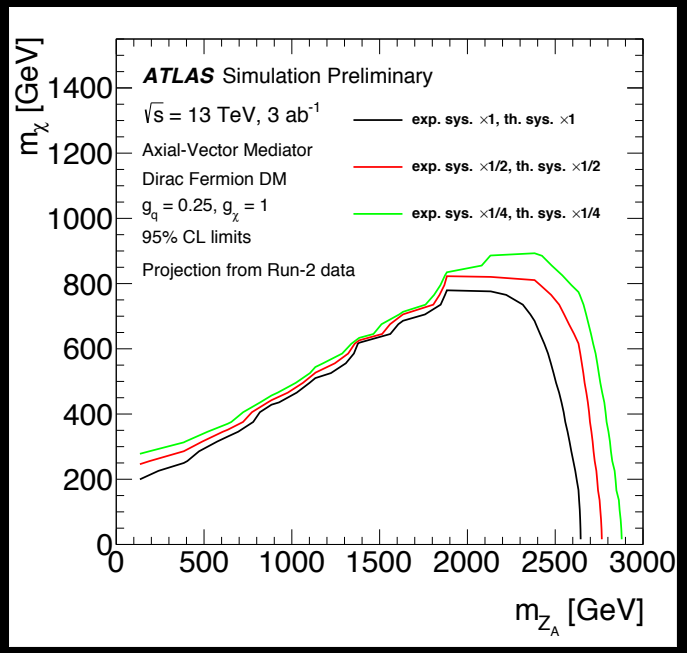

$m_{mediator}$

HL-LHC E_T^{miss} trigger threshold
CERN-LHCC-2017-020

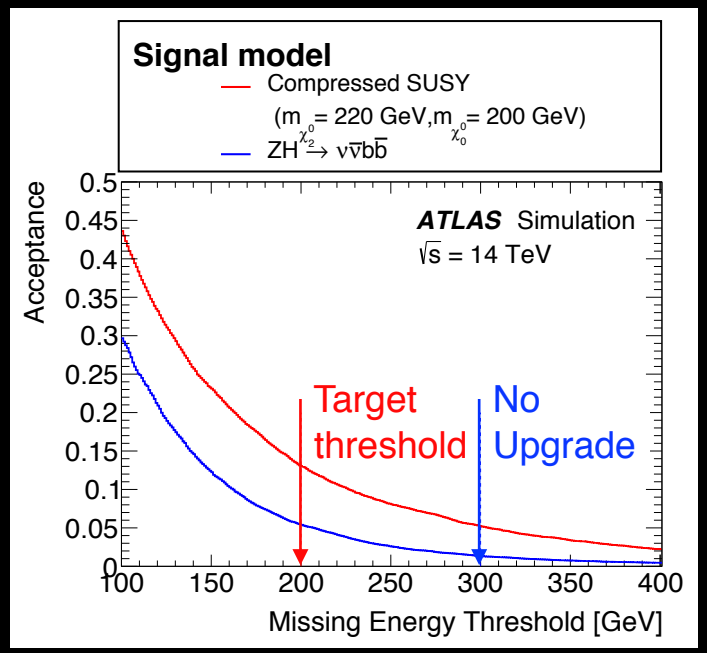

E_T^{miss}

2HDM + DM mediator *a*
ATLAS+CMS+theory [1810.09420]

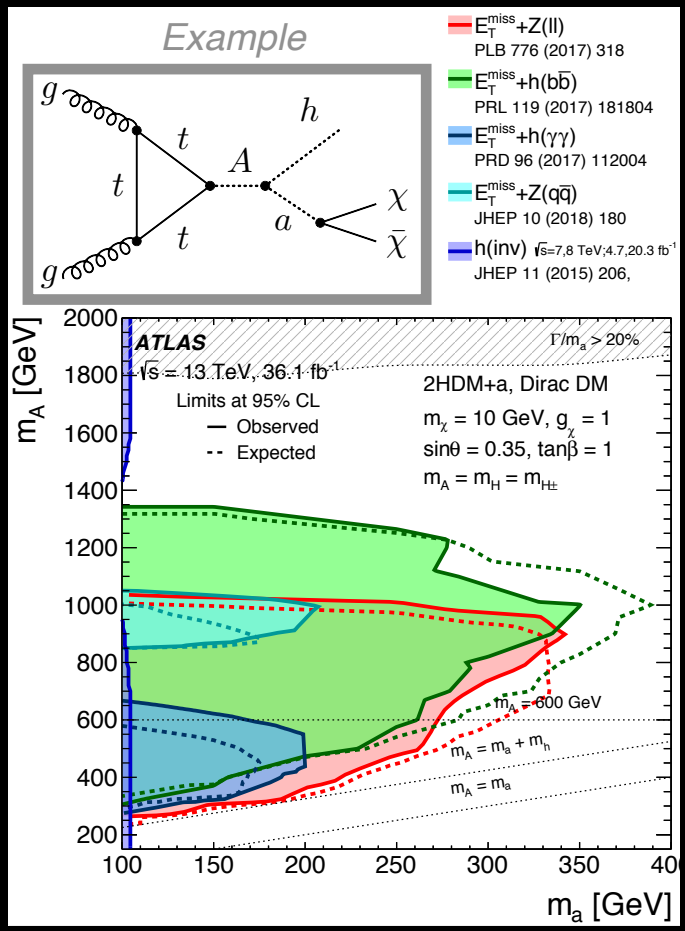

Future

Projections, Upgrades, Community effort

HL-LHC Mono-jet
ATL-PHYS-PUB-2018-043

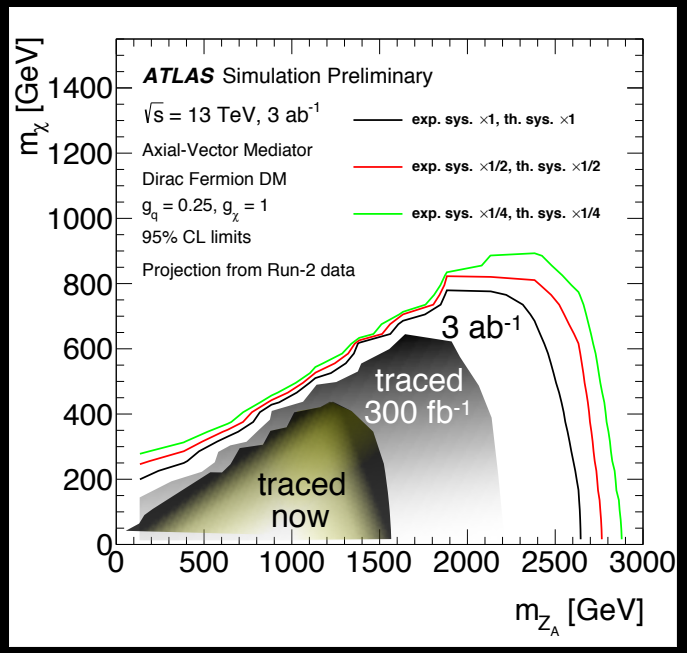

$m_{mediator}$

HL-LHC E_T^{miss} trigger threshold
CERN-LHCC-2017-020

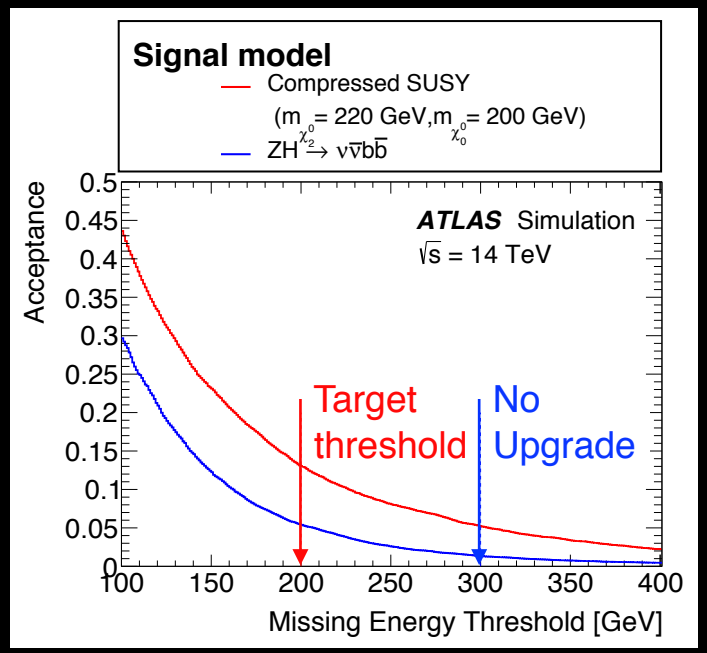

E_T^{miss}

2HDM + DM mediator *a*
ATLAS+CMS+theory [1810.09420]

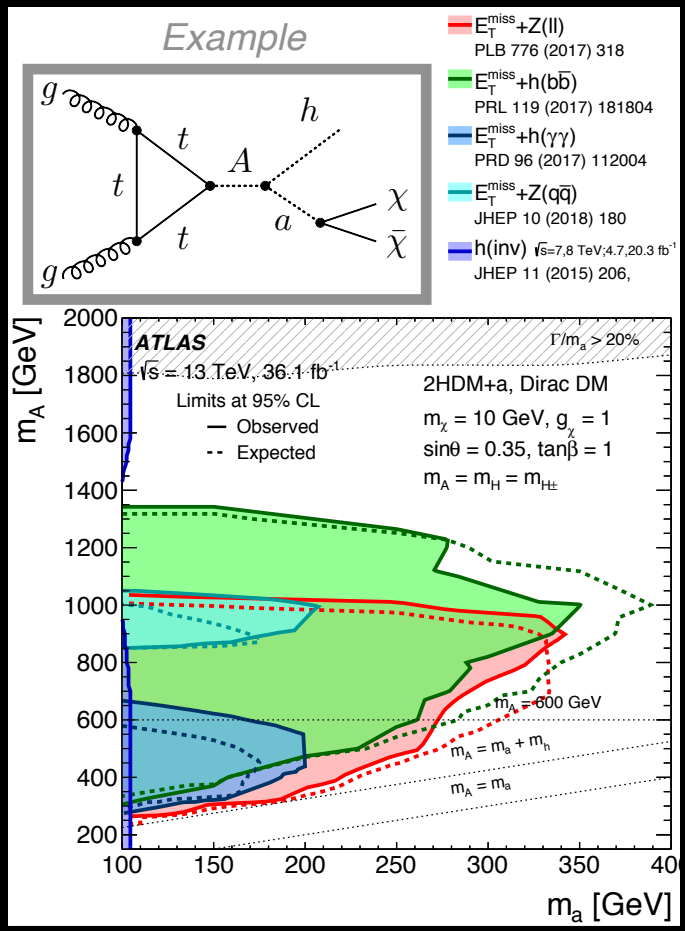

Future

Projections, Upgrades, Community effort

HL-LHC Mono-jet
ATL-PHYS-PUB-2018-043

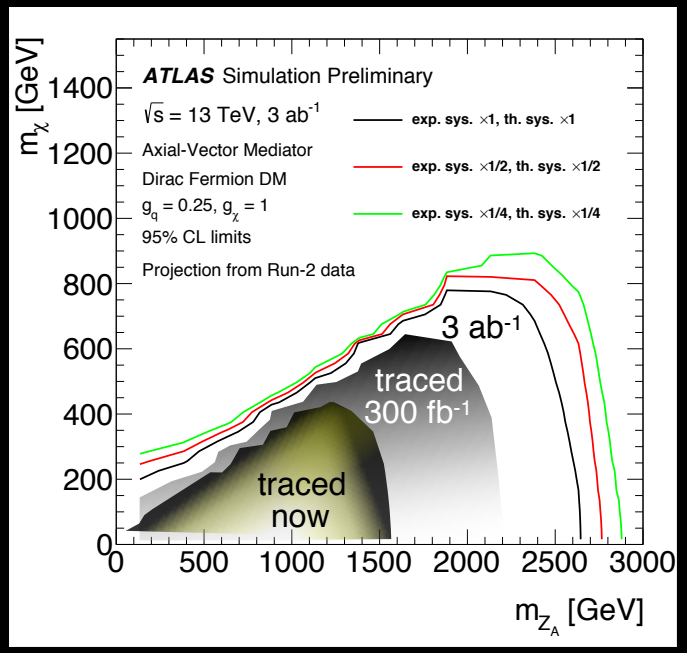

HL-LHC E_T^{miss} trigger threshold
CERN-LHCC-2017-020

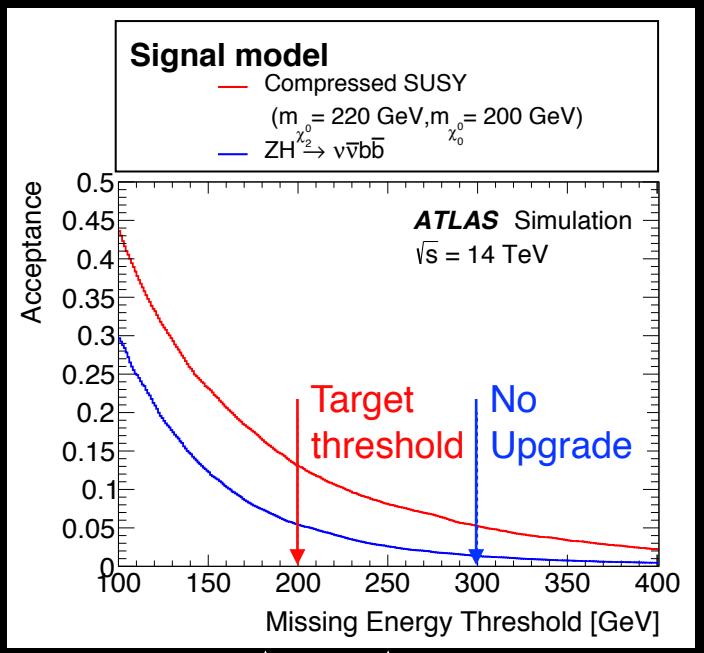

2HDM + DM mediator *a*
ATLAS+CMS+theory [1810.09420]

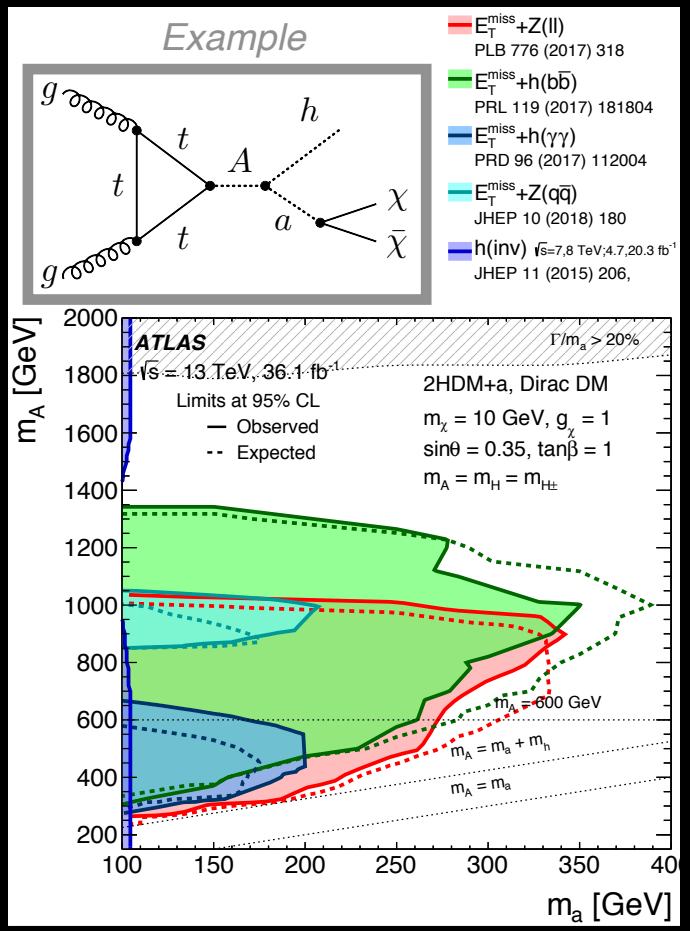

$m_{mediator}$ E_T^{miss}

Current cut for *VBF Higgs to invisible*
At "Target threshold," < 80% of current
At "No Upgrade," < 20% of current

Current cut for *Mono-jet*
< 100% because of trigger turn-on
< 80% of current WIMP on p11

Exciting challenges for HL-LHC

Last slide

Conclusion

EFT → simplifed

Dark matter → Dark matter sector ← more meas'ts

Dark matter(s)
Mediator(s)
Known matters

Fun continues

- Many interesting topics are involved, e.g.,
  - Scalars that are colored
  - Dark γ / Z that are looooooooooooooooong-lived
  - Pseudoscalar mediators
  - SUSY, R-parity conserving

Many exciting development at the LHC!

Too long; didn't read recap

Effective field theory

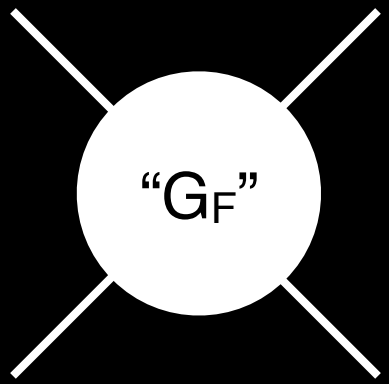

zoom in

Simplified models

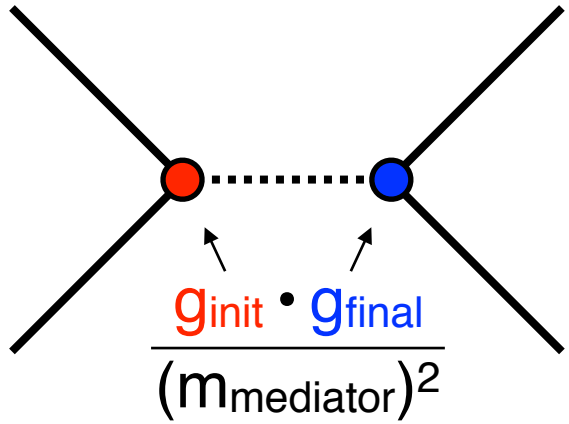

dark matter

dark matter mediator

Improved understanding of the dark matter sector

Bonus slides

(if I had 10 more minutes)

Talk abstract

The presence of a non-baryonic dark matter (DM) component in the Universe is inferred from the observation of its gravitational interaction. If dark matter interacts weakly with the Standard Model (SM) it could be produced at the LHC, escaping the detector and leaving a large missing transverse momentum as their signature. The ATLAS experiment has developed a broad and systematic search program for DM candidates, including resonance searches for the mediator which would couple DM to the SM. The results of these searches on 13 TeV pp data, their interplay and interpretation will be presented, along with some prospects for the HL-LHC.

ATLAS intro

https://youtu.be/Rwyib-gCVJ4

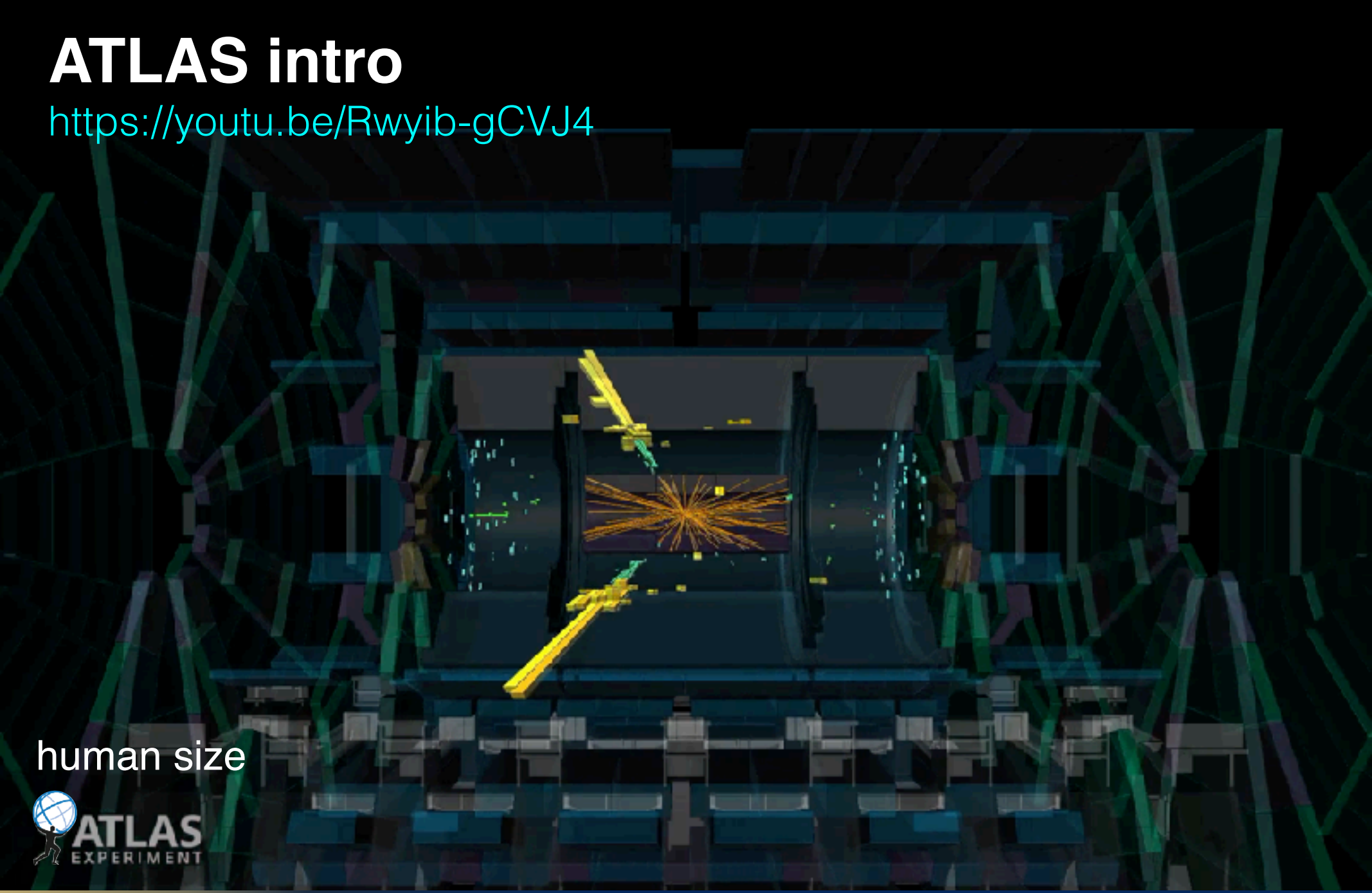

TM Hong
Pittsburgh

Di-jet event, $p_T^{jet} \sim 200$ GeV

ATLAS intro

https://youtu.be/Rwyib-gCVJ4

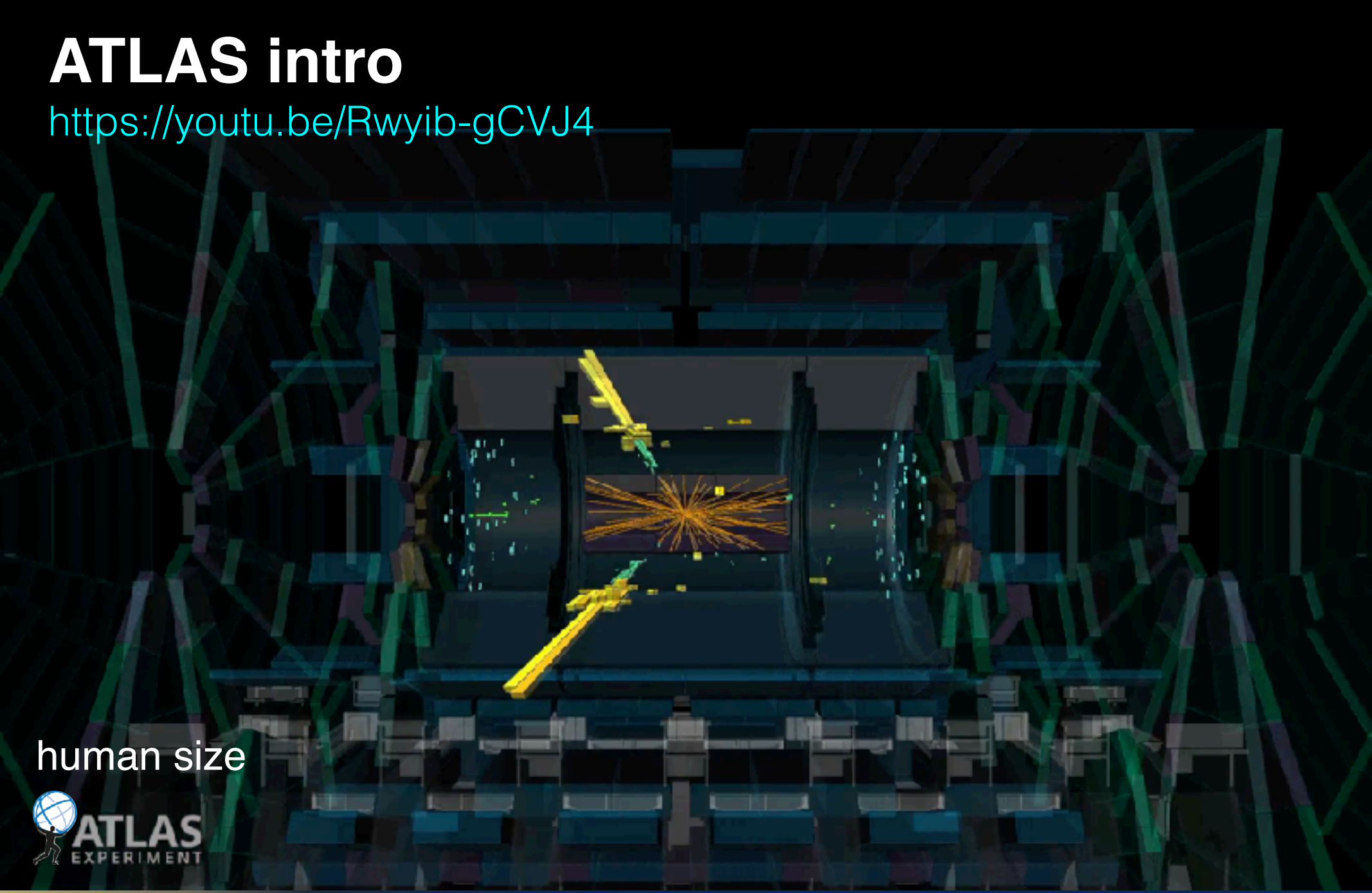

TM Hong
Pittsburgh

Di-jet event, $p_T^{jet} \sim 200$ GeV

ATLAS Experiment

JINST 3 (2008) S08003

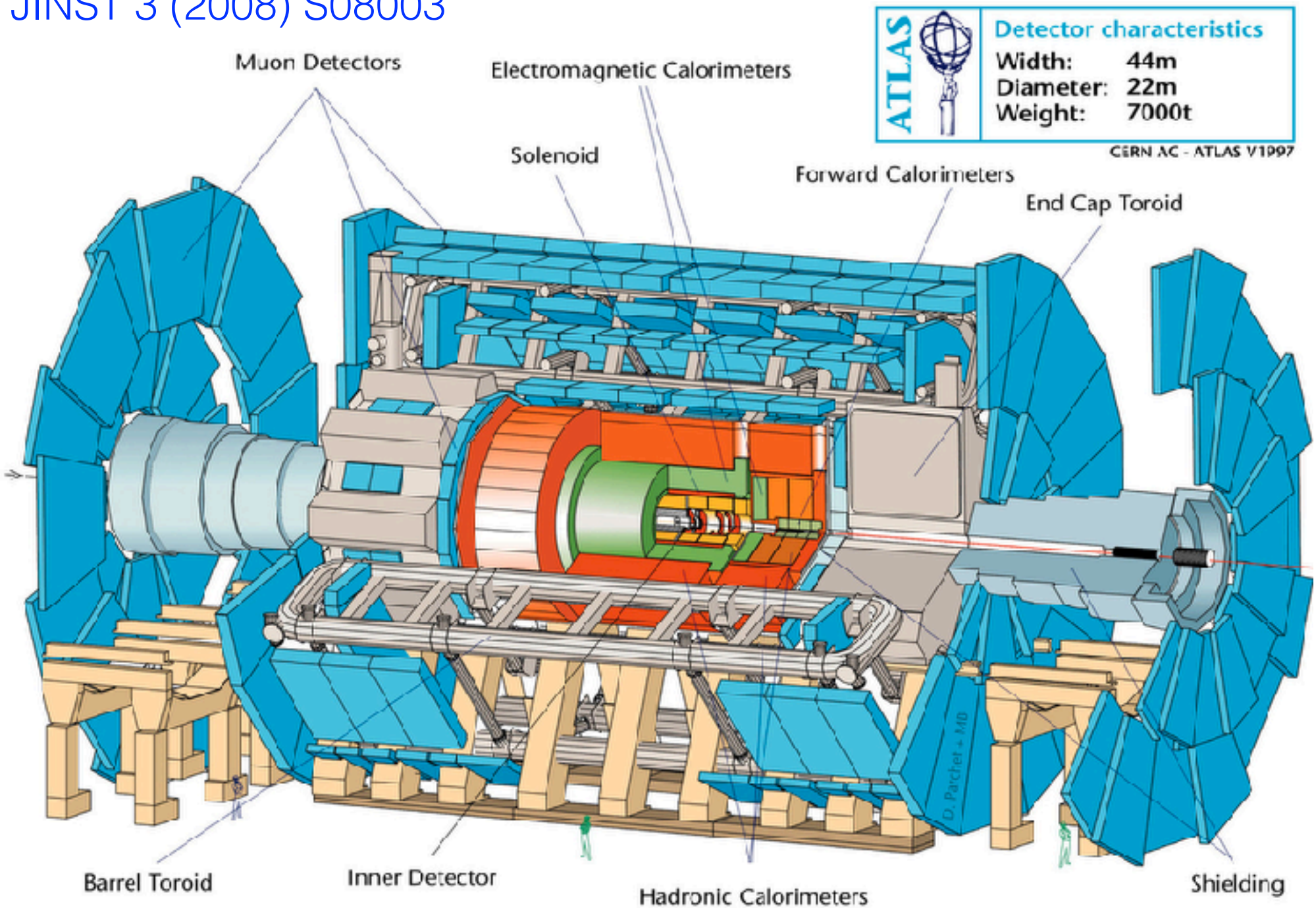

Mediator via di-jet

2016 CMS result (with blip) for pedagogy

$m_{di\text{-}jet}$

Little blip

Limit

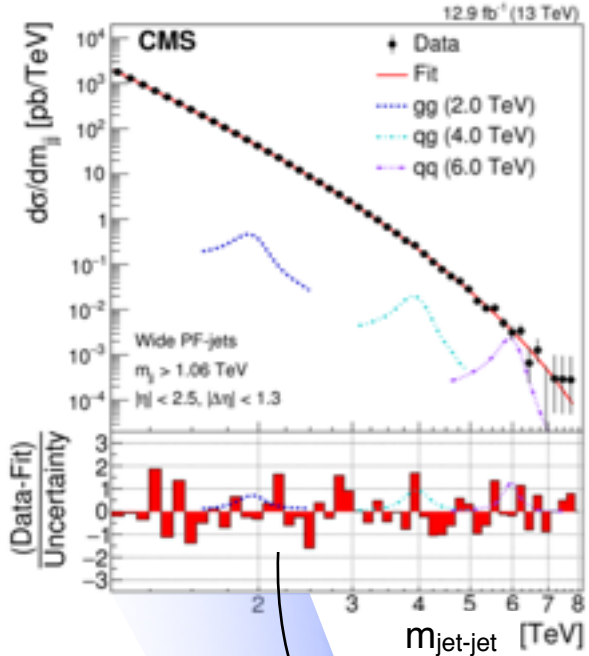

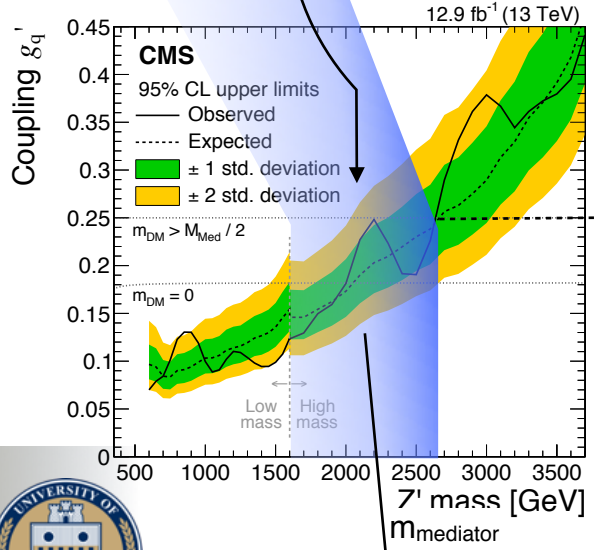

Left side by Right side
next slides by left plots

slope = ½

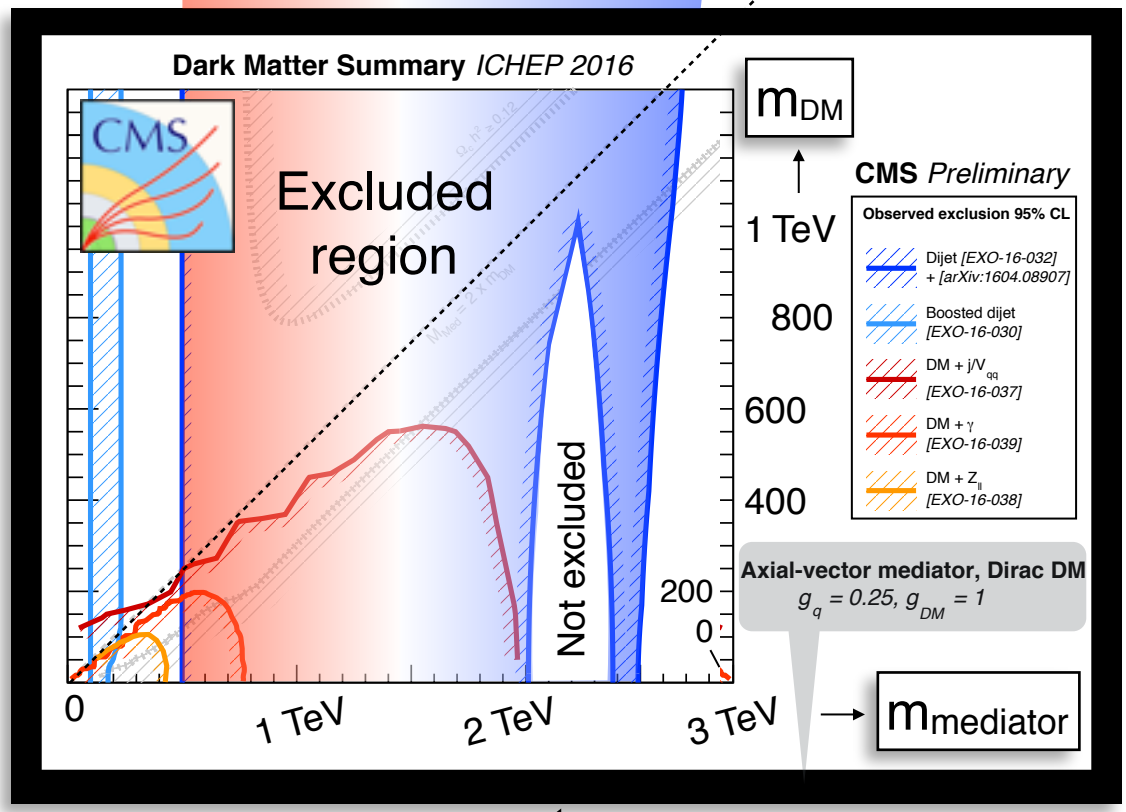

Exclusion excludes blip

Assumptions on 2 params.

TM Hong
Pittsburgh

Highest-mass di-jet

Event display

ATLAS-CONF-2019-007

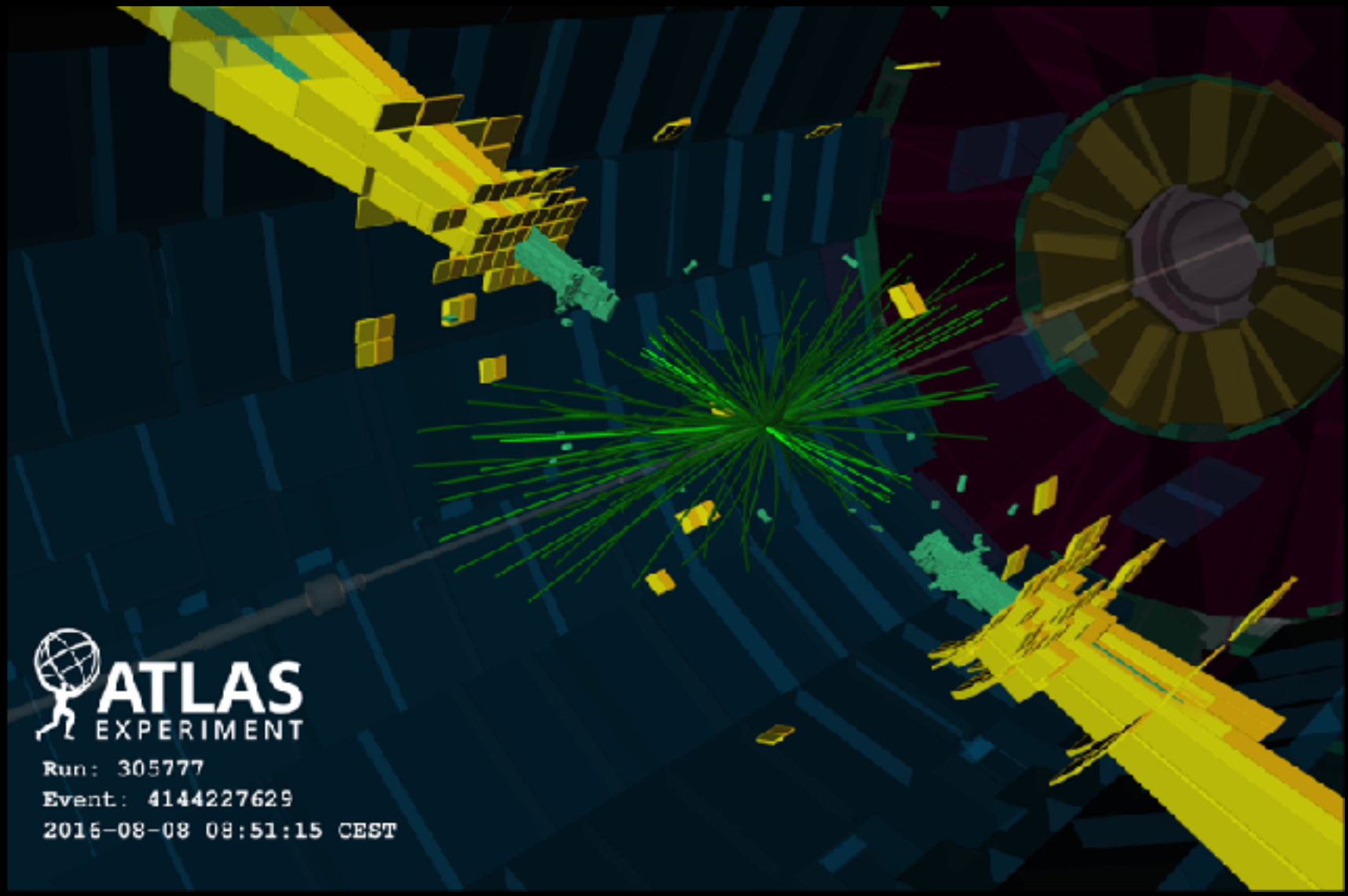

$m_{\text{di-jet}} \sim 8$ TeV

Each jet $p_T \sim 4$ TeV

Di-fermion summary, leptophobic

Generic features of results from non-LHC, LHC

Cartoon

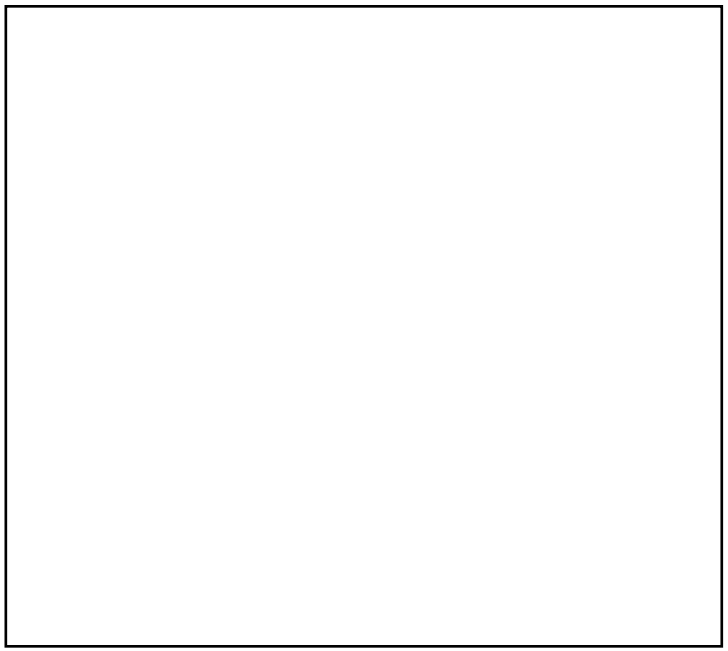

m_χ [GeV]

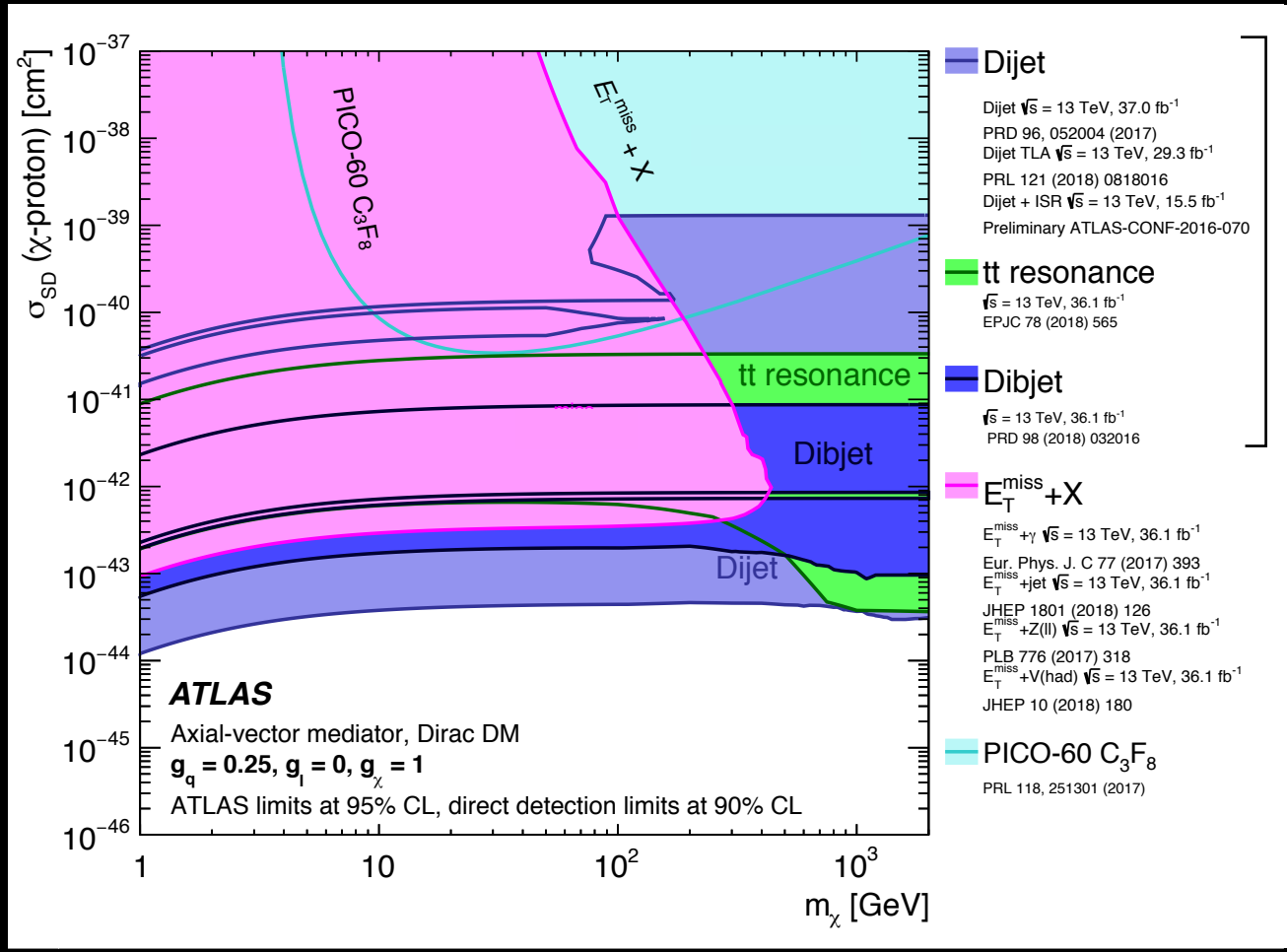

March 2019, [1903.01400]

Constraints on mediator-based dark matter and scalar dark energy models using √s =13 TeV pp collision data collected by the ATLAS detector

Complementary among various LHC results

Di-fermion summary, leptophobic

Generic features of results from non-LHC, LHC

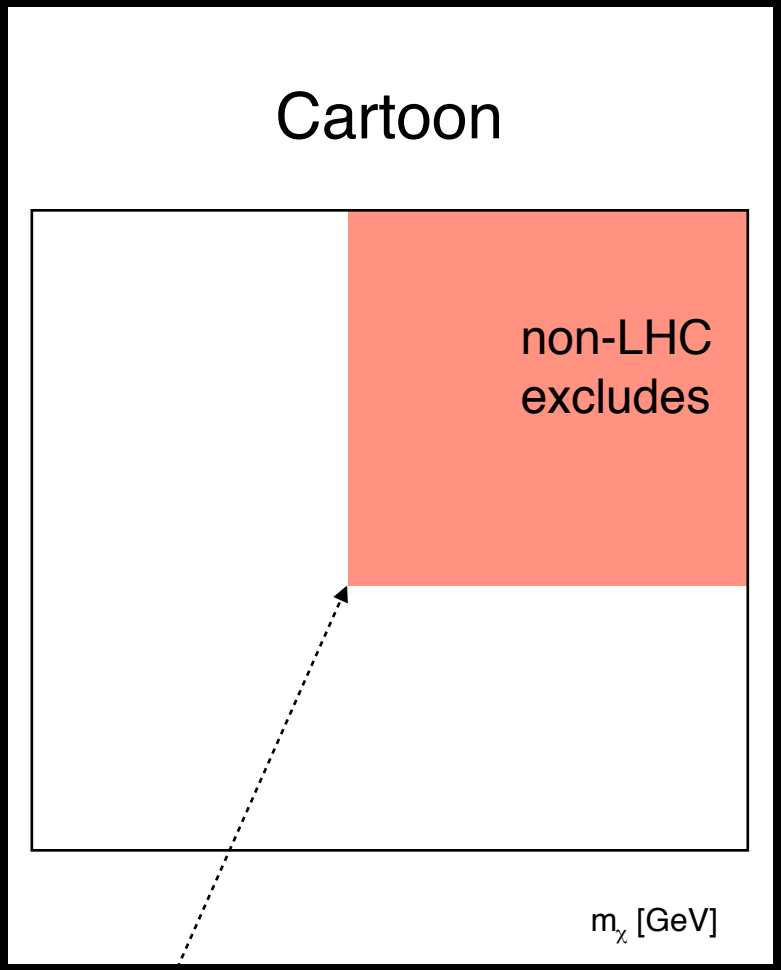

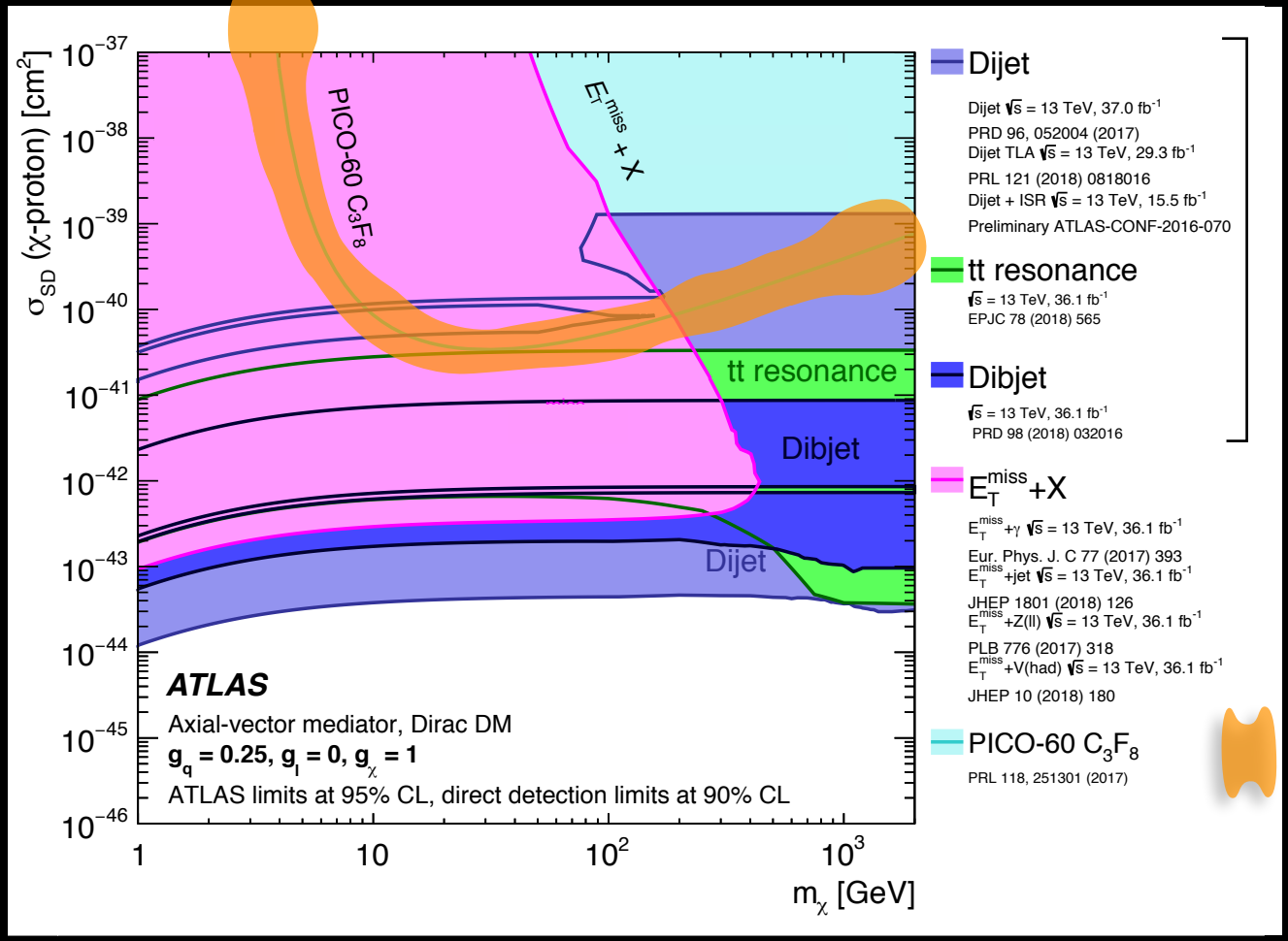

exp't limit
O(1) GeV

March 2019, [1903.01400]

Constraints on mediator-based dark matter and scalar dark energy models using √s =13 TeV pp collision data collected by the ATLAS detector

TM Hong
Pittsburgh

Complementary among various LHC results

Di-fermion summary, leptophobic

Generic features of results from non-LHC, LHC

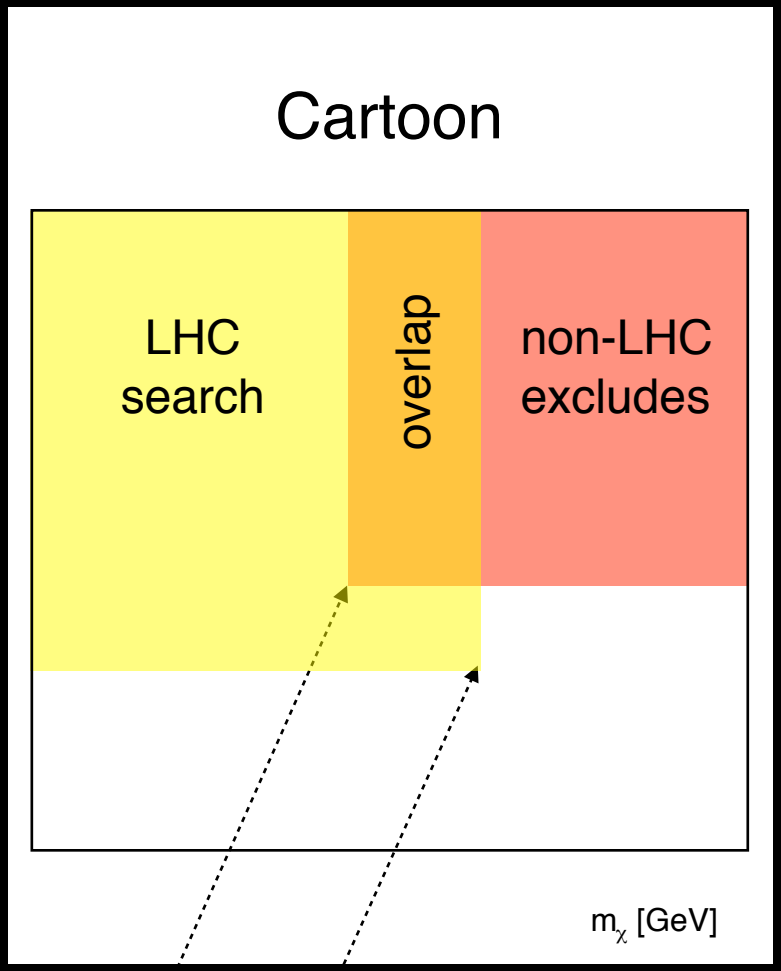

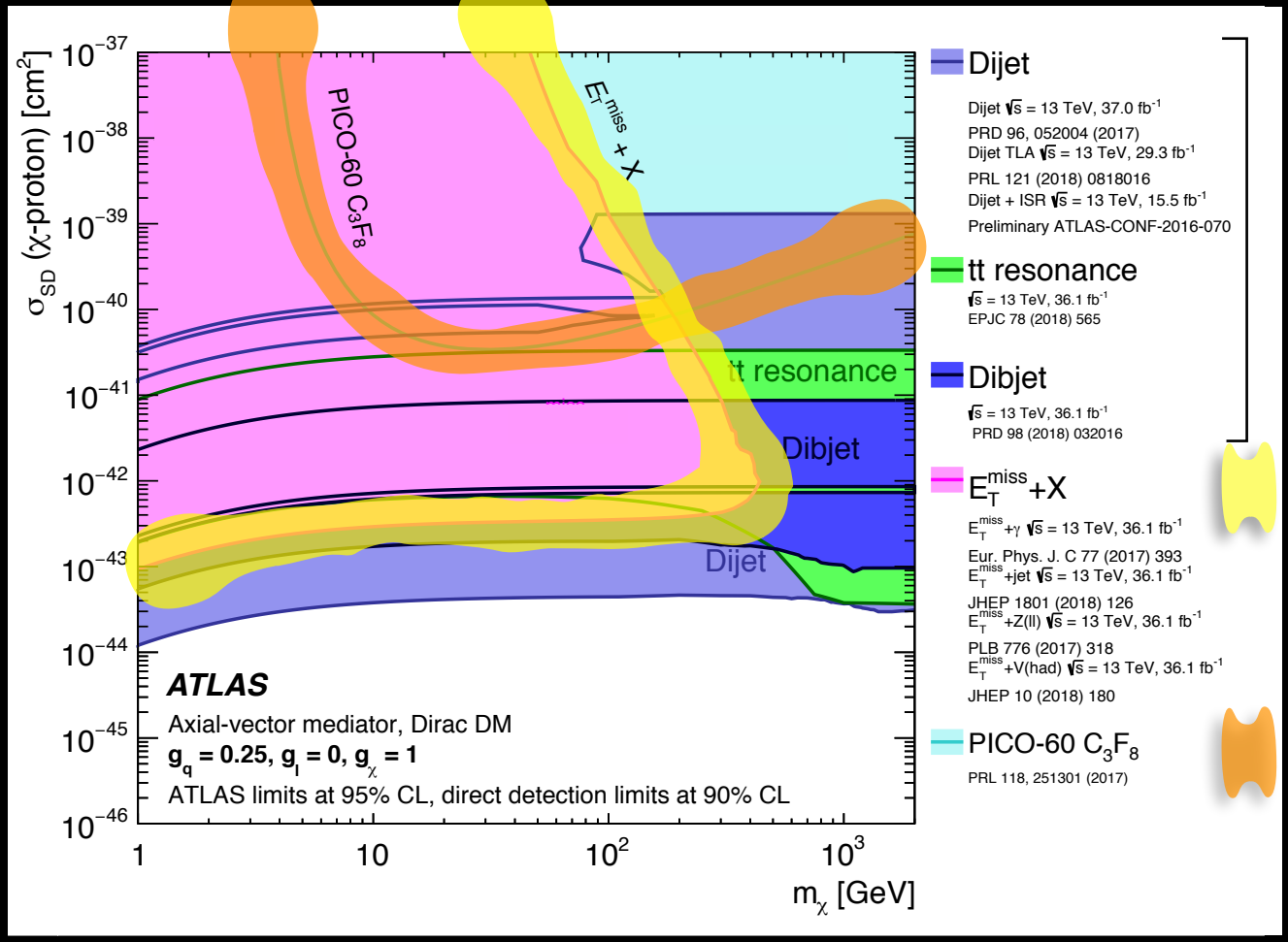

exp't limit
O(1) GeV

$m_{mediator}$
O(100) GeV

March 2019, [1903.01400]

Constraints on mediator-based dark matter and scalar dark energy models using √s =13 TeV pp collision data collected by the ATLAS detector

Complementary among various LHC results

Di-fermion summary, leptophobic

Generic features of results from non-LHC, LHC

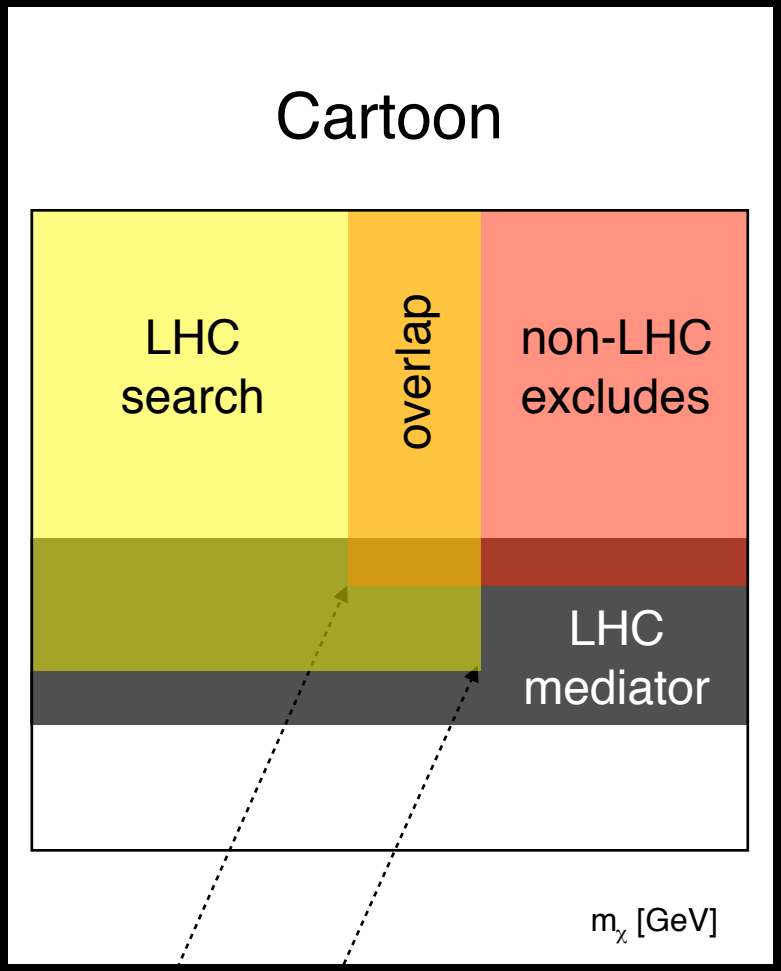

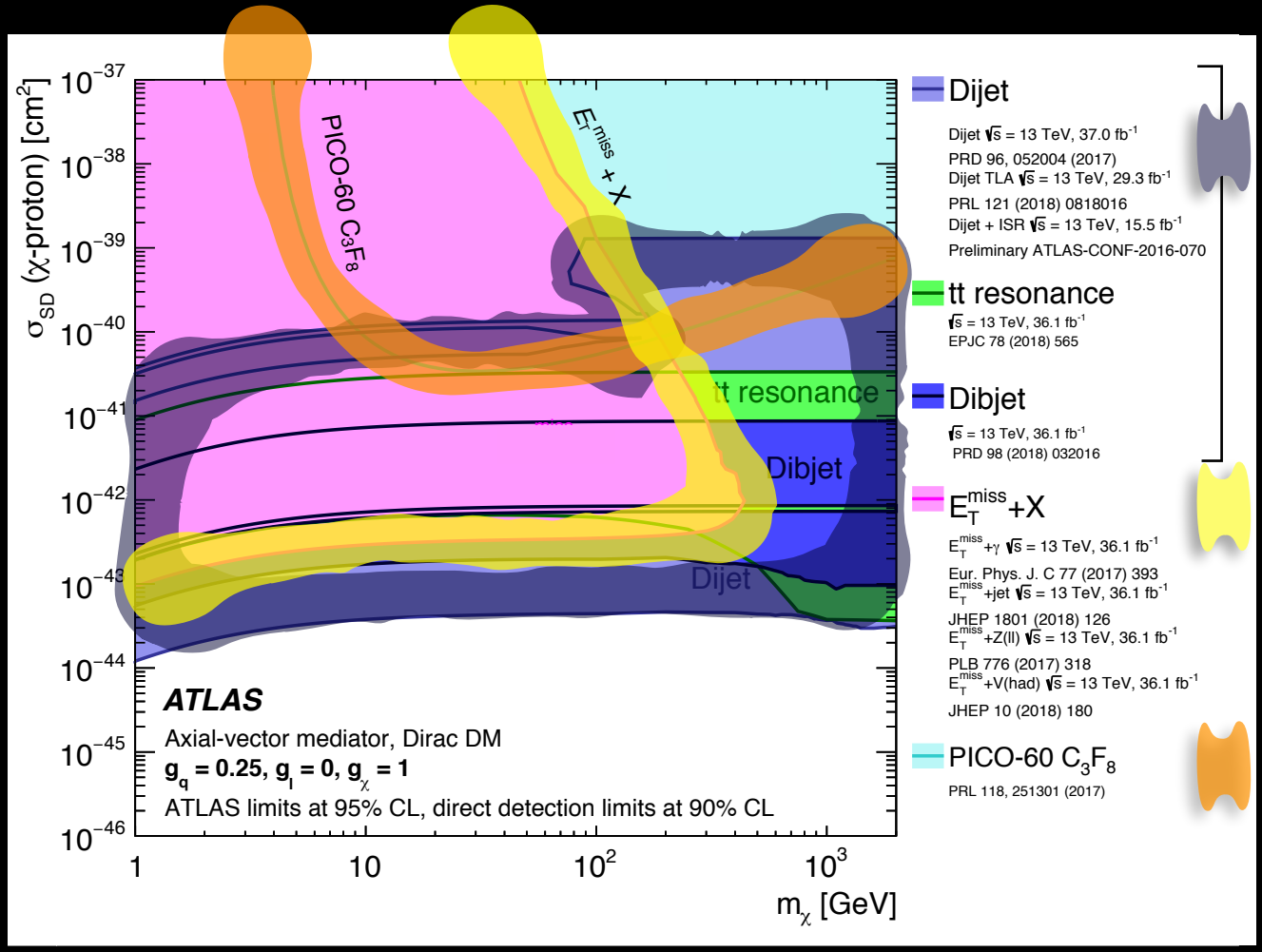

exp't limit
O(1) GeV

$m_{mediator}$
O(100) GeV

March 2019, [1903.01400]

Constraints on mediator-based dark matter and scalar dark energy models using √s =13 TeV pp collision data collected by the ATLAS detector

Complementary among various LHC results

Higgs as mediator

Motivation

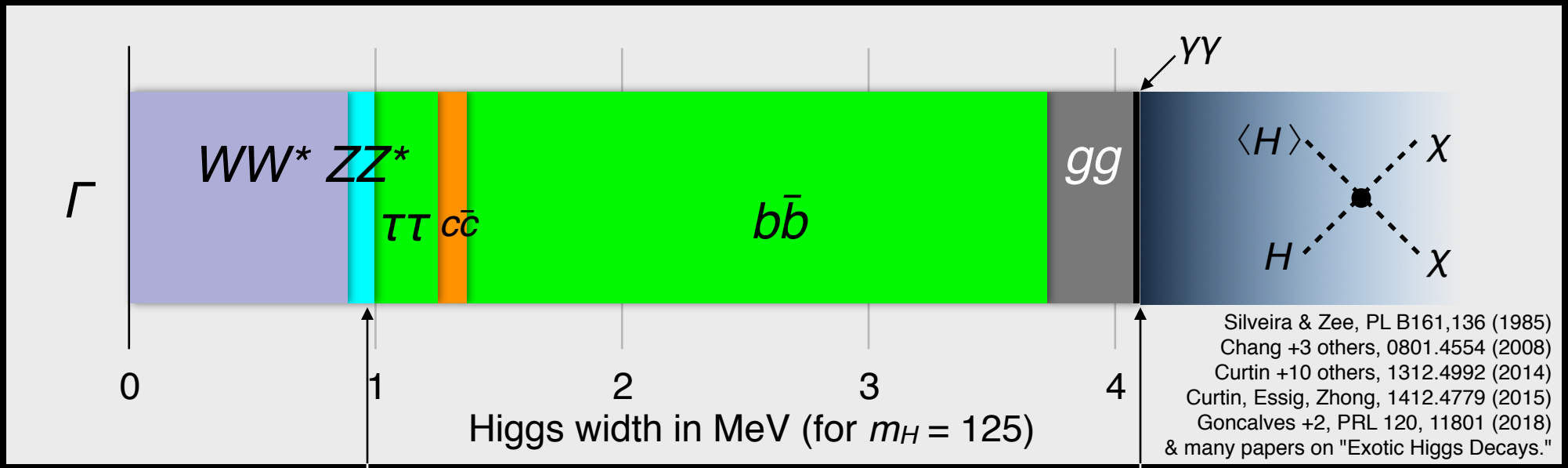

Even $g \sim 1/100$ coupling gives $\Gamma_{invisible} \sim 1$ MeV

Higgs as mediator

Motivation

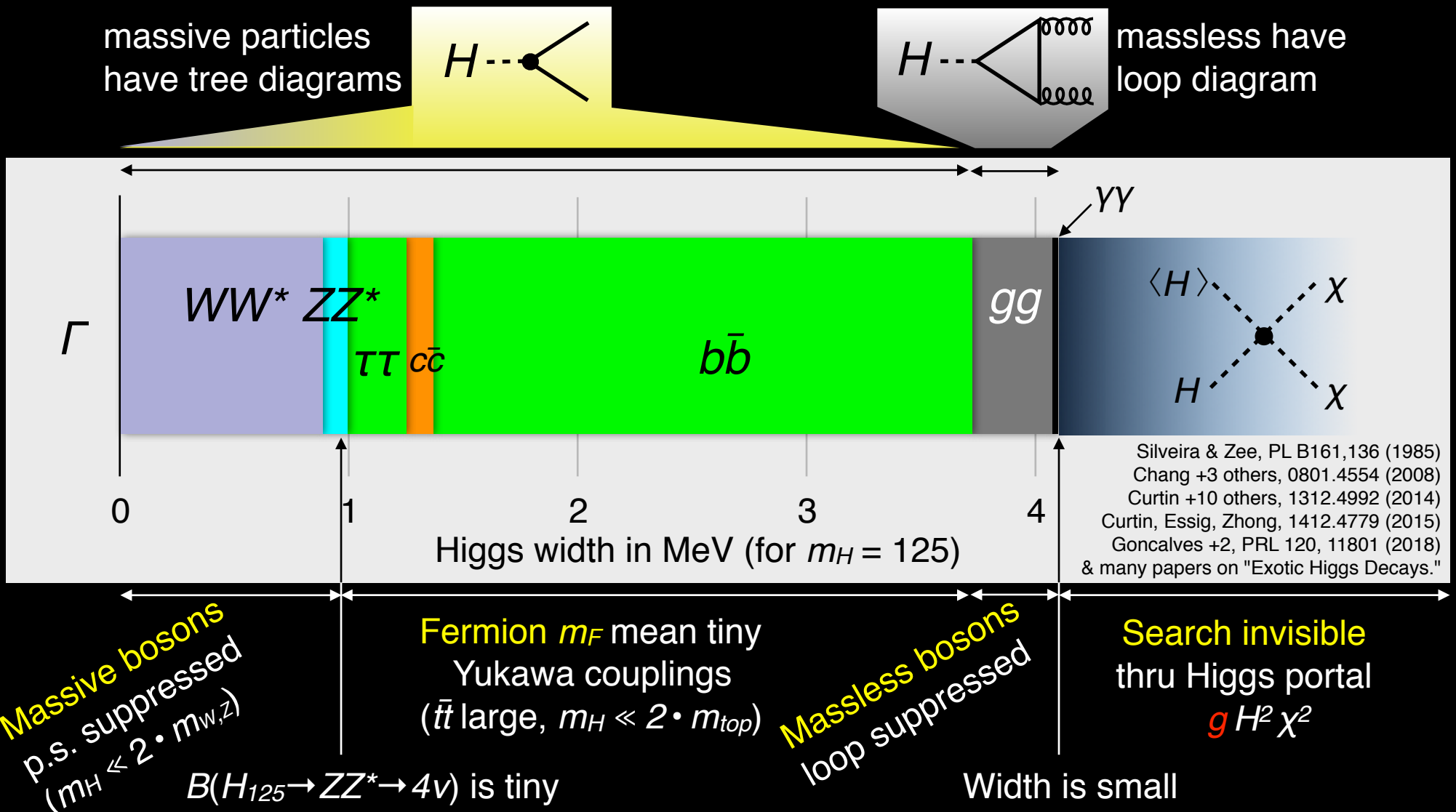

Even $g \sim 1/100$ coupling gives $\Gamma_{invisible} \sim 1$ MeV

More figures & tables

(with captions)

https://cern.ch/twiki/bin/view/AtlasPublic/TriggerOperationPublicResults

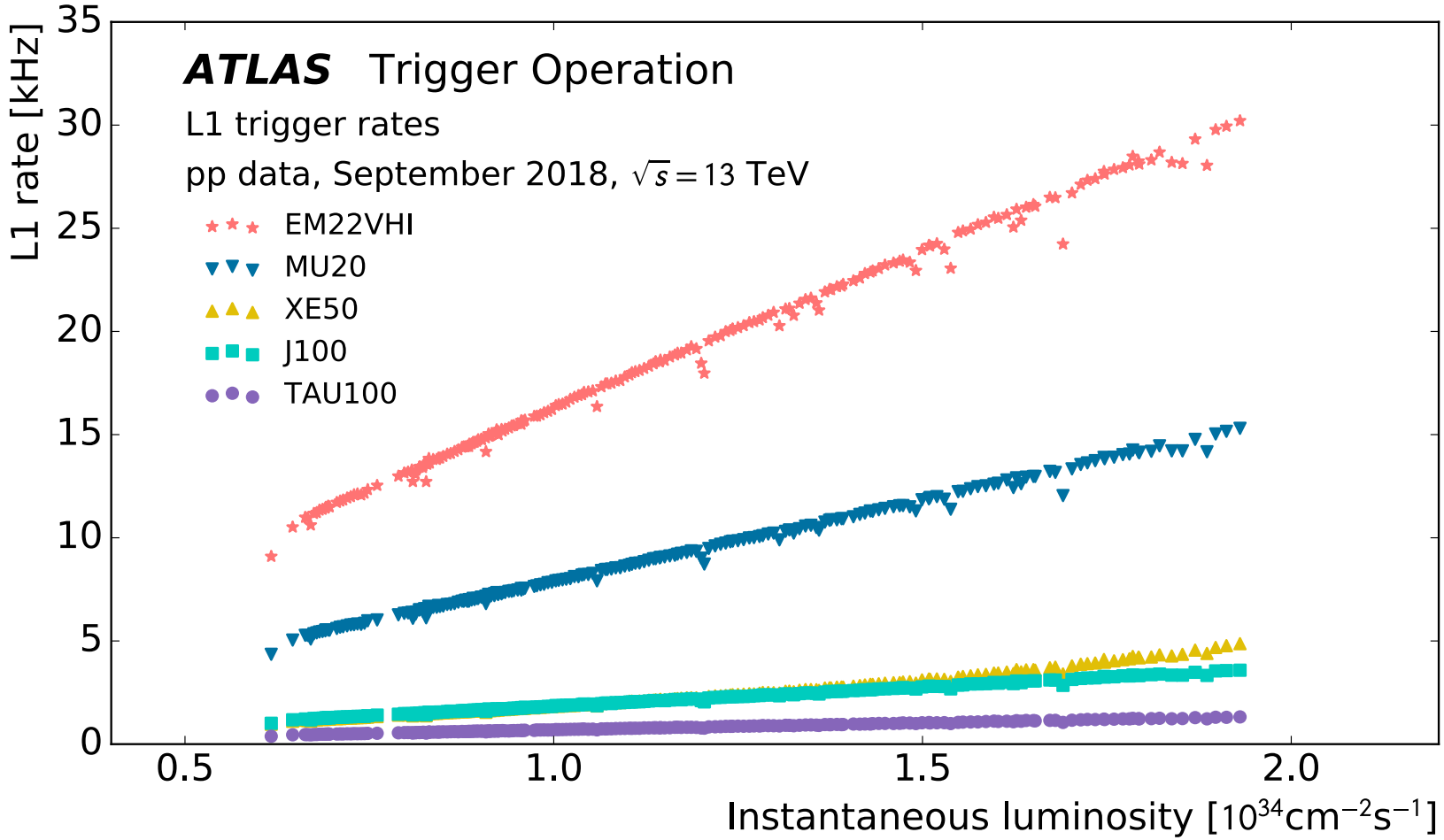

Level-1 (L1) physics trigger rates as a function of instantaneous luminosity in a fill taken in September 2018 with a peak luminosity of L = 2.0 x 1034 cm-2s-1 and a peak average number of interactions per crossing of <μ>=56. Presented are rates of some representative single-object trigger items, which have not been prescaled. These trigger items are based on such objects as electromagnetic clusters (EM), muon candidates (MU), jet candidates (J), missing transverse energy (XE) and tau candidates (TAU). The number in the trigger name denotes the trigger threshold in GeV. The letters following the threshold values refer to details of the selection: variable thresholds (V), hadronic isolation (H), and electromagnetic isolation (I). Dips in the rates are due to dead-time and spikes are caused by detector noise.

https://cern.ch/twiki/bin/view/AtlasPublic/MissingEtTriggerPublicResults

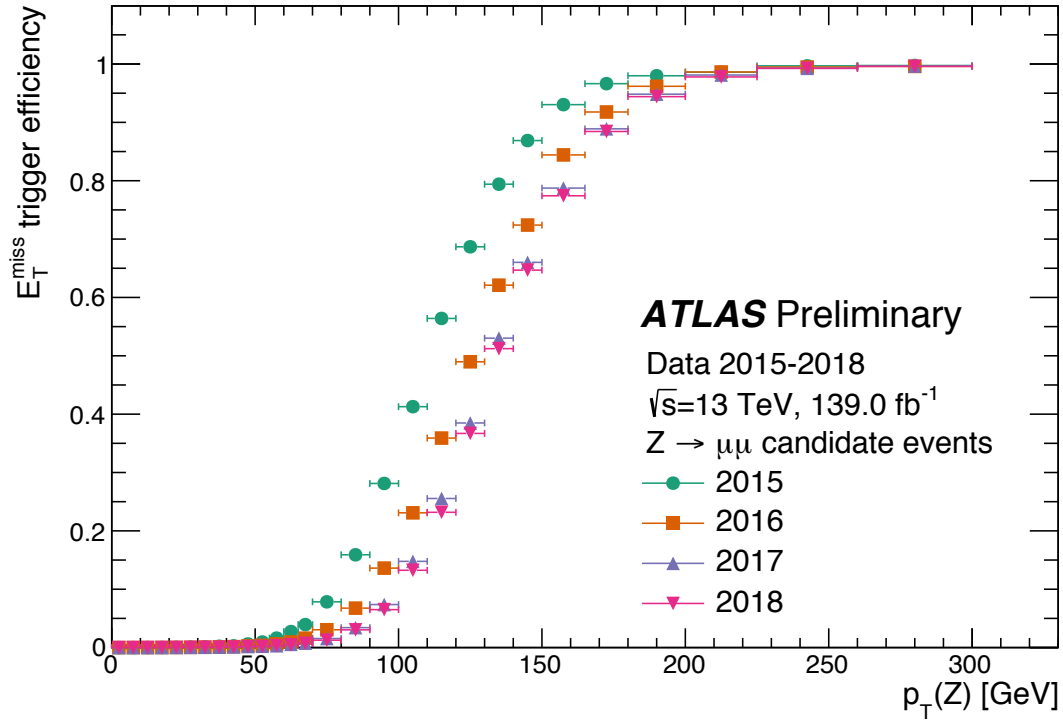

The combined L1 and HLT efficiency of the lowest unprescaled missing transverse energy triggers for the years 2015 to 2018 are shown as a function of the Z boson transverse momentum. The events are taken from data with a Z -> mumu selection, and the transverse momentum of the Z boson is used as a proxy for the missing transverse momentum in the event, as muons are treated as invisible objects by the triggers concerned. Depending on the data-taking period, the HLT E_T,miss was calculated by one or a combination of the algorithms "cell", "mht", or "pufit". In the "cell" algorithm, the E_T,miss is calculated as the negative of the transverse momentum vector sum of all calorimeter cells passing a two-sided noise cut. In the "mht" algorithm, the E_T,miss is calculated as the negative of the transverse momentum vector sum of all jets reconstructed by the anti-k_t jet finding algorithm from calorimeter topological clusters. These jets have pileup subtraction and JES calibration applied. In the "pufit" algorithm, the E_T,miss is calculated as the negative of the transverse momentum vector sum of all calorimeter topological clusters corrected for pileup. The pileup correction is done by grouping the clusters into coarser "towers" which are then marked as pileup if their E_T falls below a pileup-dependent threshold. A fit to below-threshold towers is performed, taking into account resolutions, making the assumption that the contribution of the pileup to E_T,miss is zero. The fitted pileup E_T density is used to correct the above-threshold towers. In later years, the thresholds for these algorithms were raised to compensate for increased pileup, and therefore lower efficiencies in the turn on region were observed. High efficiency was maintained for events with E_T,miss > 200 GeV throughout all years.

Mono-jet, Phys. Rev. D 94 (2016) 032005

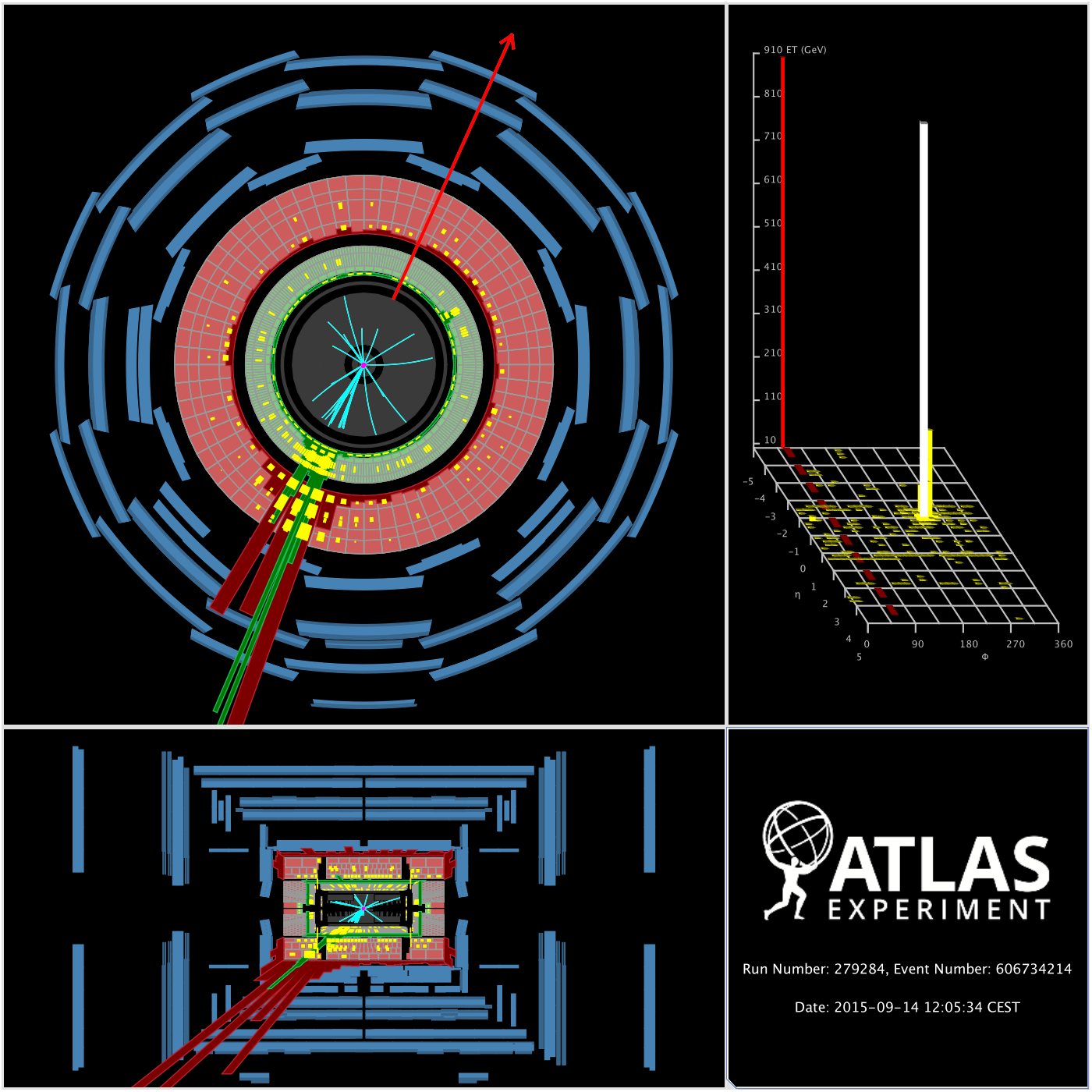

Figure 9:
The highest E_T^{miss} monojet event in the 2015 ATLAS data (Event 606734214, Run 279284). A jet with p_T of 973 GeV, indicated by the green and red bars corresponding to the energy deposition in the calorimeters, is balanced by a E_T^{miss} of 954 GeV, shown as the red arrow. Tracks with p_T above 2 GeV are displayed in the inner detector.

Mono-jet, JHEP 01 (2018) 126

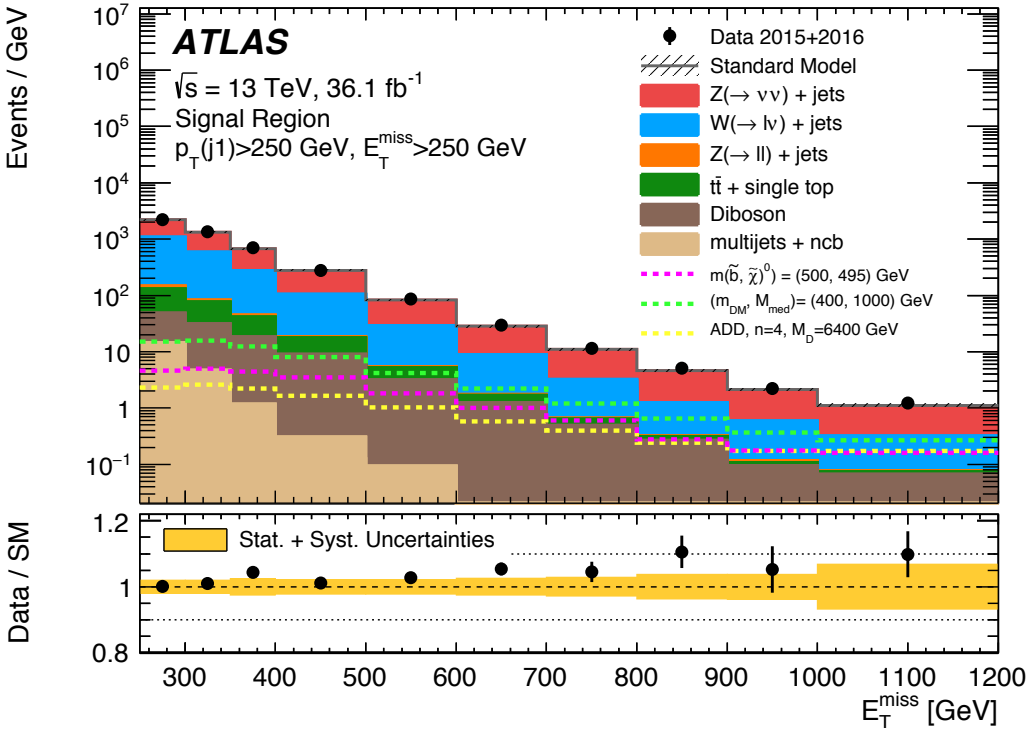

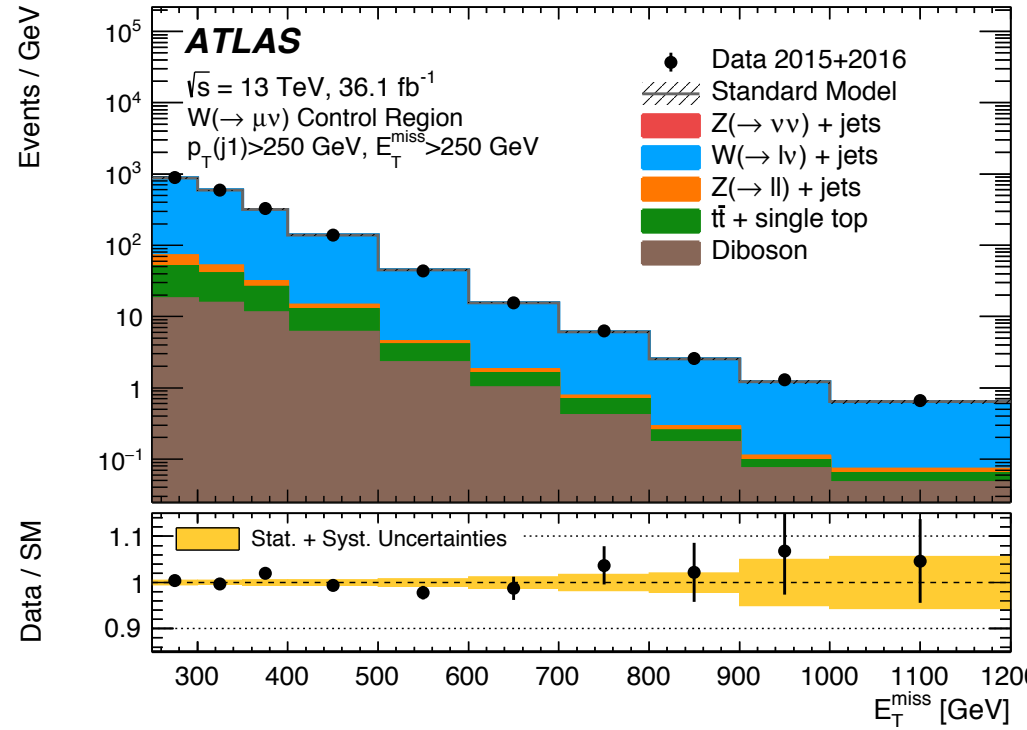

Figure 4a:
Measured distributions of the (a) E_T^{miss}, (b) leading-jet p_T, (c) leading-jet $|\eta|$, and (d) jet multiplicity for the E_T^{miss} >250GeV selection compared to the SM predictions. The latter are normalized with normalization factors as determined by the global fit that considers exclusive E_T^{miss} regions. For illustration purposes, the distributions of example ADD, SUSY, and WIMP scenarios are included. The error bands in the ratios shown in the lower panels include both the statistical and systematic uncertainties in the background predictions. The last bin of the E_T^{miss} and leading-jet p_T distributions contains overflows. The contributions from multijet and non-collision backgrounds are negligible and are only shown in the case of the E_T^{miss} distribution.

Figure 2a:
The measured (a),(c),(e) E_T^{miss} and (b),(d),(f) leading-jet p_T distributions in the W(→ μ ν)+jets, W(→ e ν)+jets, and Z/γ*(→ μ⁺μ⁻)+jets control regions, for the E_T^{miss} > 250GeV inclusive selection, compared to the background predictions. The latter include the global normalization factors extracted from the fit. The error bands in the ratios include the statistical and systematic uncertainties in the background predictions as determined by the binned-likelihood fit to the data in the control regions. The last bin of the E_T^{miss} and leading-jet p_T distributions contains overflows. The contributions from multijet and non-collision backgrounds are negligible and are not shown in the Figures.

Mono-jet, JHEP 01 (2018) 126

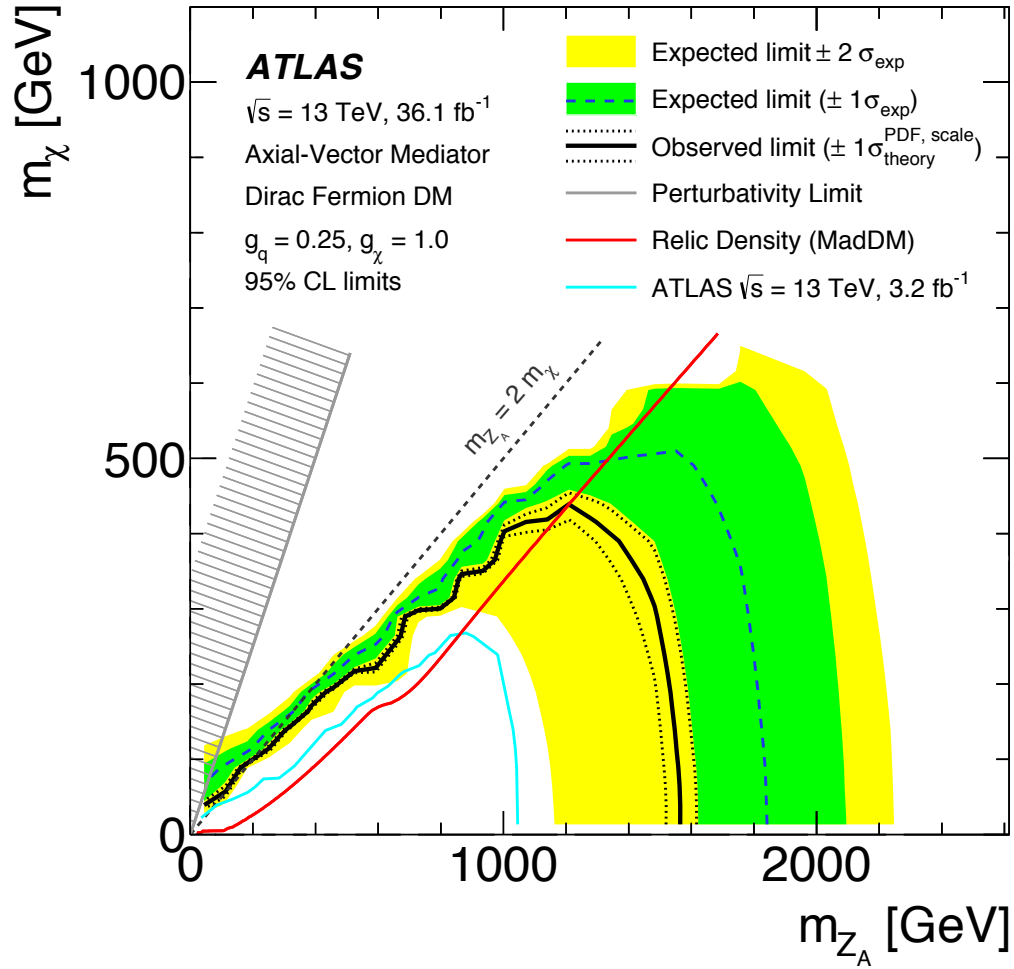

Figure 5a:
(a) Axial-vector 95% CL exclusion contours in the m_{ZA}–m_{χ} parameter plane. The solid (dashed) curve shows the observed (expected) limit, while the bands indicate the ± 1σ theory uncertainties in the observed limit and ± 1σ and ± 2σ ranges of the expected limit in the absence of a signal. The red curve corresponds to the set of points for which the expected relic density is consistent with the WMAP measurements (i.e. $\Omega h^2 = 0.12$), as computed with MadDM [95]. The region on the right of the curve corresponds to higher predicted relic abundance than these measurements. The region excluded due to perturbativity, defined by $m_{\chi} > \sqrt{\pi}/2\ m_{ZA}$, is indicated by the hatched area. The dotted line indicates the kinematic limit for on-shell production $m_{ZA} = 2 \times m_{\chi}$. The cyan line indicates previous results at 13TeV [1] using 3.2 fb^{-1}.
(b) A comparison of the inferred limits (black line) to the constraints from direct detection experiments (purple line) on the spin-dependent WIMP–proton scattering cross section in the context of the simplified model with axial-vector couplings. Unlike in the m_{ZA}–m_{χ} parameter plane, the limits are shown at 90% CL. The results from this analysis, excluding the region to the left of the contour, are compared with limits from the PICO [96] experiment. The comparison is model-dependent and solely valid in the context of this model, assuming minimal mediator width and the coupling values g_q=1/4 and g_{χ}=1.

Mono-$H_{b\bar{b}}$, ATLAS-CONF-2018-039

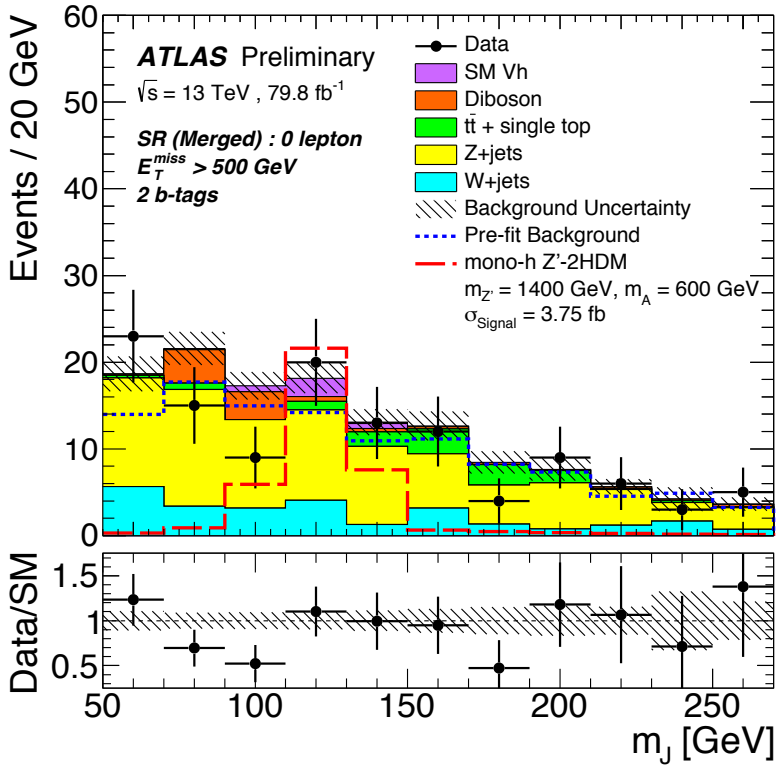

Figure 6d:
Distributions of the invariant mass of the Higgs boson candidates $m_h = m_{jj}$, m_J with two b-tagged jets in the SR for the four E_T^{miss} categories that are used as inputs to the fit. The upper panels show a comparison of data to the SM expectation before (dashed lines) and after the fit (solid histograms) with no signal included. The lower panels display the ratio of data to SM expectations after the background-only fit, with its systematic uncertainty considering correlations between individual contributions indicated by the hatched band. The expected signal from a representative Z′-2HDM model is also shown (long-dashed line), and it is scaled up by a factor of 1000 and 100 for the lowest two E_T^{miss} bins [150 GeV, 200 GeV) and [200 GeV, 350 GeV), respectively.

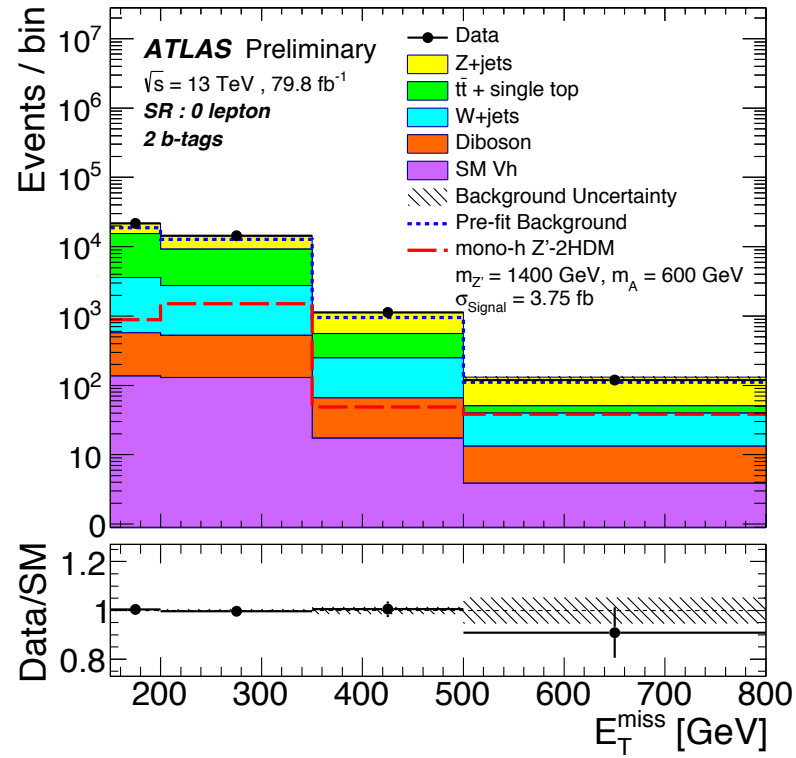

Figure 7:
E_T^{miss} distribution for the resolved and the merged signal regions combined. The upper panel shows a comparison of data to the SM expectation before (dashed lines) and after the fit (solid histograms) with no signal included. The lower panels display the ratio of data to SM expectations after the background-only fit, with its systematic uncertainty considering correlations between individual contributions indicated by the hatched band. The expected signal from a representative Z′-2HDM model is also shown (long-dashed line).

Mono-$H_{b\bar{b}}$, ATLAS-CONF-2018-039

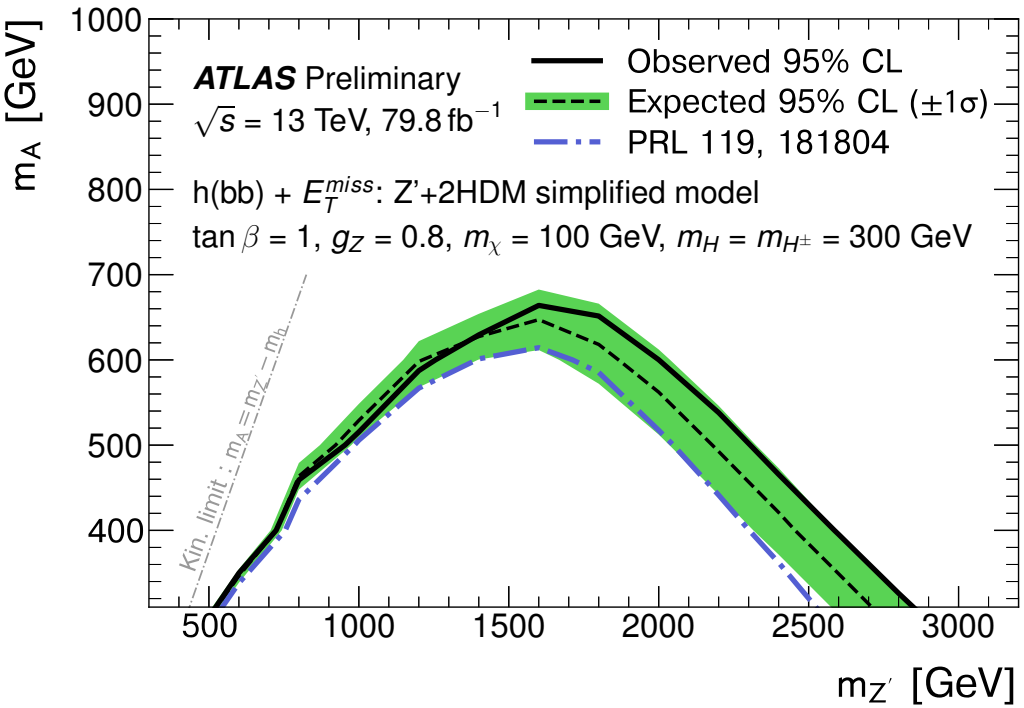

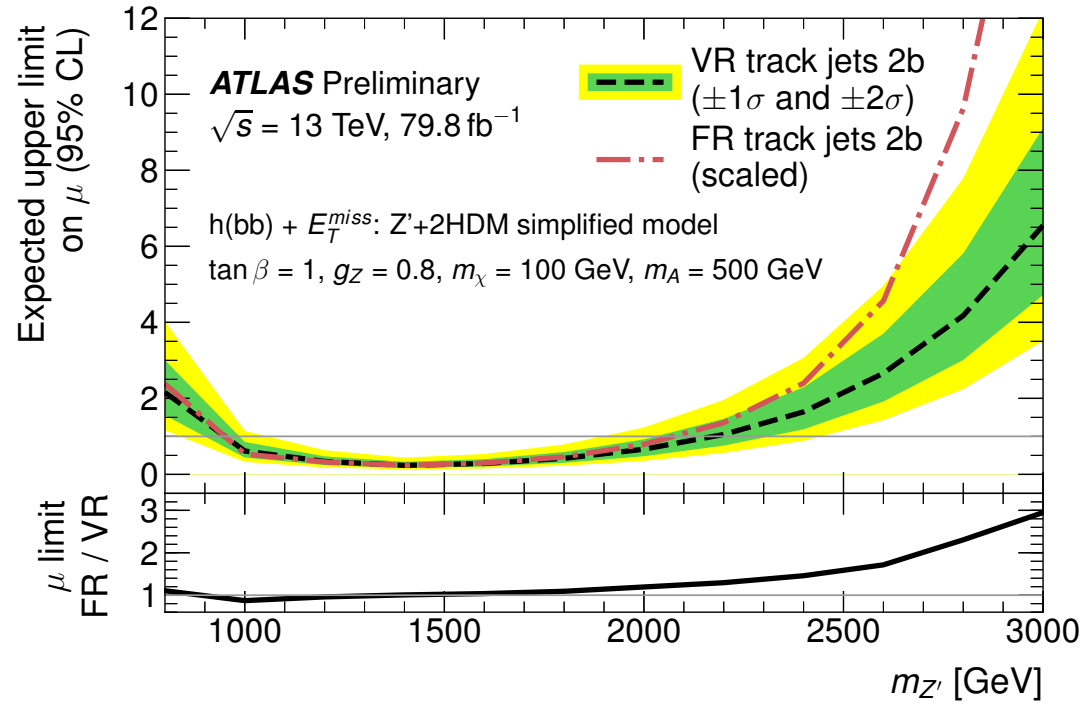

Figure 8:
Exclusion contours for the Z′-2HDM scenario in the ($m_{Z'}$,m_A) plane for tan(β) = 1, $g_{Z'}$=0.8, and m_χ=100 gev. The observed limits (solid line) are consistent with the expectation under the SM-only hypothesis (densely dashed line) within uncertainties (filled band). Observed limits from previous ATLAS results at √s = 13 TeV (dash-dotted line) are also shown.

Figure 9:
Comparison of the expected upper limits on the signal strength μ for the analysis using variable-radius (VR) track-jets (dashed line) against the previous iteration of the analysis performed with fixed-radius (FR) track-jets (dash-dotted line) with two b-tagged jet and scaled to 79.8 fb^{-1}, for fixed m_A = 500 GeV and different values of $m_{Z'}$ of the Z′-2HDM benchmark model. Other differences between the two analyses include the suppression of the multijet background using the object-based E_T^{miss} significance, reduced uncertainties from the MC statistics, and the improve calibration of the b-tagging efficiency in the VR analysis. The lower panel is the ratio of the upper limits, showing a significant improvement in the high $m_{Z'}$ region.

High-mass di-jet, ATLAS-CONF-2019-007

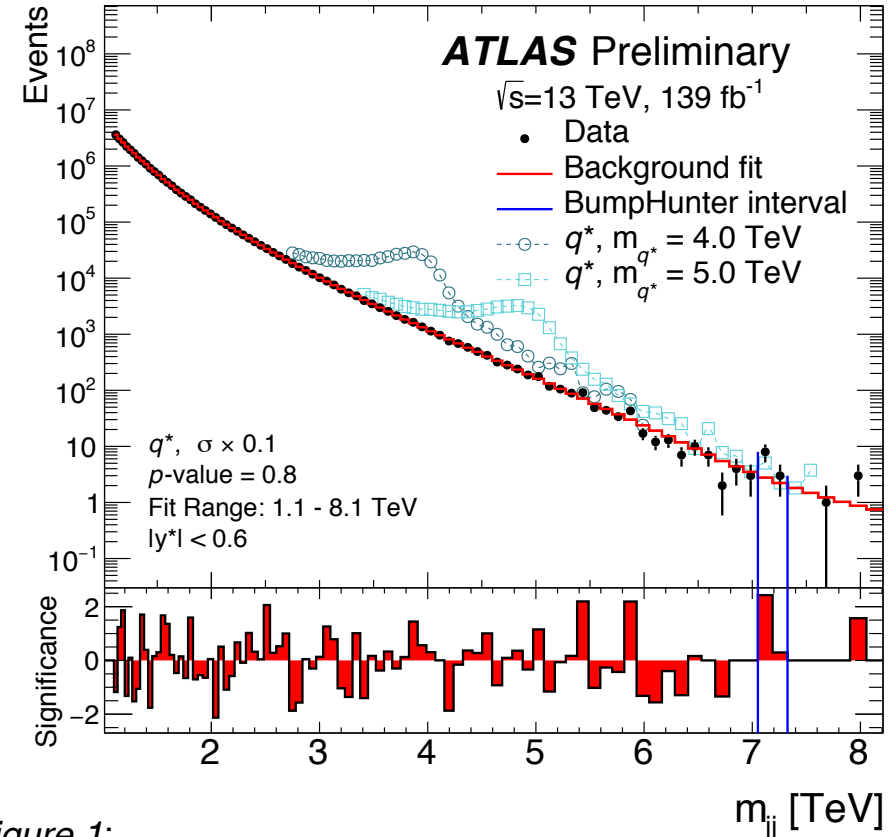

Figure 1:
The reconstructed dijet mass distribution, m_{jj}, is shown for events with $p_T > 150$,GeV for the two leading jets, with $|y^*| < 0.6$, and m_{jj} greater than 1.1,TeV (filled points). The solid line depicts the background prediction from the sliding-window fit. The vertical lines indicate the most discrepant interval identified by the BumpHunter algorithm [49,50], for which the p-value is reported in the figure. The expected contributions for q^* signal with a mass of 4 and 5 TeV are overlaid, normalized to 0.1 times their predicted cross section. The lower panel shows the bin-by-bin significance of the data-fit discrepancy, based only on statistical uncertainties.

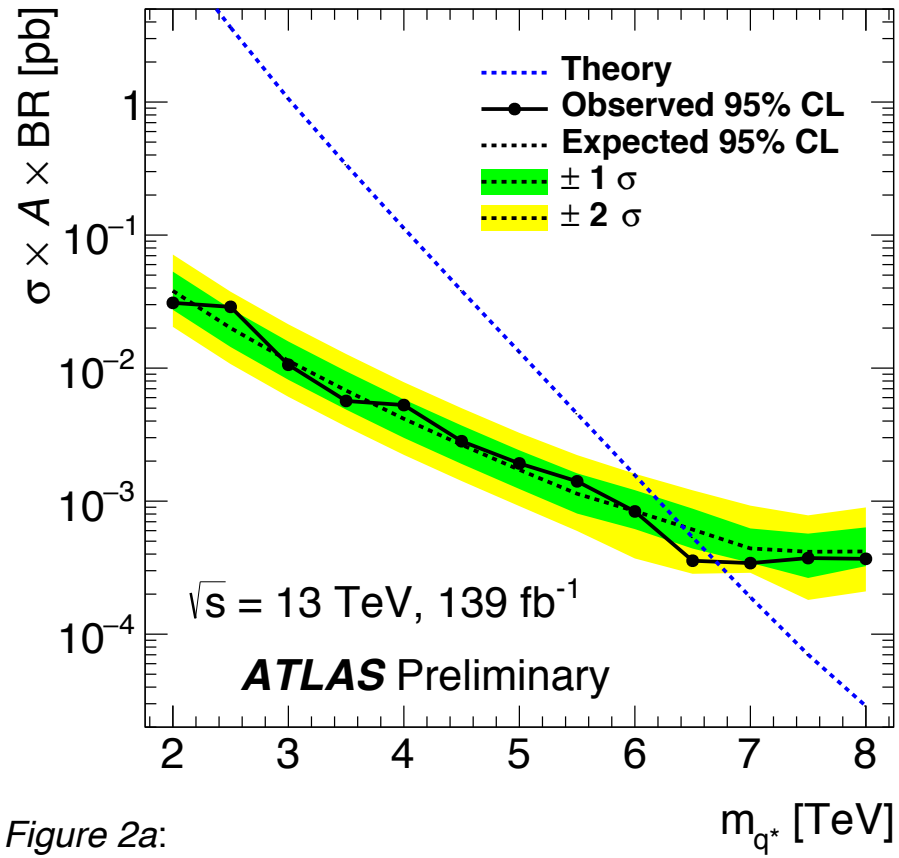

Figure 2a:
The 95% CL upper limit obtained from the dijet invariant mass (m_{jj}) distribution on cross-section times acceptance times branching ratio to two jets, σ× A × BR, as a function of (a) the mass of a q^* signal (m_{q^*}) and (b) the mass of a hypothetical signal that produces a Gaussian-shaped contribution to the m_{jj} distribution. For Gaussian-shaped signals the observed limits are reported for different width hypotheses σ_G. The expected limit and corresponding ±1σ and ±2σ uncertainty bands are also indicated for the q^* model in (a). Limits corresponding to a Gaussian-shaped signal with a relative width of 15% are set up to m_G=6,TeV due to the poor background estimation when a broad signal overlaps the upper end of the m_{jj} spectrum.

High-mass di-jet, ATLAS-CONF-2019-007

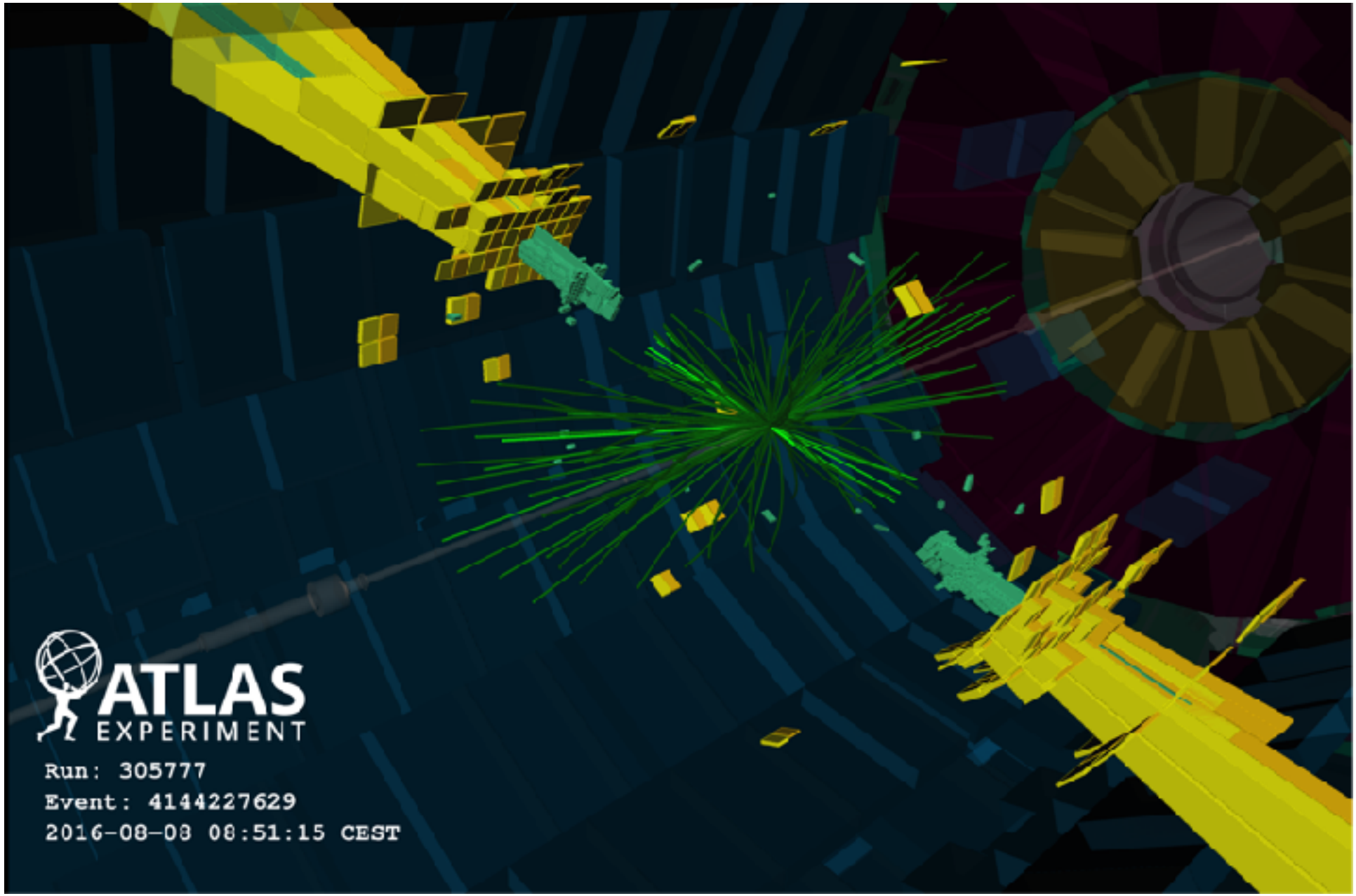

Figure 3:
A visualization of the highest-mass dijet event, (Event 4144227629, Run 305777) recorded in 2016: the two central high-p_T jets each have transverse momenta of 3.74 TeV, they have a y^* of 0.38 and their invariant mass is 8.02 TeV.

High-mass di-jet, ATLAS-CONF-2019-007

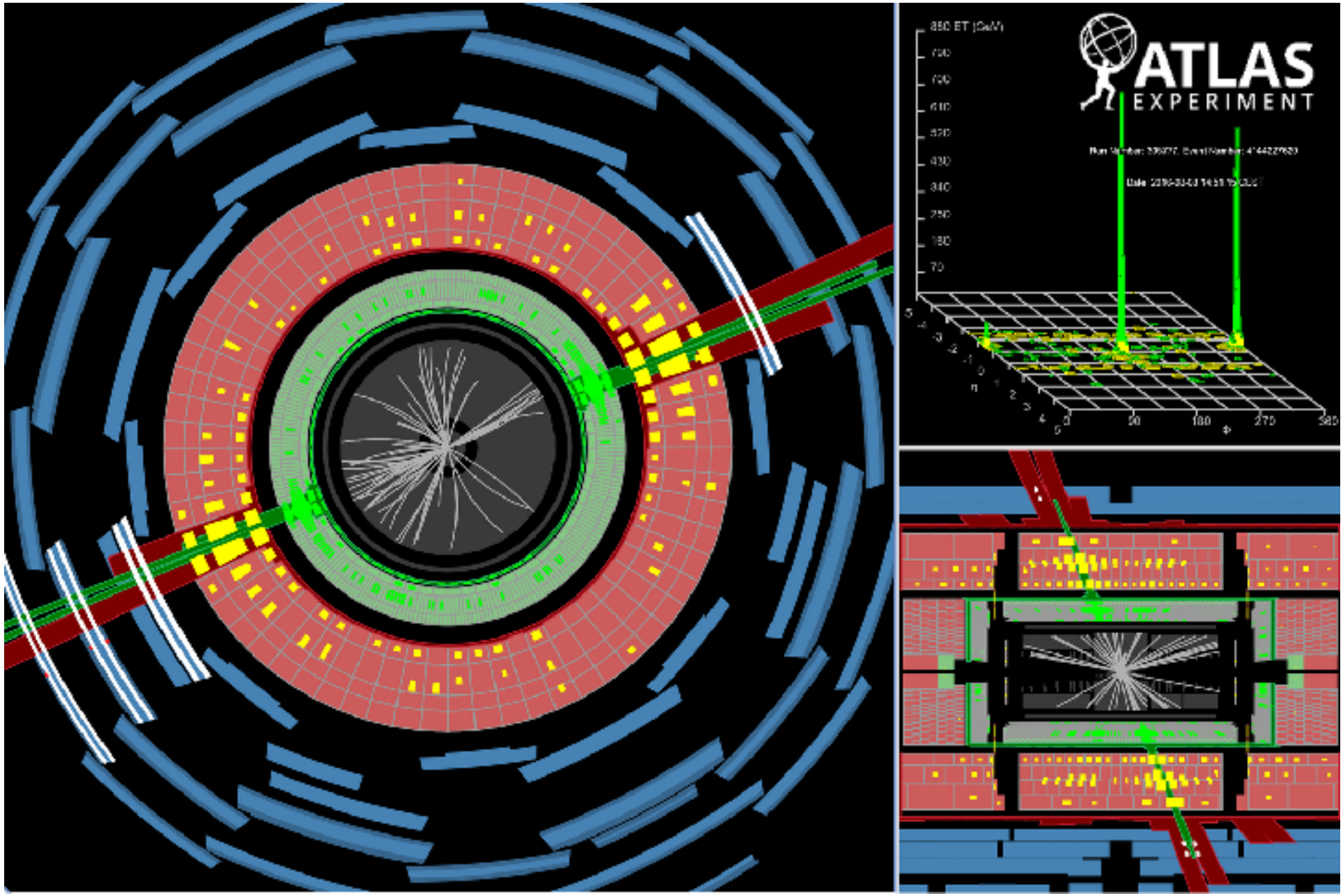

Figure 4 (same event as 3):
A visualization of the highest-mass dijet event, (Event 4144227629, Run 305777) recorded in 2016: the two central high-p_T jets each have transverse momenta of 3.74 TeV, they have a y^* of 0.38 and their invariant mass is 8.02 TeV.

High-mass di-jet, ATLAS-CONF-2019-007

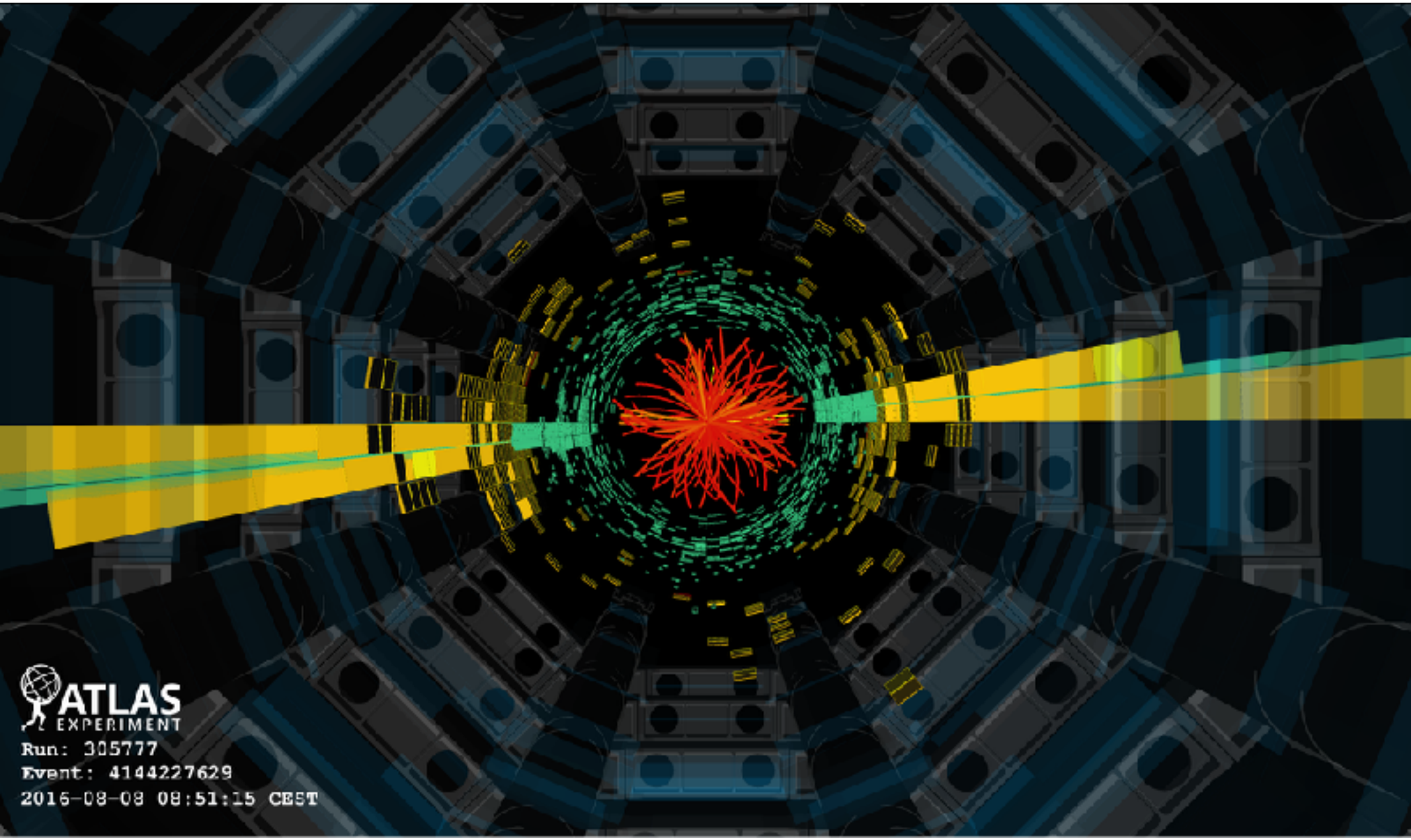

Figure 5 (same event as 3):
A visualization of the highest-mass dijet event, (Event 4144227629, Run 305777) recorded in 2016: the two central high-p_T jets each have transverse momenta of 3.74 TeV, they have a y^* of 0.38 and their invariant mass is 8.02 TeV.

DM summary paper, JHEP 05 (2019) 142

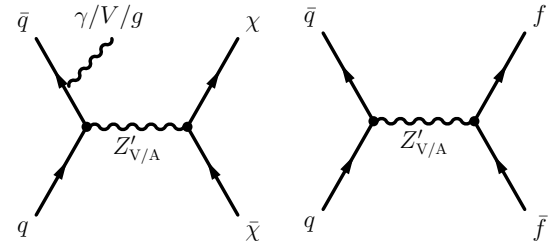

Figure 1: Schematic representation of the dominant production and decay modes for the V/AV model.

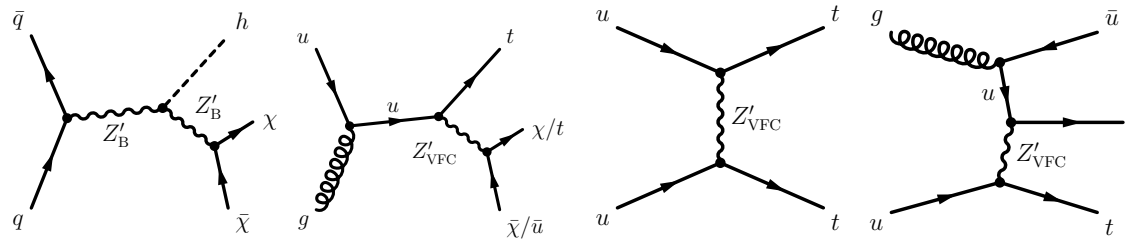

Figure 2: Schematic representation of the dominant production and decay modes for the (a) VBC model and (b,c,d) VFC model.

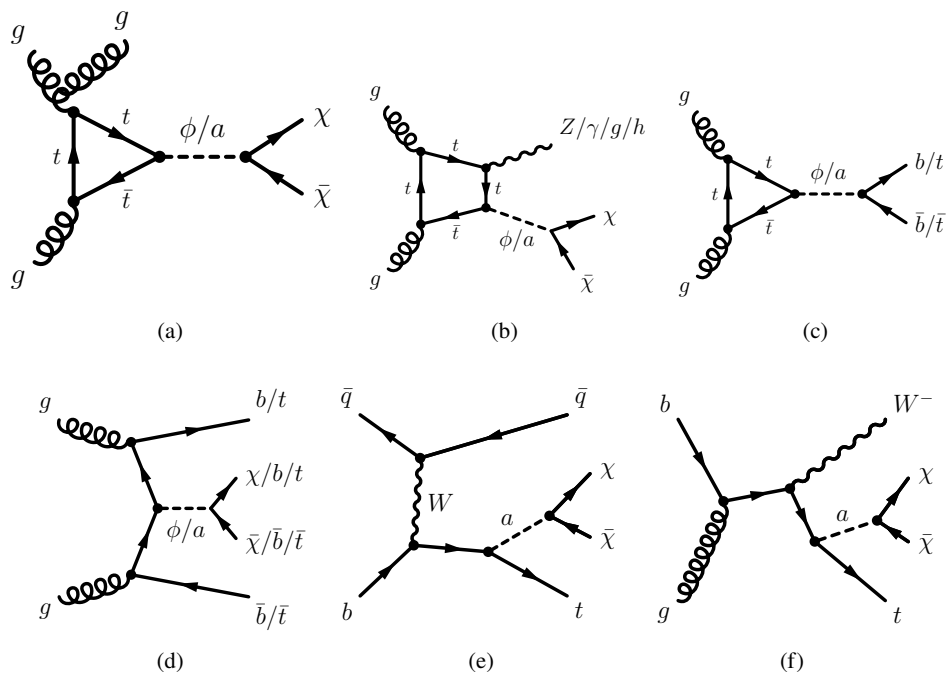

Figure 3: Schematic representation of the dominant production and decay modes for the S/PS models.

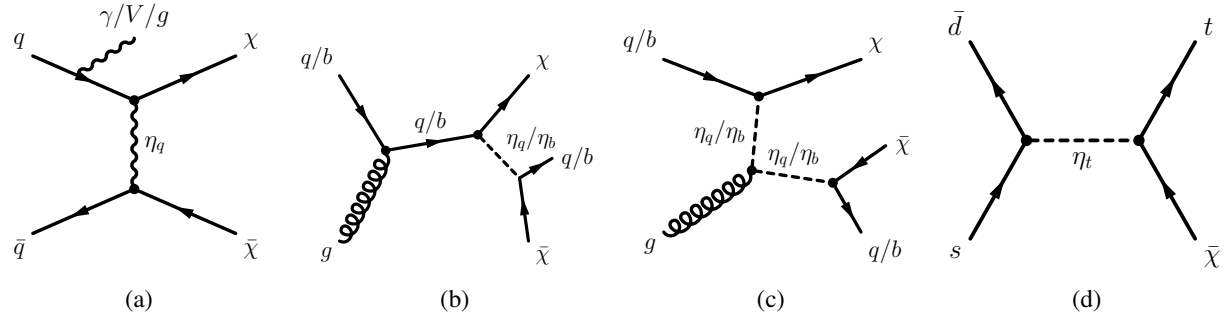

Figure 4: Schematic representation of the dominant production and decay modes for the SCC models.

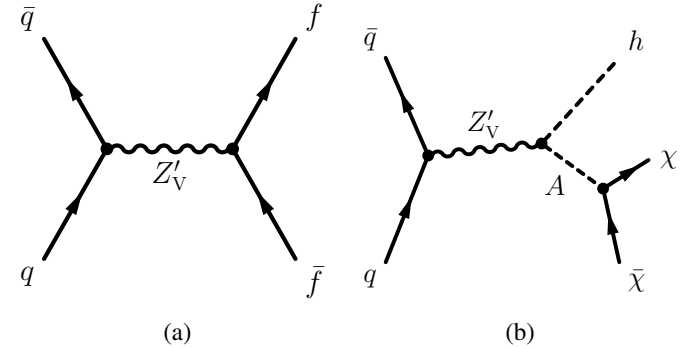

Figure 5: Schematic representation of the dominant production and decay modes for the 2HDM+Z'_{V} model.

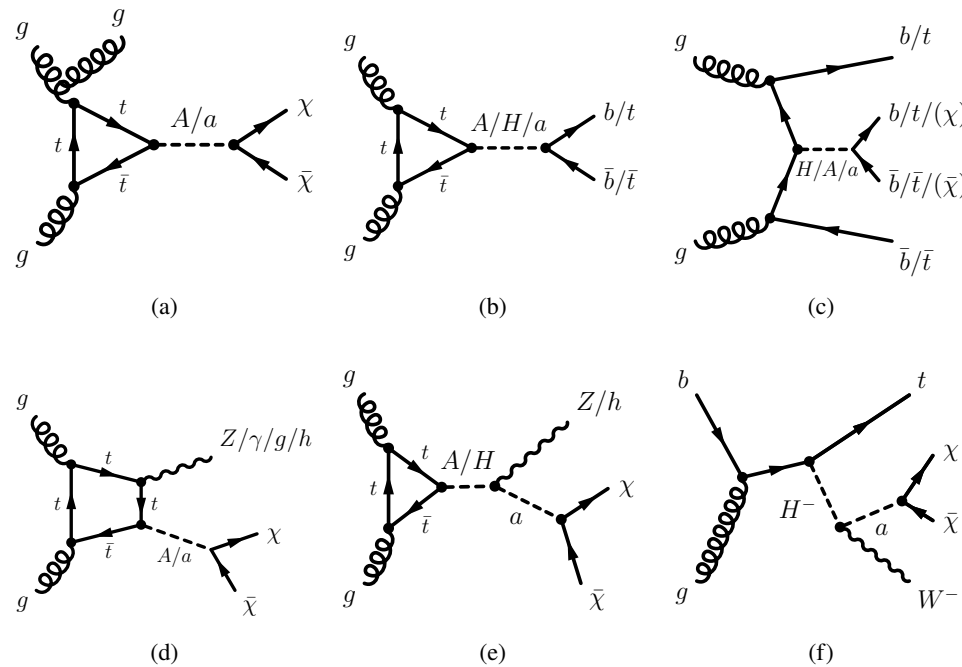

Figure 6: Schematic representation of the dominant production and decay modes for the 2HDM+a model.

DM summary paper, JHEP 05 (2019) 142

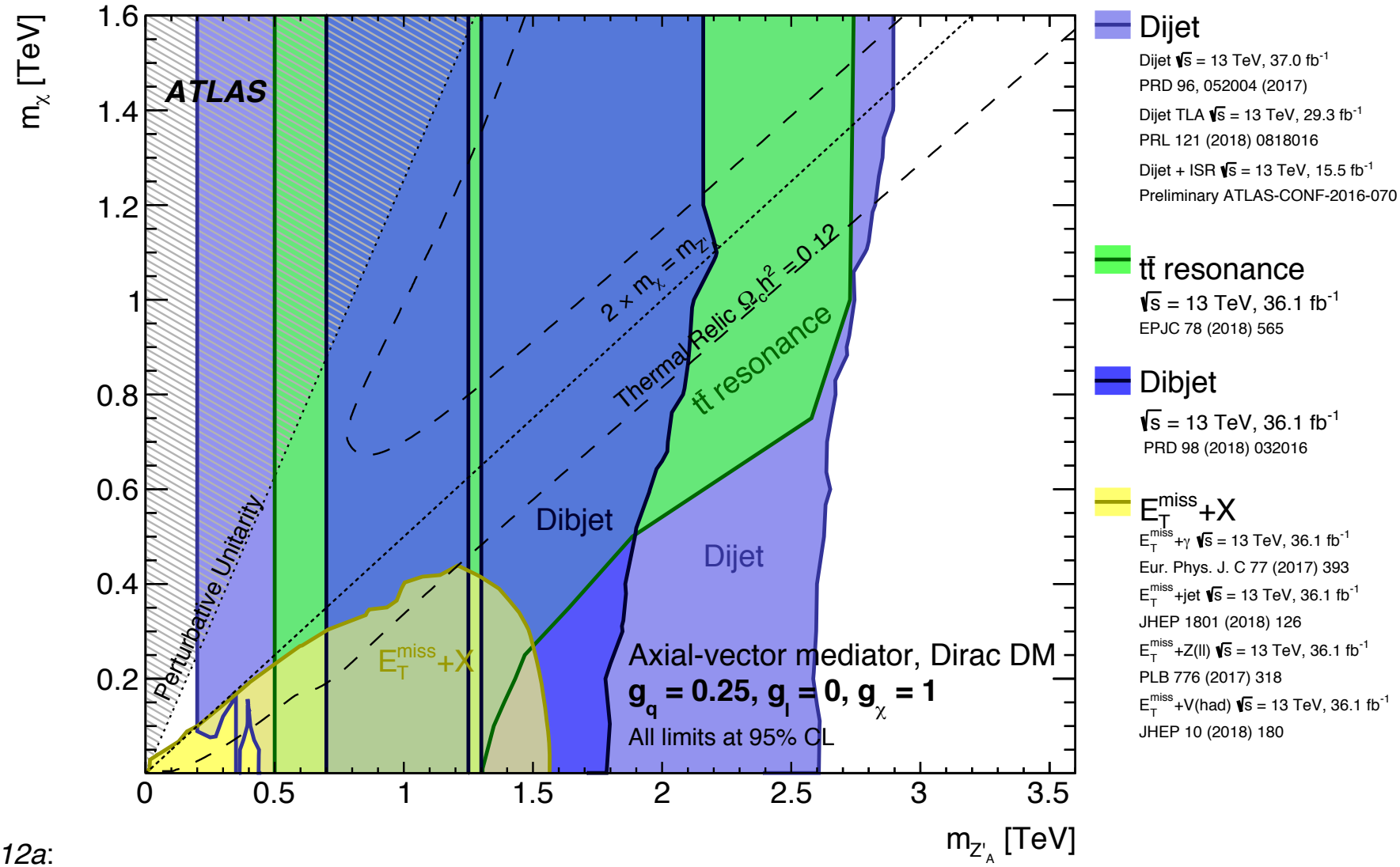

Figure 12a:
Regions in a (mediator-mass, DM-mass) plane excluded at 95% CL by visible and invisible searches, for leptophobic (a) or leptophilic (b) axial-vector mediator simplified models. The exclusions are computed for a DM coupling g_χ, quark coupling g_q, universal to all flavours, and lepton coupling g_ℓ; as indicated in each case. Dashed curves labelled ``thermal relic'' correspond to combinations of DM and mediator mass values that are consistent with a DM density of $\Omega h^2 = 0.12$ and a standard thermal history, as computed in MadDM [arXiv:1703.05703,arXiv:1509.03683]. Between the two curves, annihilation processes described by the simplified model deplete Ωh^2 to below 0.12 . A dotted line indicates the kinematic threshold where the mediator can decay on-shell into DM. Excluded regions that are in tension with the perturbative unitary considerations of [arXiv:1510.02110] are indicated by shading in the upper left corner.

DM summary paper, JHEP 05 (2019) 142

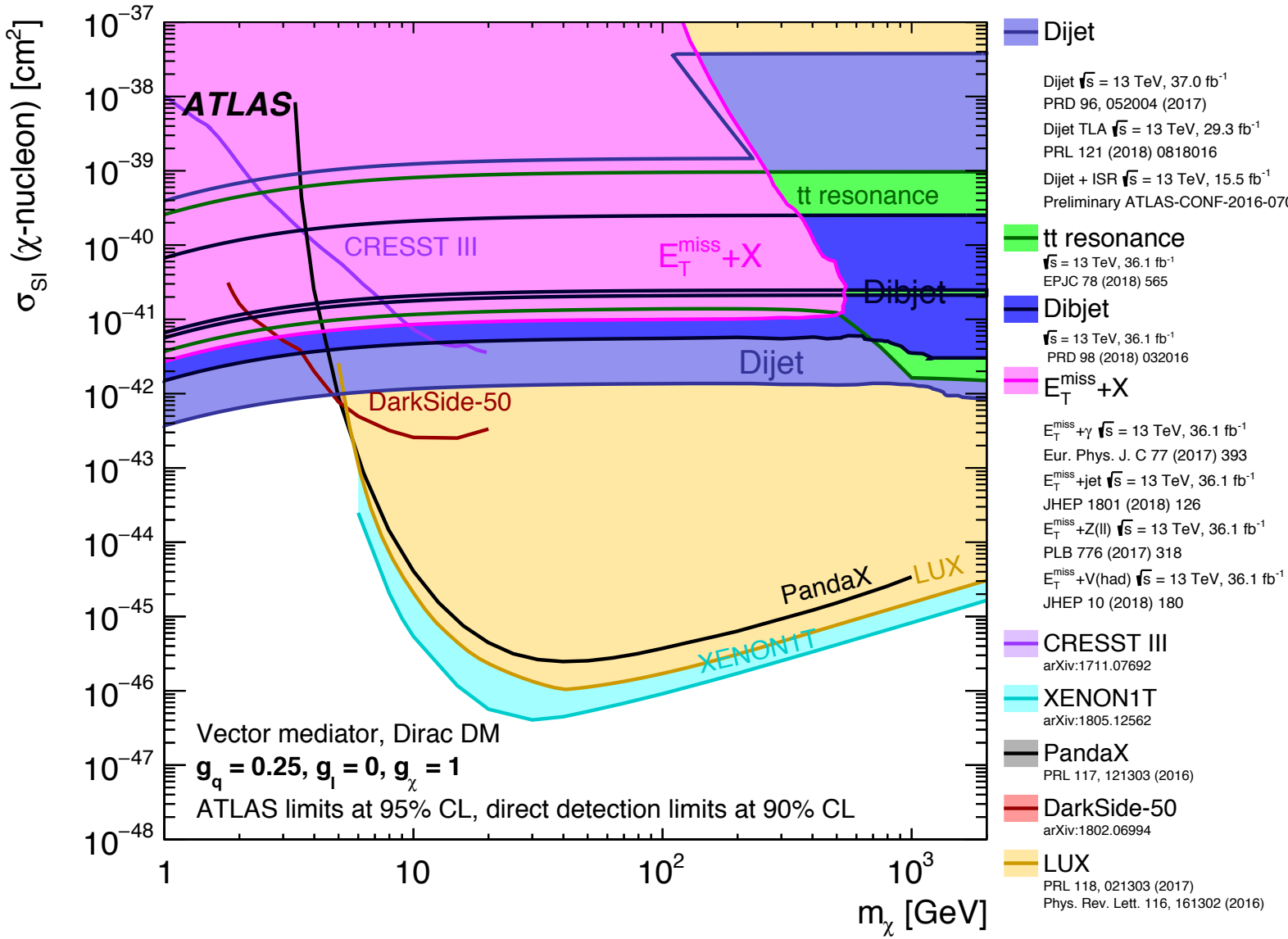

Figure 13a:
A comparison of the inferred limits with the constraints from direct detection experiments on (a) the spin-dependent WIMP--proton scattering cross-section in the context of the vector leptophobic model and (b) the spin-independent WIMP--nucleon scattering cross-section in the context of the axial-vector leptophilic model. The results from this analysis, excluding the region inside or to the left of the contour, are compared with limits from direct detection experiments. ATLAS limits are shown at 95% CL and direct detection limits at 90% CL. ATLAS searches and direct detection experiments exclude the shaded areas. Exclusions beyond the canvas are not implied for the ATLAS results. The dijet and E_T^{miss}+X exclusion regions represent the union of exclusions from all analyses of that type.

DM summary paper, JHEP 05 (2019) 142

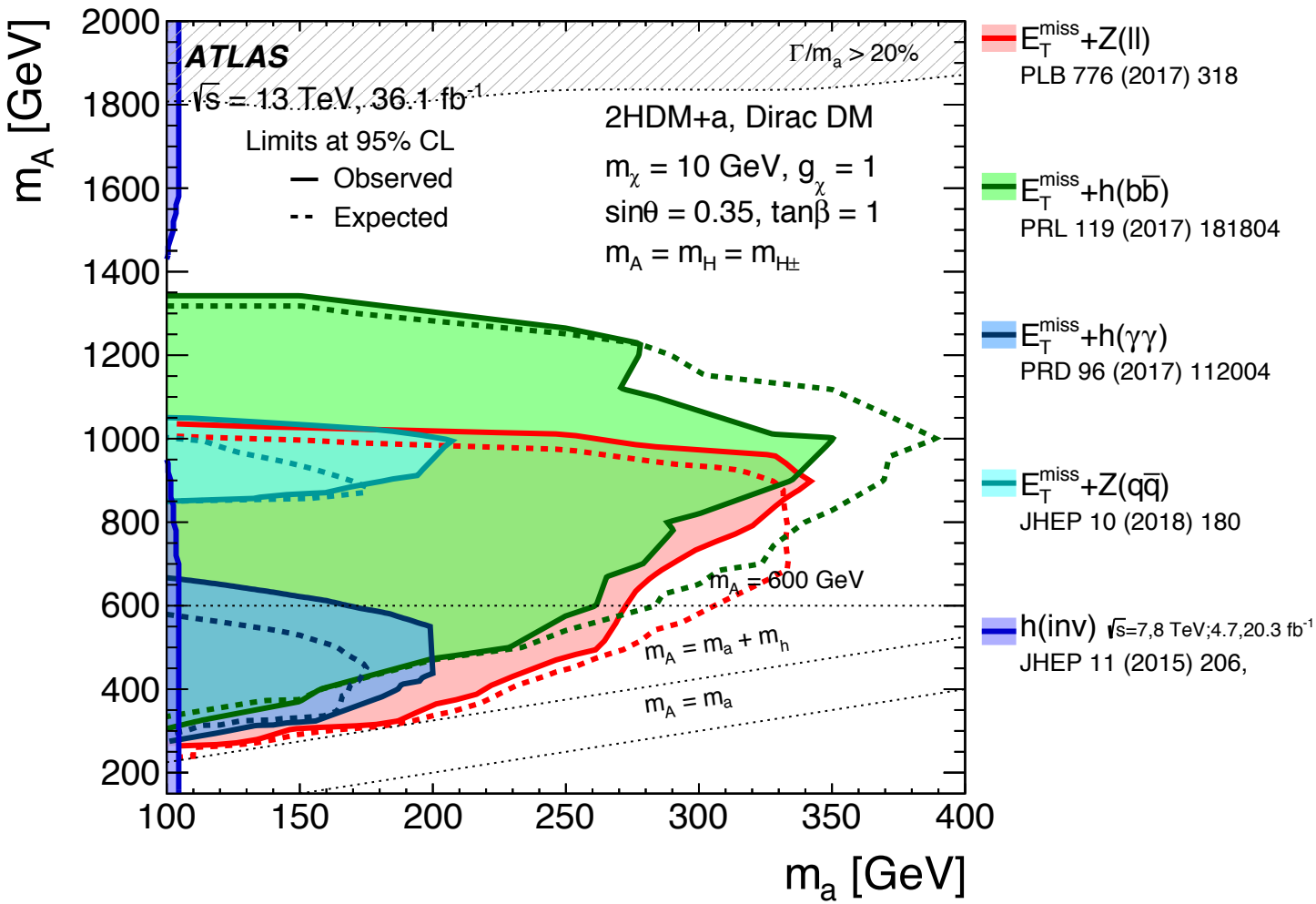

Figure 19a:
Regions in the (a) (m_a,m_A) and (b) (m_a,tanβ) planes excluded by data at 95% CL by X+E_T^{miss} and $t\bar{t}t\bar{t}$ analyses, following the parameter choices of scenarios 1 and 2 of the 2HDM+a model. The dashed grey regions at the top of (a) and the bottom of (b) indicate the region where the width of any of the Higgs bosons exceeds 20% of its mass. The exclusion limits presented above conservatively neglect the contribution from $b\bar{b}$-initiated production, which might be sizeable for tanβ ≥ 3 for the Z+E_T^{miss} channel and, to a lesser extent, for the h+E_T^{miss} one.

DM summary paper, JHEP 05 (2019) 142

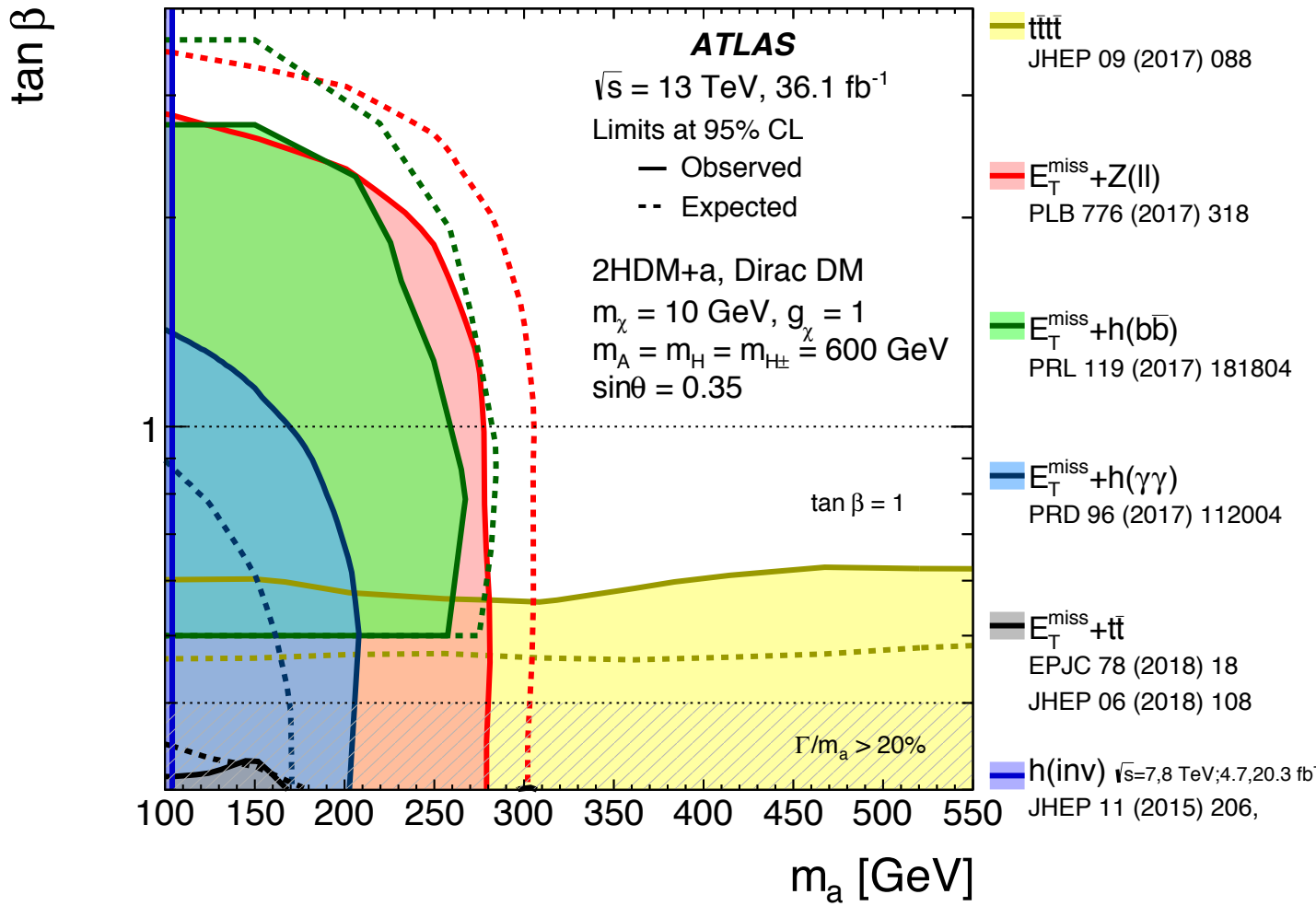

Figure 19b:
Regions in the (a) (m_a,m_A) and (b) (m_a,tanβ) planes excluded by data at 95% CL by X+E_T^{miss} and $t\bar{t}t\bar{t}$ analyses, following the parameter choices of scenarios 1 and 2 of the 2HDM+a model. The dashed grey regions at the top of (a) and the bottom of (b) indicate the region where the width of any of the Higgs bosons exceeds 20% of its mass. The exclusion limits presented above conservatively neglect the contribution from $b\bar{b}$-initiated production, which might be sizeable for tanβ ≥ 3 for the Z+E_T^{miss} channel and, to a lesser extent, for the h+E_T^{miss} one.

Low-mass di-jet, [1901.10917]

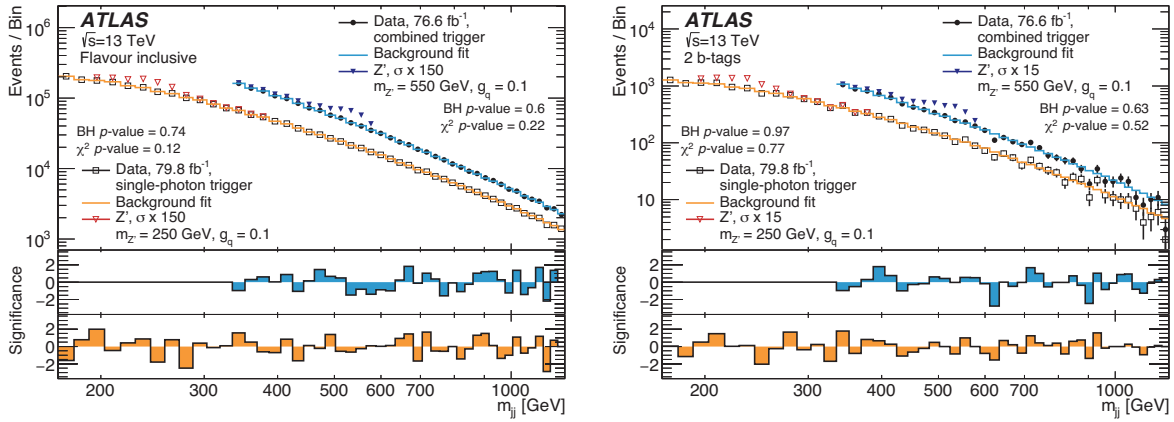

(a) (b)

Figure 1: Dijet mass distributions for the (a) flavour-inclusive and (b) b-tagged categories. In both figures, the distribution for the sample collected using the combined trigger with $E_{\mathrm{T}}^{\gamma} > 95\,\mathrm{GeV}$ and two $p_{\mathrm{T}}^{\mathrm{jet}} > 25\,\mathrm{GeV}$ jets (filled circles) and the distribution for the sample collected using the single-photon trigger with $E_{\mathrm{T}}^{\gamma} > 150\,\mathrm{GeV}$ (open squares) are shown separately. The solid lines indicate the background estimated from the fitting method described in the text. Also shown are the p-values both by a χ^2 comparison of data to background estimate and by BumpHunter (BH). The solid and empty triangles represent a Z' injected signal with $g_{\mathrm{q}} = 0.1$, masses of 550 and 250 GeV, respectively, where the theory-cross section is multiplied by the factor shown in the legend. The bottom panels show the significances of bin-by-bin differences between the data and the fits for the combined trigger (middle) and single-photon trigger (bottom). These Gaussian significances are calculated from the Poisson probability, considering only statistical uncertainties on the data.

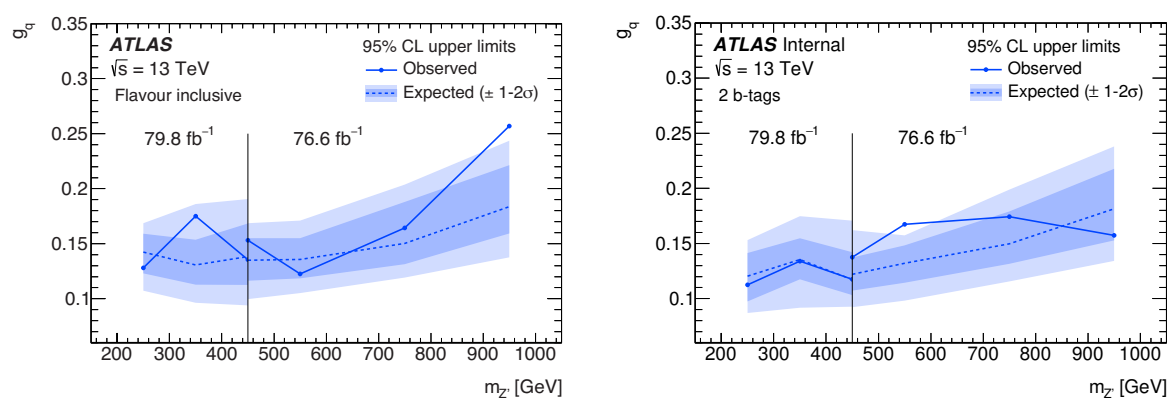

(a) (b)

Figure 2: Excluded values of the coupling between a Z' and quarks, at 95% CL, as a function of $m_{Z'}$, from (a) the flavour-inclusive and (b) the b-tagged categories. Below 450 GeV the distribution of events selected by the single-photon trigger is used for hypothesis testing, while above 450 GeV the combined trigger is used.

VBF + Invisible Higgs, PLB 793 (2019) 499

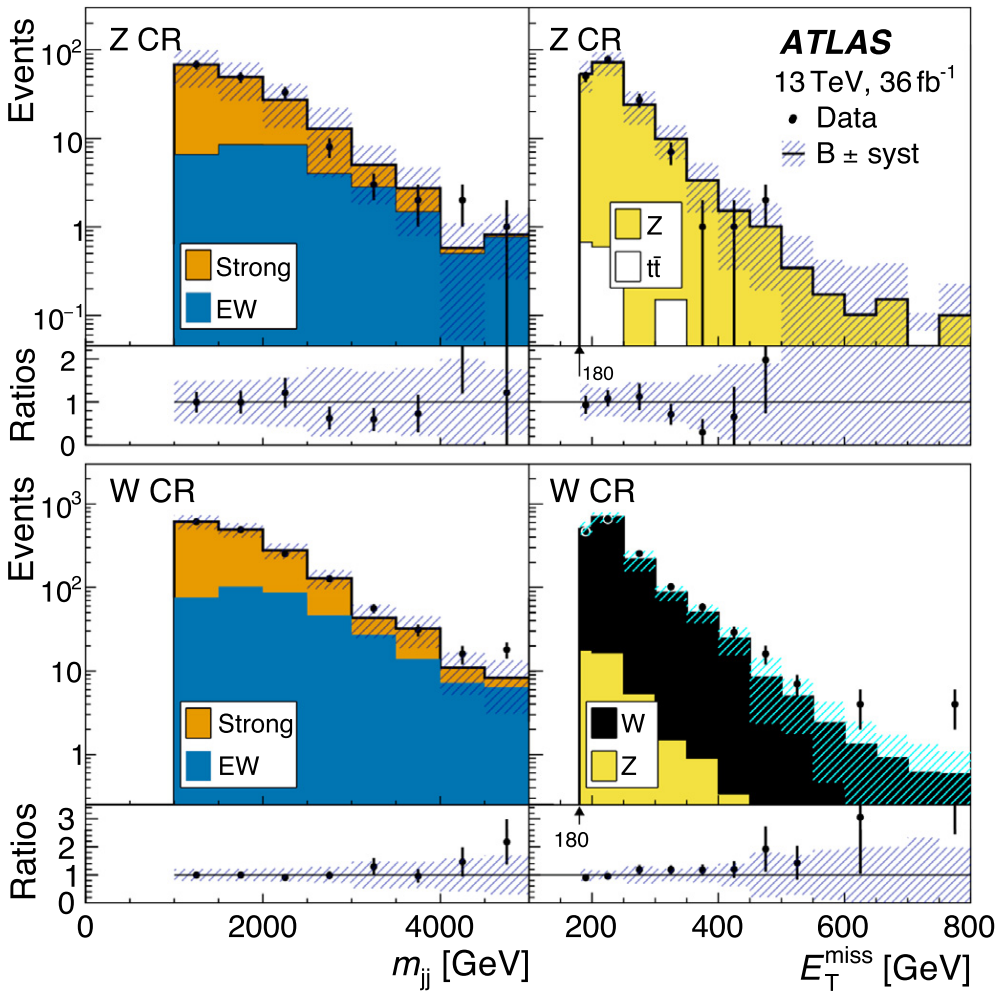

Fig. 2. Distribution of event yields in the Z (top) and W (bottom) control regions. The *postfit* normalizations for m_{jj} (left) and E_T^{miss} (right) are summed over the subsamples. The E_T^{miss} distributions start at 180 GeV as indicated. The observed data N (dots) are superimposed on the sum of the backgrounds B (stacked histogram with shaded systematic uncertainty bands). The breakdown of the B is given in the lower left box in each panel. The bottom panels show the ratios of N to B with the systematic uncertainty band shown on the line at 1. The "other," as listed in Table 1, contribute a few events at low values of m_{jj} and E_T^{miss}, and are omitted. The last bin in each plot contains the overflow.

Table 1
Event yields in the signal region (SR) and control regions (CR) summed over lepton charge and flavor. The yields are the *prefit* values for $m_{jj} > 1$ TeV. The observed data (N), the background estimate (B), and the signal (S for $m_H = 125$ GeV with $\mathcal{B}_{inv} = 1$) are given. The B and S values for individual processes are rounded to a precision commensurate with the sampling uncertainty associated with the finite MC sample size. For all processes the fractions of electroweak production [EW] are given. "Other" is defined in the text.

Description	SR		W CR		Z CR	
	Yield	[EW]	Yield	[EW]	Yield	[EW]
N, observed	2252		1602		166	
B, expected	2243		1648		183	
$Z \to \nu\nu$	1111	[18%]	–		–	
$Z \to ee, \mu\mu$	12	[9%]	38	[9%]	181	[23%]
$Z \to \tau\tau$	10	[16%]	11	[16%]	–	
$W \to e\nu, \mu\nu$	540	[16%]	1400	[30%]	–	
$W \to \tau\nu$	533	[20%]	130	[34%]	–	
Other	36		67		2	
S, signal	1070		–		–	
VBF	930		–		–	
Gluon fusion	140		–		–	

For the SR, an event is required to have

- no isolated electron or muon,
- a leading jet with $p_T > 80$ GeV,
- a subleading jet with $p_T > 50$ GeV,
- no additional jets with $p_T > 25$ GeV,
- $E_T^{miss} > 180$ GeV,
- $H_T^{miss} > 150$ GeV.

The two jets are required to have the following properties:

- not be aligned with $\vec{E}_T^{miss}$, $|\Delta\phi_{j\text{-MET}}| > 1$,
- not be back-to-back, $|\Delta\phi_{jj}| < 1.8$,
- be well separated in η, $|\Delta\eta_{jj}| > 4.8$,
- be in opposite η hemispheres, $\eta_{j_1} \cdot \eta_{j_2} < 0$,
- $m_{jj} > 1$ TeV.

VBF + Invisible Higgs, PLB 793 (2019) 499

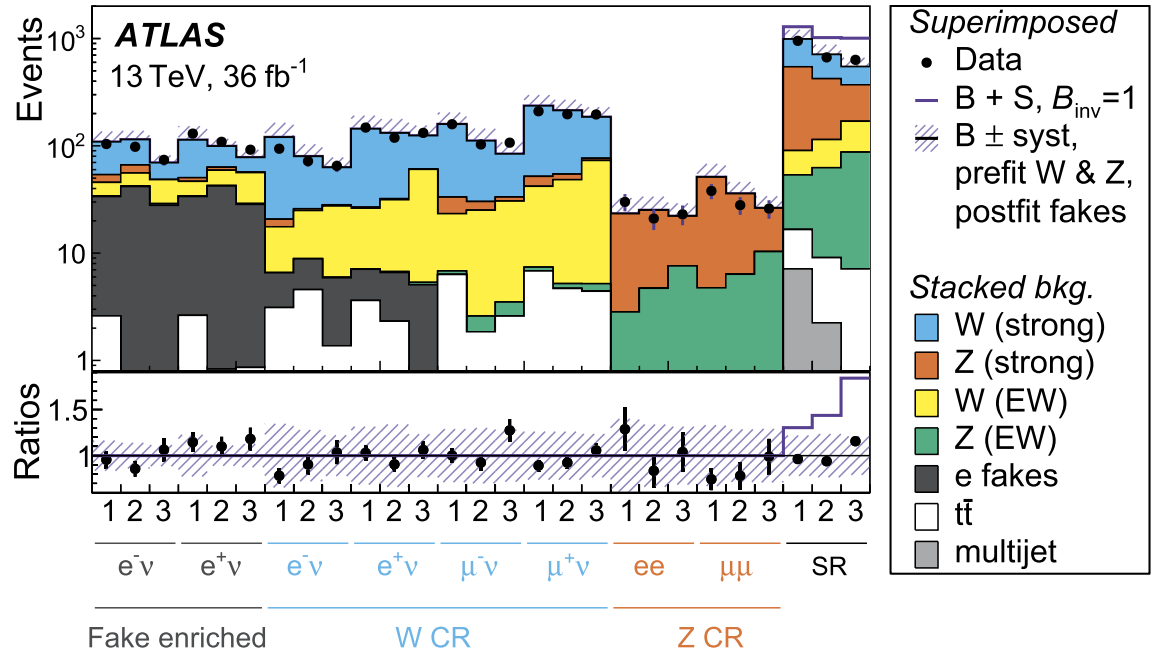

Prefit

Fig. 1. Data-to-MC yield comparisons in the 27 subsamples used in the statistical fit. The observed data N (dots) are superimposed on the *prefit* backgrounds B (stacked histogram with shaded systematic uncertainty bands). The hypothetical signal S (empty blue histogram) is shown on top of B for $\mathcal{B}_{\text{inv}} = 1$. The bottom panels show the ratios of N (dots) and $B + S$ (blue line) to B with the systematic uncertainty band shown on the line at 1. The 1, 2, and 3 bin labels corresponds to $1 < m_{jj} \leq 1.5\,\text{TeV}$, $1.5 < m_{jj} \leq 2\,\text{TeV}$, and $m_{jj} > 2\,\text{TeV}$, respectively. The "e fakes" refers to $S_{\text{MET}} < 4\sqrt{\text{GeV}}$ selection and is determined by the fit, so *postfit* values are shown for the purposes of illustration. The diboson contribution is included in the electroweak (EW) W and Z bosons.

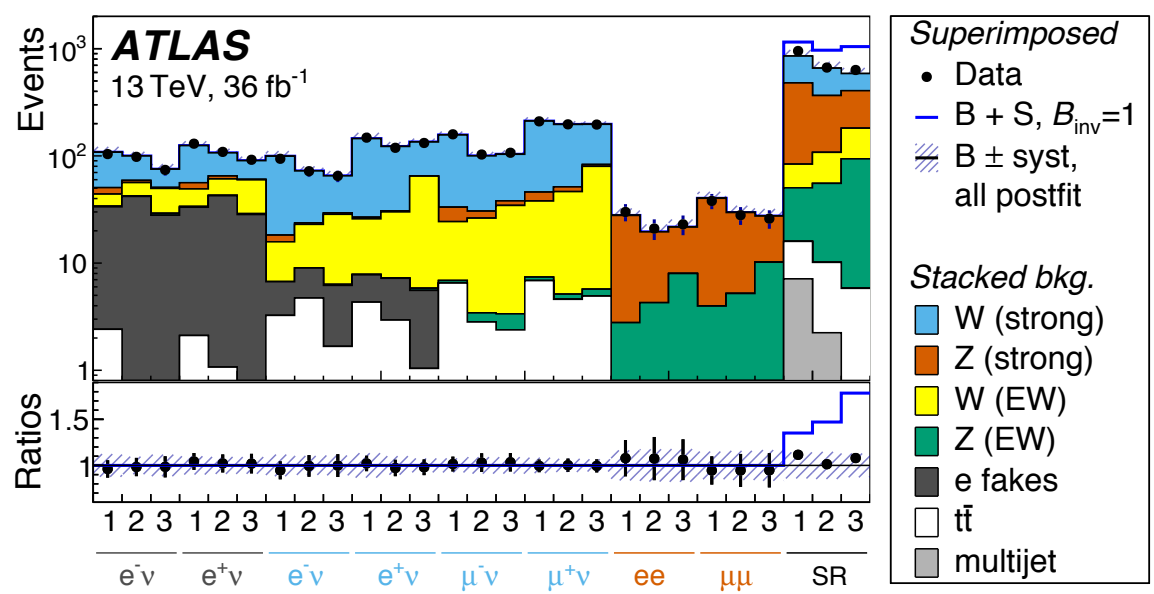

Postfit

VBF + Invisible Higgs, PLB 793 (2019) 499

Table 2
Sources of uncertainty. The first set shows Δ, the *relative* improvement of the 95% CL upper limit on $\mathcal{B}_{\text{inv}}$ when the source of uncertainty is "removed" by fixing it to its best-fit value. The "visual" column shows bars whose lengths from the center tick are proportional to Δ. The second set shows the effect on the yields and the α transfer factors for the $1 < m_{jj} \leq 1.5$ TeV bin. The yields are for the signal process in the SR (S), Z MC in the SR (B_Z^{SR}), and Z MC in the CR (B_Z^{CR}). The α_Z is given to demonstrate the reduction in the uncertainty in the ratio $B_Z^{\text{SR}}/B_Z^{\text{CR}}$. The individual yields for the W are not shown because the cancellation effects are similar to the Z counterparts. The value for "3rd jet veto" corresponds only to the uncertainty related to jet bin migration for signal processes; the corresponding effect for the background processes are evaluated in the various jet energy and theoretical variations. The abbreviations for the theoretical sources are described in the text. The '-' indicates that the quantity is not applicable. The "combined" rows at the bottom are not simple sums of the rows above because of the Δ metric; the symbols ($\dagger, \ddagger, \star$) are parenthetically defined in the table. The penultimate (last) row shows the summary impact of removing the systematic uncertainties due to the experimental and theoretical sources (as well as statistical uncertainties of the MC samples).

Source	$\mathcal{B}_{\text{inv}}$ improve. [%] using all m_{jj} bins		Yields, α changes (%) in $1 < m_{jj} \leq 1.5$ TeV				
	Δ	visual	S	B_{SR}^Z	B_{CR}^Z	α_Z	α_W
Experimental ($\dagger$)							
Jet energy scale	10		12	7	8	8	6
Jet energy resol.	2		2	0	1	1	4
$E_{\text{T}}^{\text{miss}}$ soft term	1		2	2	2	2	2
Lepton id., veto	2		–	–	–	0	4
Pileup distrib.	1		3	1	2	3	1
Luminosity	0		2	2	2	–	–
Theoretical ($\ddagger$)							
Resum. scale	1		–	2	3	0	2
Renorm., fact.	2		–	20	19	1	2
CKKW matching	4		–	2	3	1	5
PDF	0		1	1	2	1	1
3rd jet veto	2		7	–	–	–	–
Statistical							
MC sample ($\star$)	12		4	5	9	10	9
Data sample	21		6	5	12	12	6
Combined							
All $\dagger$ sources	17						
All $\ddagger$ sources	10						
Combine $\dagger$, $\ddagger$	28						
Combine $\dagger$, $\ddagger$, $\star$	42						

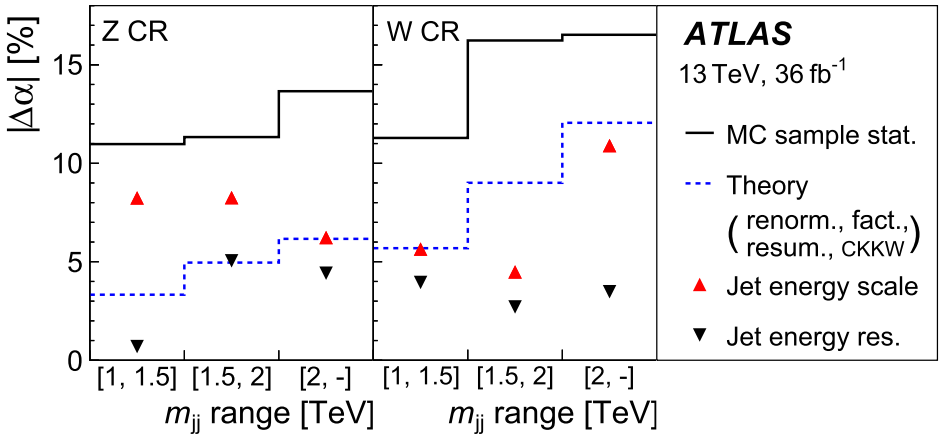

Fig. 4. Contributions to the relative uncertainty in the transfer factors α_Z (left) and α_W (right) in the three m_{jj} bins of the SR. The theoretical uncertainties from the sources noted in the legend are combined in quadrature.

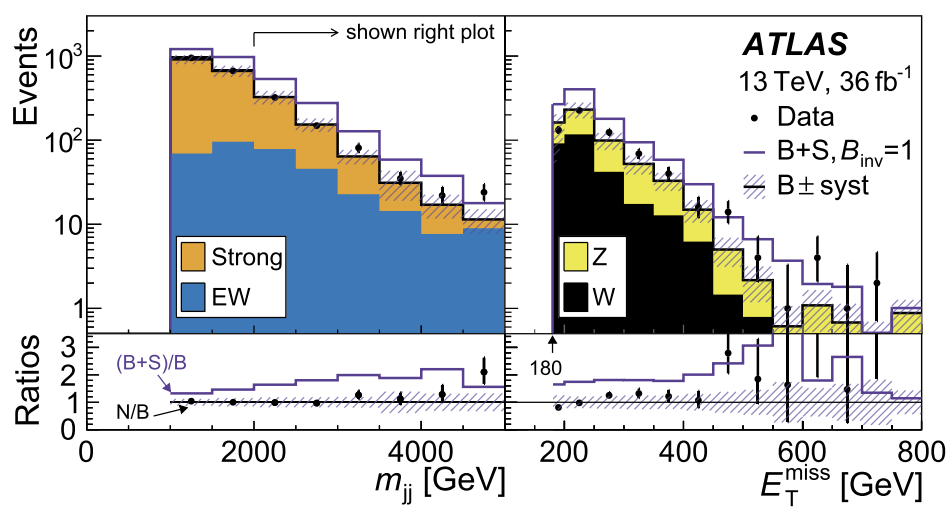

Fig. 5. Distribution of event yields in the signal region for m_{jj} (left) and $E_{\mathrm{T}}^{\mathrm{miss}}$ (right). The $E_{\mathrm{T}}^{\mathrm{miss}}$ distributions start at 180 GeV and shows the most sensitive $m_{jj} > 2$ TeV subset of the SR as indicated by the arrow. The *postfit* normalizations for m_{jj} ($E_{\mathrm{T}}^{\mathrm{miss}}$) distributions use separate background, B, normalizations in the three (one) m_{jj} bins of $1 < m_{jj} \leq 1.5$ TeV, $1.5 < m_{jj} \leq 2$ TeV, and $m_{jj} > 2$ TeV ($m_{jj} > 2$ TeV), and sum the contributions from W and Z bosons (electroweak and strong production modes). The hypothetical signal S (empty blue histogram) is shown on top of B for $\mathcal{B}_{\mathrm{inv}} = 1$. The bottom panels show the ratios of N (dots) and $B + S$ (blue line) to B with the systematic uncertainty band shown on the line at 1. The bin width in the m_{jj} plots ($E_{\mathrm{T}}^{\mathrm{miss}}$) is 500 GeV (50 GeV except for the first bin with the non-zero entry, which is 20 GeV). See the caption of Fig. 2 for other plotting details.

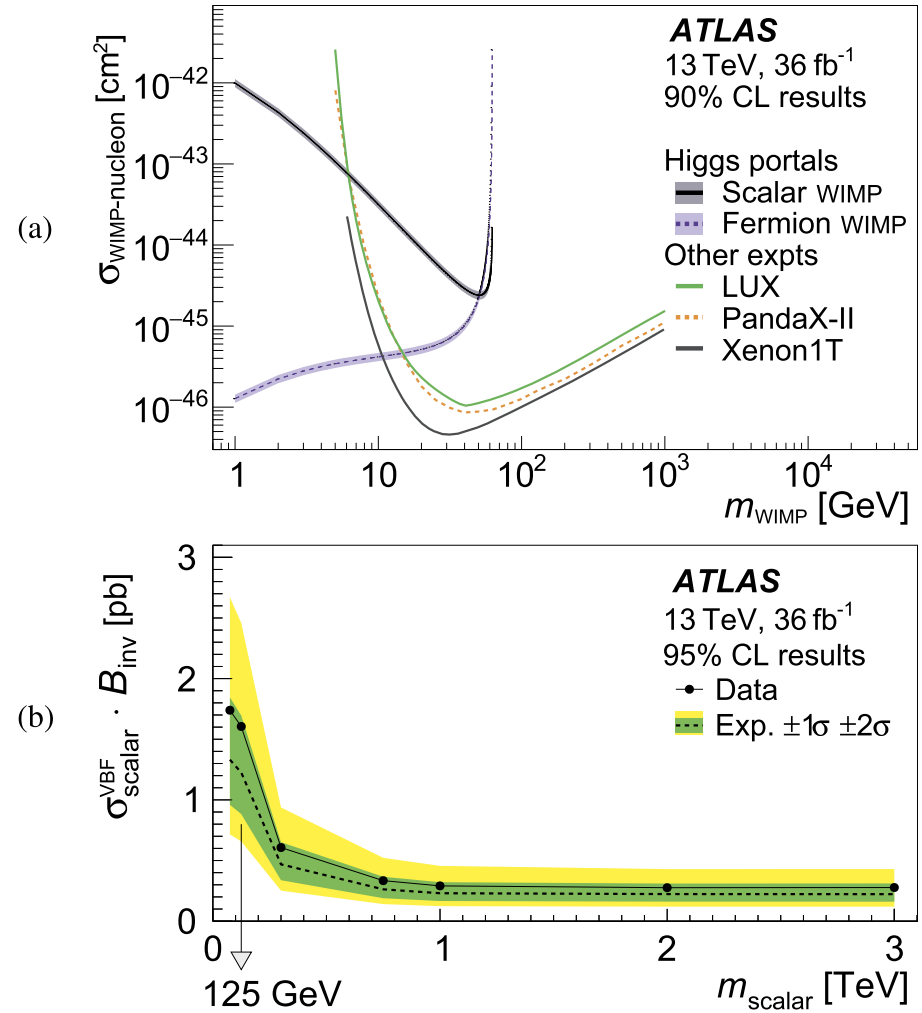

Fig. 6. Upper limits on (a) the spin-independent WIMP–nucleon cross section using Higgs portal interpretations of $\mathcal{B}_{\mathrm{inv}}$ at 90% CL vs. m_{WIMP} and (b) the VBF cross section times the branching fraction to invisible decays at 95% CL vs. m_{scalar}. The top plot shows results from Ref. [85–87].

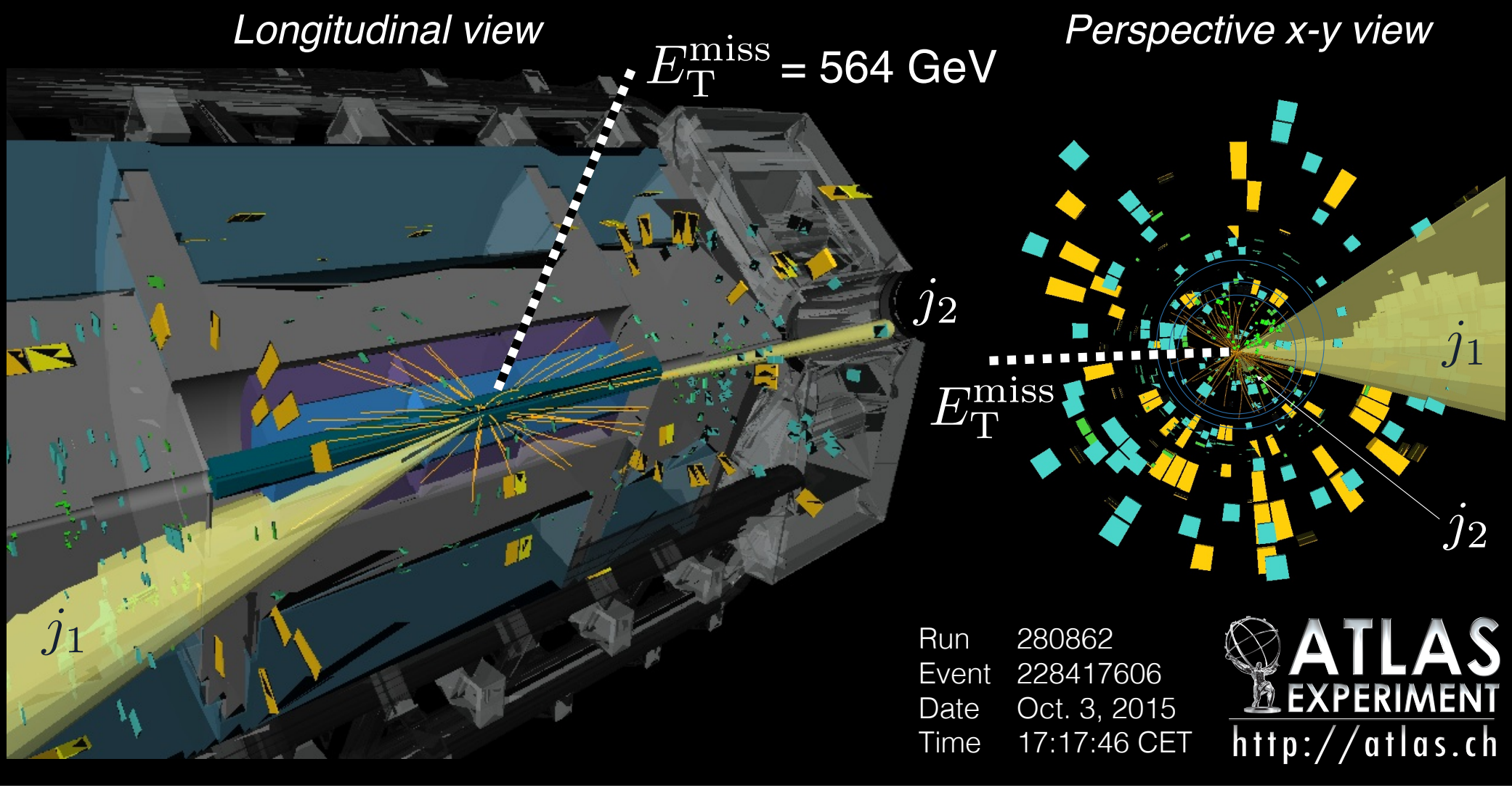

Figure 4a:
Event display of a candidate in the signal region. The image on the top (bottom) shows calorimeter cell energy deposits for $E_{\mathrm{T}} > 0.25$ (1) GeV and charged tracks for $p_{\mathrm{T}} > 1$ (2) GeV. For each image, the left (right) shows a longitudinal (transverse *x*-*y*) view. In the transverse view, the concentric circles on the right correspond to the perspective view of the TRT subdetector system shown in the longitudinal view; the leading (subleading) jet j_1 (j_2) is coming out of (going into) the page. The two jets shown have the properties ($p_{\mathrm{T,j1}}$ = 450 GeV, ($p_{\mathrm{T,j2}}$ = 110 GeV, η_{j1} = -1.8, η_{j2} = 3.7) that result in the dijet properties (m_{jj} = 3.6 TeV, $\Delta\eta_{jj}$ = 5.5, $\Delta\phi_{jj}$ = 0.1) and $\vec{E}_{\mathrm{T}}^{\mathrm{miss}}$ quantities ($E_{\mathrm{T}}^{\mathrm{miss}}$ = 564 GeV, = 2.8). During the run in which this event was recorded, the peak averaged number of *pp* interactions per event was around 17.

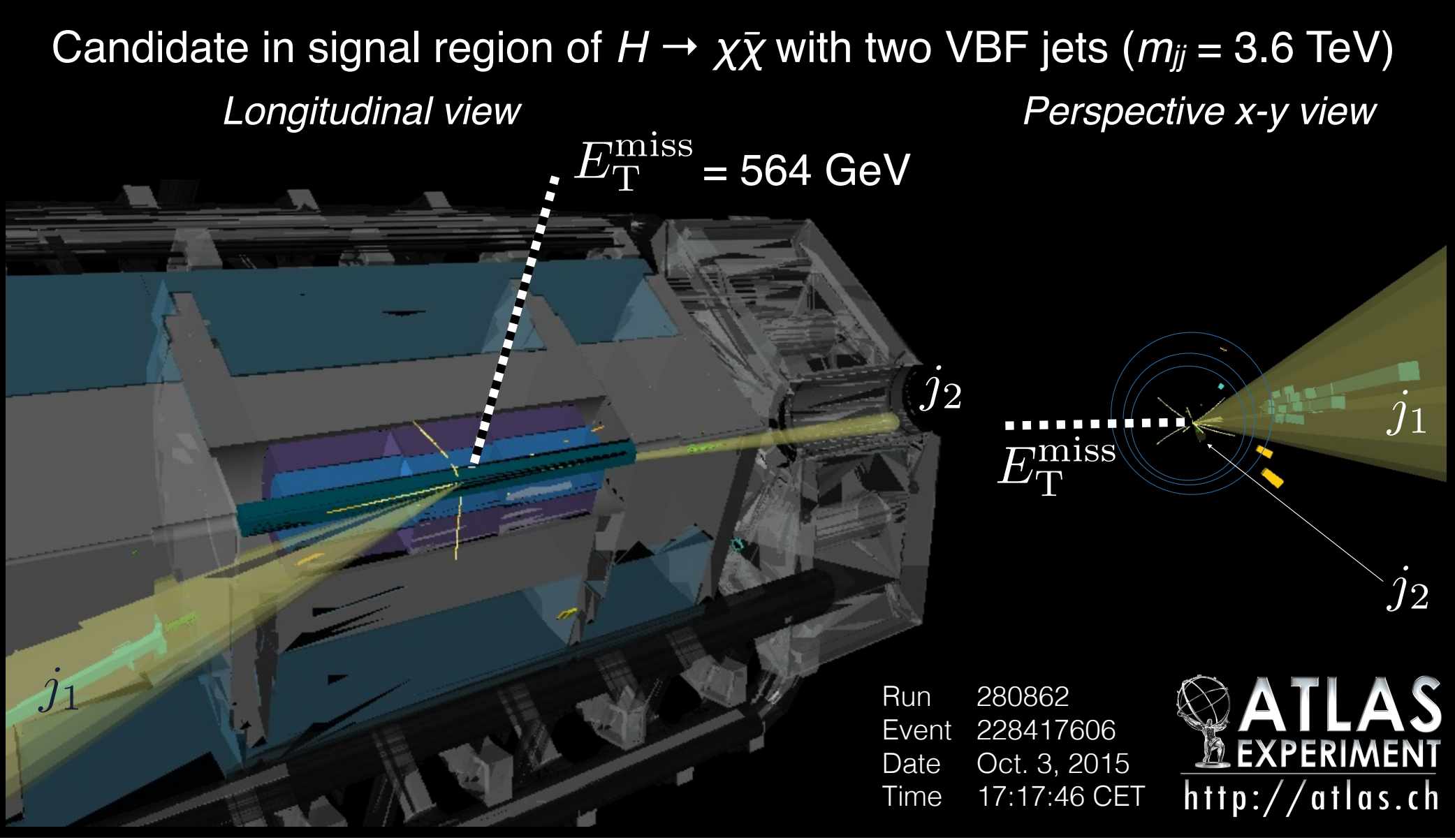

Figure 4b:
Event display of a candidate in the signal region. The image on the top (bottom) shows calorimeter cell energy deposits for $E_{\mathrm{T}} > 0.25$ (1) GeV and charged tracks for $p_{\mathrm{T}} > 1$ (2) GeV. For each image, the left (right) shows a longitudinal (transverse *x*-*y*) view. In the transverse view, the concentric circles on the right correspond to the perspective view of the TRT subdetector system shown in the longitudinal view; the leading (subleading) jet j_1 (j_2) is coming out of (going into) the page. The two jets shown have the properties ($p_{\mathrm{T,j1}}$ = 450 GeV, ($p_{\mathrm{T,j2}}$ = 110 GeV, η_{j1} = -1.8, η_{j2} = 3.7) that result in the dijet properties (m_{jj} = 3.6 TeV, $\Delta\eta_{jj}$ = 5.5, $\Delta\phi_{jj}$ = 0.1) and $\vec{E}_{\mathrm{T}}^{\mathrm{miss}}$ quantities ($E_{\mathrm{T}}^{\mathrm{miss}}$ = 564 GeV, = 2.8). During the run in which this event was recorded, the peak averaged number of *pp* interactions per event was around 17.

VBF + Invisible Higgs, PLB 793 (2019) 499

Table 6:
Analysis updates. Notable changes to the analysis with respect to Ref. [28] are listed.

Topic	Ref. [1]	This paper	Comments
Objects			
Jet tagger	JVF [2]	JVT	Only in the tracking volume
$E_{\mathrm{T}}^{\mathrm{miss}}$ soft term	Calorimeter based	Track based	-
MC			
W and Z	SHERPA v1.4.5	SHERPA v2.2.1	NLO for up to two jets
Selection			
$E_{\mathrm{T}}^{\mathrm{miss}}$	> 150 GeV	> 180 GeV	Fake low $E_{\mathrm{T}}^{\mathrm{miss}}$ introduced by using JVT[a]
m_{jj}	One bin > 1 TeV	Three bins in [1, 1.5, 2, -]	-
Third-jet p_{T}	> 30 GeV	> 25 GeV	-
Estimation			
Z	$Z_{\ell\ell}$ and $W_{\ell\nu}$ samples	$Z_{\ell\ell}$ sample	Using $W_{\ell\nu}$ involves W-to-Z extrapolation
W	Fit m_{T} template	Fake-enriched & -depleted	-
Multijet	Inverted $\Delta\phi(j, E_{\mathrm{T}}^{\mathrm{miss}})$ sample	Rebalance-and-smear	-
Results			
Signal	Higgs at 125 GeV	Higgs at 125 GeV & up to 3 TeV	-

[a] Going from 150 to 180 GeV reduces the signal yield to about two-thirds of the original amount.

Mono-jet projections, ATL-PHYS-PUB-2018-043

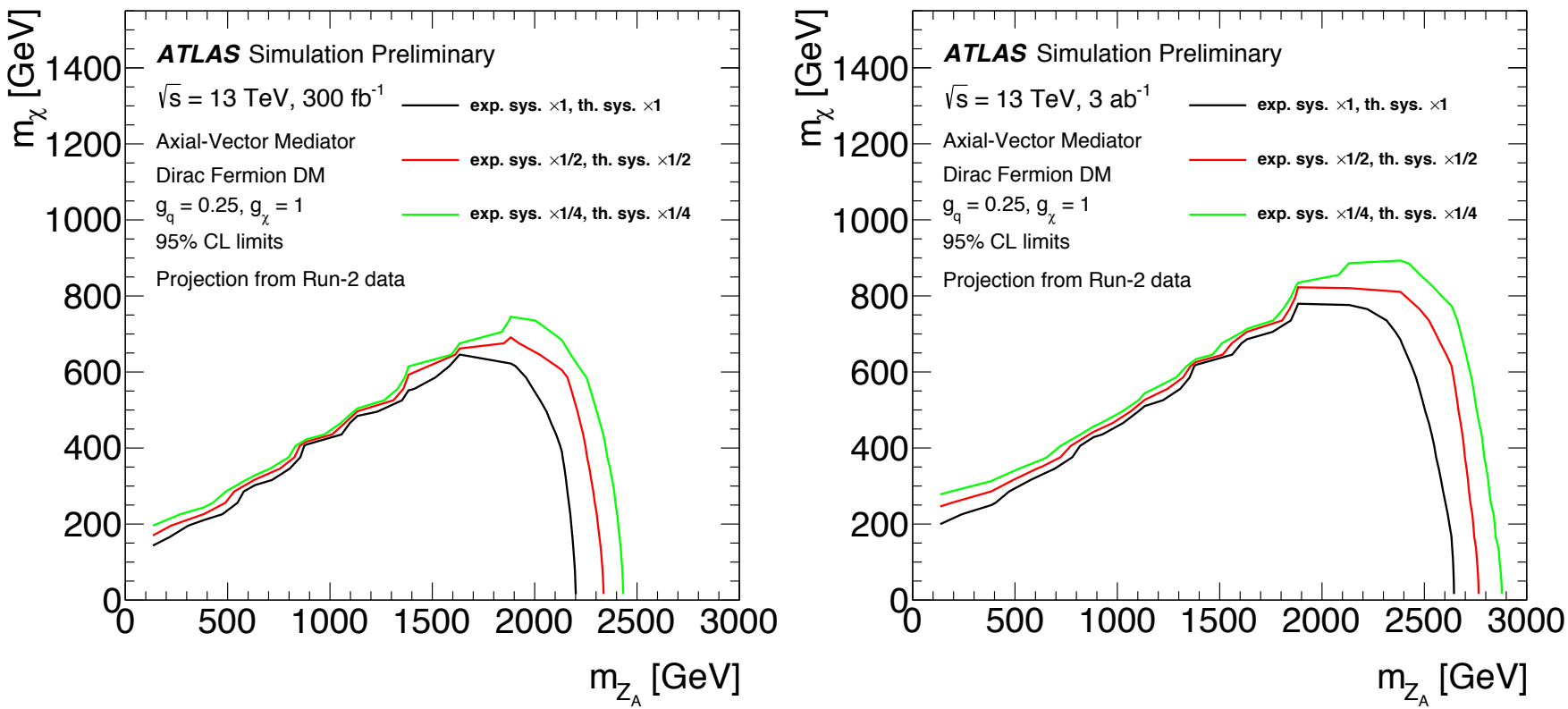

Figure 1: Expected 95% CL excluded regions on the (m_χ, m_{Z_A}) mass plane for the axial-vector simplified model with couplings $g_\chi = 1$ and $g_q = 0.25$, for a luminosity of 300 fb^{-1} (left) and 3000 fb^{-1} (right). Three contours are shown in each plot, corresponding to the three different systematic uncertainty scenarios: standard (black), reduced by a factor 2 (red) and 4 (green). More details in the text.

Trigger projections, CERN-LHCC-2017-020

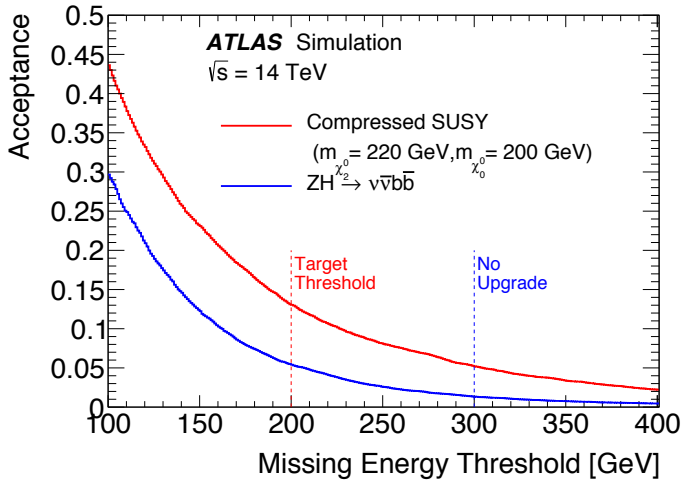

Figure 2.11: *The integrated acceptance as a function of the missing transverse energy threshold for representative channels. A representative compressed SUSY model and $ZH \to \nu\nu bb$ are shown.*

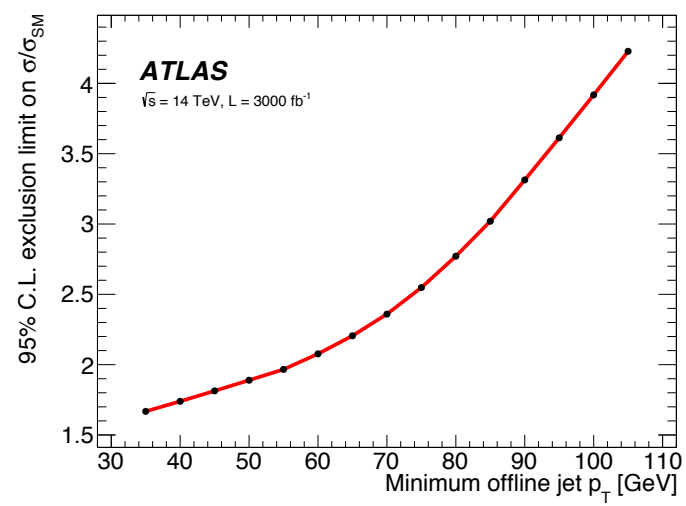

Figure 2.9: *Expected 95% C.L. upper limit on the cross-section ratio $\sigma(HH \to 4b)/\sigma(HH \to 4b)_{SM}$ as a function of the minimum p_T requirement applied to the fourth-leading jet, assuming that systematics are not a strong limitation on the result. As discussed in Section 2.2, modifications of the Higgs self-coupling can modify the cross-section by factors of order unity. Results with systematics show similar trigger impacts. For a more detailed discussion, see Section 6.13.*

CERN-LPCC-2018-02

LHC Dark Matter Working Group: Next-generation spin-0 dark matter models

Tomohiro Abe,[1,2] **Yoav Afik,**[3] **Andreas Albert,**[4] **Christopher R. Anelli,**[5] **Liron Barak,**[6] **Martin Bauer,**[7] **J. Katharina Behr,**[8] **Nicole F. Bell,**[9] **Antonio Boveia,**[10,*] **Oleg Brandt,**[11] **Giorgio Busoni,**[9] **Linda M. Carpenter,**[10] **Yu-Heng Chen,**[8] **Caterina Doglioni,**[12,*] **Alison Elliot,**[13] **Motoko Fujiwara,**[14] **Marie-Helene Genest,**[15] **Raffaele Gerosa,**[16] **Stefania Gori,**[17] **Johanna Gramling,**[18] **Alexander Grohsjean,**[8] **Giuliano Gustavino,**[19] **Kristian Hahn,**[20,*] **Ulrich Haisch,**[21,22,23,*] **Lars Henkelmann,**[11] **Junji Hisano,**[2,14,24] **Anders Huitfeldt,**[25] **Valerio Ippolito,**[26] **Felix Kahlhoefer,**[27] **Greg Landsberg,**[28] **Steven Lowette,**[29] **Benedikt Maier,**[30] **Fabio Maltoni,**[31] **Margarete Muehlleitner,**[32] **Jose M. No,**[33,34] **Priscilla Pani,**[8,35] **Giacomo Polesello,**[36] **Darren D. Price,**[37] **Tania Robens,**[38,39] **Giulia Rovelli,**[40] **Yoram Rozen,**[3] **Isaac W. Sanderson,**[9] **Rui Santos,**[41,42] **Stanislava Sevova,**[43] **David Sperka,**[44] **Kevin Sung,**[20] **Tim M. P. Tait,**[17,*] **Koji Terashi,**[45] **Francesca C. Ungaro,**[9] **Eleni Vryonidou,**[23] **Shin-Shan Yu,**[46] **Sau Lan Wu,**[47] **and Chen Zhou.**[47]

[1]Institute for Advanced Research, Nagoya University, Furo-cho Chikusa-ku, Nagoya, Aichi, 464-8602, Japan

[2]Kobayashi-Maskawa Institute for the Origin of Particles and the Universe, Nagoya University, Furo-cho Chikusa-ku, Nagoya, Aichi, 464-8602, Japan

[3]Department of Physics, Technion: Israel Institute of Technology, Haifa, Israel

[4]III. Physikalisches Institut A, RWTH Aachen University, Physikzentrum, Otto-Blumenthal-Straße, Aachen, Germany

[5]University of Victoria, Department of Physics and Astronomy, Elliott Building, room 101, University of Victoria, Victoria, Canada

[6]Tel Aviv University, Haim Levanon (Ramat Aviv), Tel Aviv 69978, Israel

[7]Institute for Particle Physics Phenomenology, Department of Physics, Durham University, South Road, Durham DH1 3LE, UK

That's all!